INTERNATIONAL ATOMIC ENERGY AGENCY
UNITED NATIONS EDUCATIONAL, SCIENTIFIC AND CULTURAL ORGANIZATION
INTERNATIONAL CENTRE FOR THEORETICAL PHYSICS
I.C.T.P., P.O. BOX 586, 34100 TRIESTE, ITALY, CABLE: CENTRATOM TRIESTE

H4.SMR/676-11

SECOND SCHOOL ON THE USE OF SYNCHROTRON RADIATION IN SCIENCE AND TECHNOLOGY: *"JOHN FUGGLE MEMORIAL"*

25 October - 19 November 1993

Miramare - Trieste, Italy

Some Notes on the Design of Beamlines for Soft X-ray SR-Sources of the 3rd Generation

W.B. Peatman
BESSY
Berlin, Germany

Some Notes on the Design of Beamlines for Soft X-ray SR-Sources of the 3rd Generation

W.B. Peatman
Berliner Elektronenspeicherring-Gesellschaft
für Synchrotronstrahlung mbH (BESSY)
Lentzeallee 100, D-1000 Berlin 33, FRG

* No text. References only (see 10).

Some Notes on the Design of Beamlines for Soft X-ray SR-Sources of the 3rd Generation

W.B. Peatman
Berliner Elektronenspeicherring-Gesellschaft
für Synchrotronstrahlung mbH (BESSY)
Lentzeallee 100, D-1000 Berlin 33, FRG

1. Introduction

Up until the development of synchrotron radiation (SR) sources in the 1960's and 1970's research in the extreme VUV and soft x-ray range of the electromagnetic spectrum was limited to single wavelengths produced by line sources and to the helium continuum which produces 10 - 20 eV photons. Most research employing line sources was done without monochromators and without elaborate beamlines. Thus, in the 1970's the need for monochromators and optical systems to handle the continous radiation emitted from synchrotrons and storage rings marked a dramatic and abrupt change in the course of the development of practical optics. Although the theoretical basis for what was to come had long existed, the practical aspects of the design of optical systems for photon energies between 10 eV and 2000 eV, and of the manufacture of suitable optical elements for these energies had until that time never been in significant demand and had therefore been neglected.

Most of the original SR sources, which had been designed for the needs of high energy physics and not as light sources have been succeeded by SR sources of the second generation: electron or positron storage rings with a relatively high brightness in the dipole magnets. BESSY in Berlin, Germany, offering user operation since 1982 is just one example of such an SR-Facility. The SR is emitted from electrons undergoing centripetal acceleration in the bending magnets. Since then still better sources of high brightness SR have been developed: wigglers and undulators. At present the world is experiencing a building boom of SR-sources of the third generation: storage rings in which the primary sources of SR are undulators and where wigglers and dipole sources take a secondary, albeit important role. The general characteristics of SR are shown in figure 1.0.1-1.0.3, the differences between dipole, wiggler and undulator radiation in figure 1.0.4.

Fig. 1.0.1: Important Characteristics of Synchrotron Radiation

1) 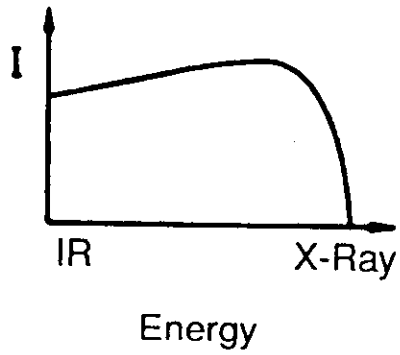

Continuous spectrum

2) 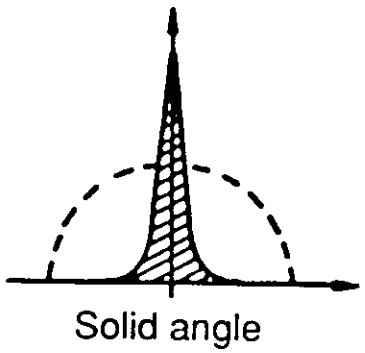

Emission in small solid angle

3) 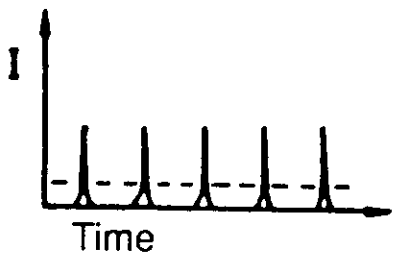

Pulsed time structure

4) 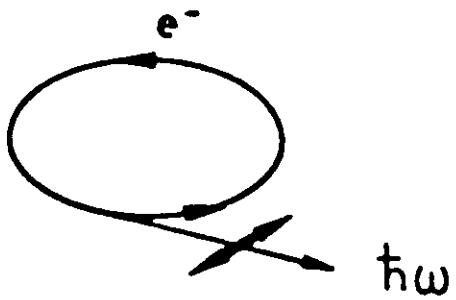

High degree of polarisation

5) Properties can be calculated/predicted

Figure 1.0.2: Time Structure of Synchrotron Radiation [2.12]

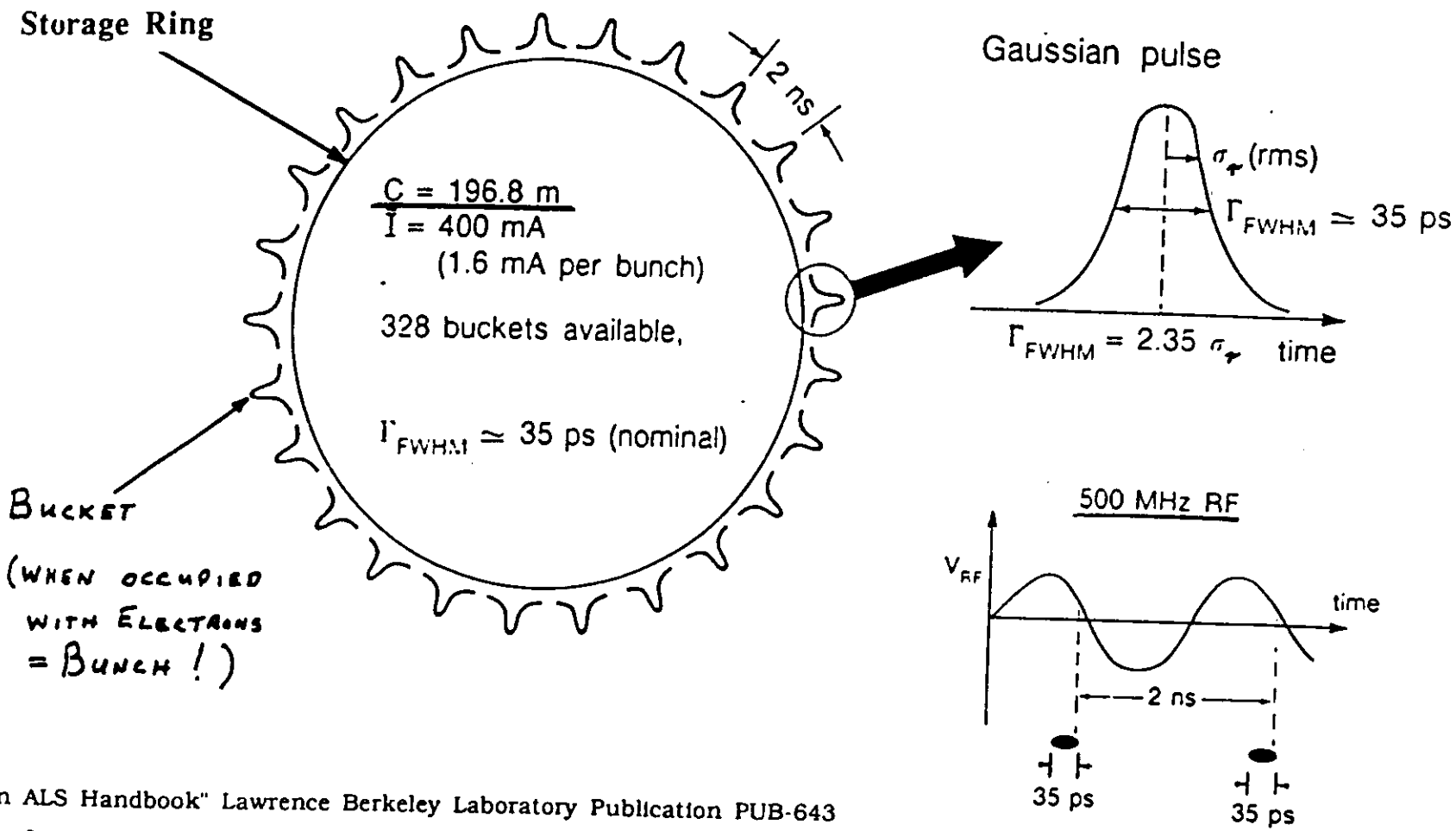

"An ALS Handbook" Lawrence Berkeley Laboratory Publication PUB-643 Rev. 2, April 1989

Figure 1.0.3: SR Intensity Versus Number of Electrons

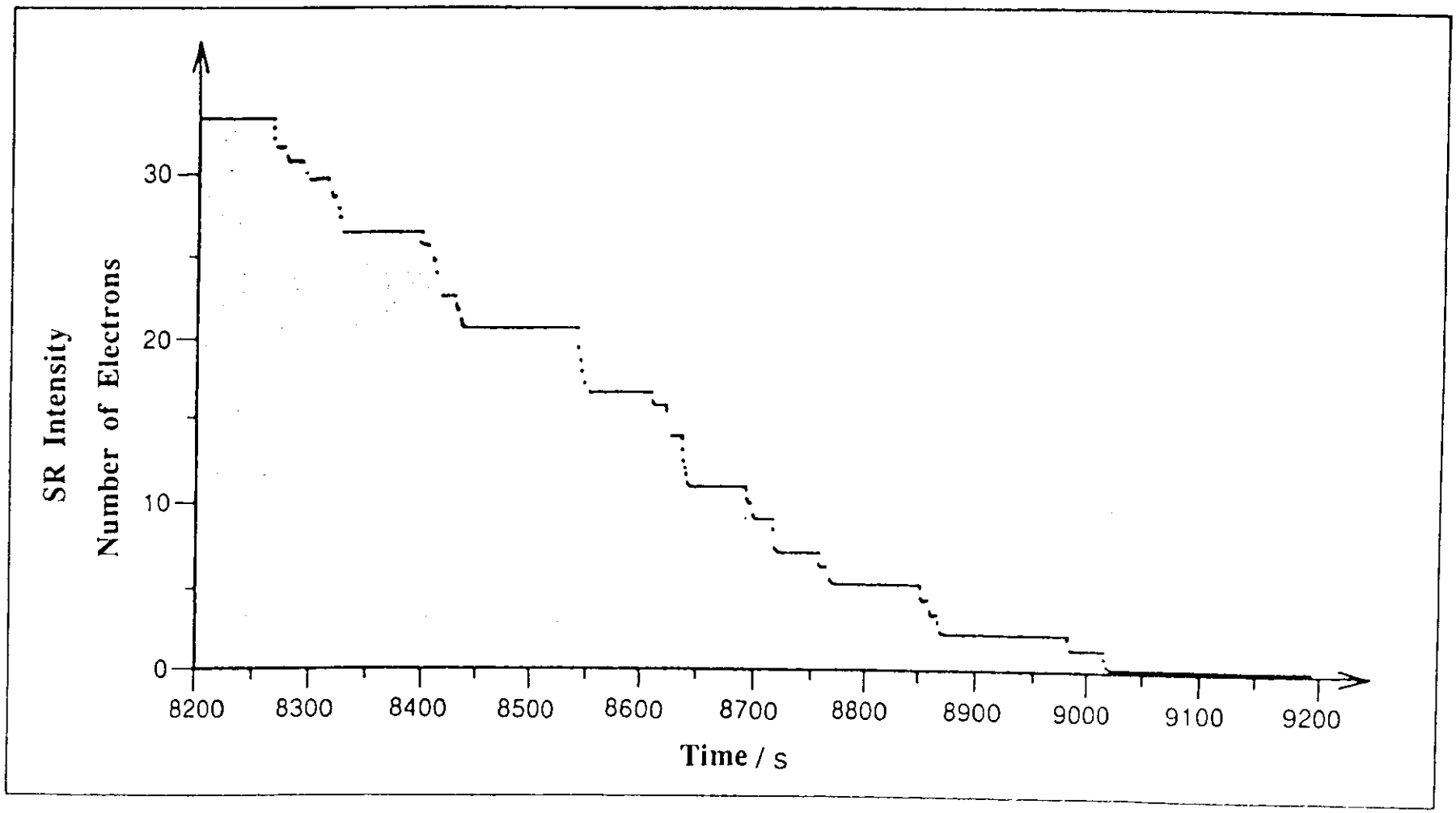

Fig. 1.0.4 SR-Sources

Dipole Magnet

Horizontal source divergence

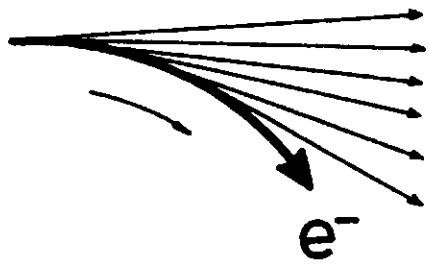

many mrad

Flux typically

$1 \cdot 10^{12}$ Photons / sec·100mA

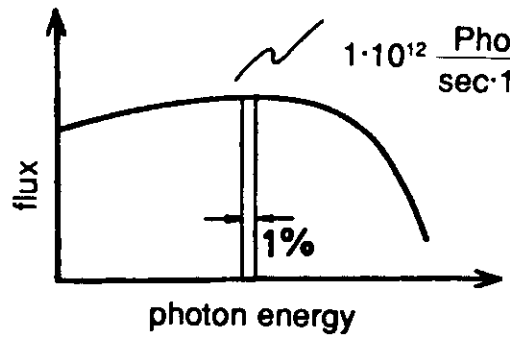

Wiggler

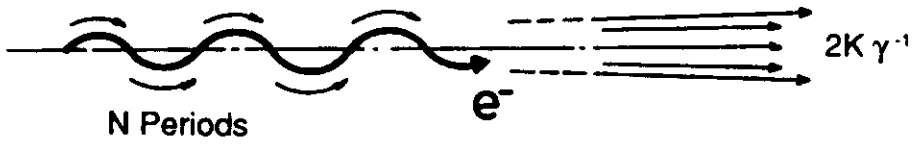

SR-collimated

Intensity 2 N times that of a dipole source with the same number of mrad

Undulator

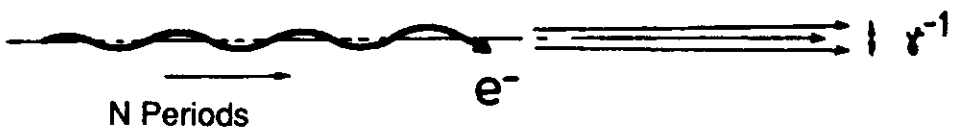

Interference effects lead to up to N^2 times the brilliance of a comparable dipole source

line spectrum

well collimated

typically

$1 \cdot 10^{15}$ Photons / sec·100mA

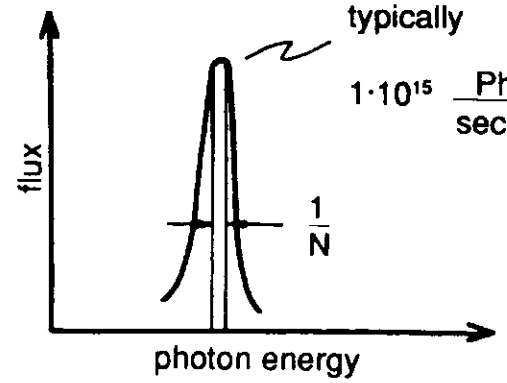

These notes are intended for those who have been intrusted with the design of the optical system which accepts SR from the source and brings it in the desired form to the experiment. We restrict ourselves to storage rings with an electron energy of 1.5-2.0 GeV and emphasize the development of high resolution monochromators for photon energies of ca. 10 - 1000 eV [1.6]. The problems associated with high energy storage rings ($E_{el} > 3$ GeV) and with hard x-ray radiation are not dealt with here. The problem of heat loading of optical elements will only be alluded to and indeed chapters 6 - 9 will be handled only in that relevant references have been provided in part 10 for the reader's convenience. Similarly, many tables and figures will be found here for which there is no corresponding text. Their relevance should be evident from their placement in the development.

The number of references in chapter 10 is an indication of how many people have been making contributions to this field. Equally important for the present endeavour have been the discussions with colleagues in the experimental and machine groups here at BESSY as well as with friends and colleagues at sister institutions around the world. Their patience and interest is most gratefully acknowledged.

We hope the information provided here is found to be useful and request the reader to make known to the author errors and suggestions for improvement.

WBP March 1992

1.1 Coupling the source to the experiment: Brightness and flux

The word "brightness" has already been mentioned several times without having been defined.

$$\text{Brightness}^* = \frac{\text{Photons/sec}}{I} \cdot \frac{1}{\sigma_x\sigma_y \cdot \sigma_x'\sigma_y' \cdot BW}$$

where I = electron current in the storage ring
$\sigma_x\sigma_y$ = the transverse extent of the electron beam
$\sigma_x'\sigma_y'$ = the solid angle into which the SR is emitted
BW = Bandwidth of the monochromator

* In Europe the term "Brilliance" is generally used for this quantity.

It is assumed here that all the above distributions are gaussian.
In general, the researcher needs a certain minimum number of photons/sec or "Flux" at his experiment. These photons will have been monochromatized to a larger or smaller extent (BW) and will be focussed down to a spot of some particular characteristics. Thus, where the researcher thinks of flux at his experiment, the beamline designer quickly discovers that the second half of the brightness equation is as important as the first half in determining the success or failure of his efforts. But the brightness equation given above is only the first link in the chain: the source. In order to optimize the coupling of the source to the experiment, the brightness of the source must be conserved, as well as possible, as the SR is reflected and dispersed in the beamline. A bad optical design, faulty optical elements or instability of the various "links" are just a few of the things which irrevocably lead to loss of brightness. Thus, in order to obtain a high flux of SR of the desired qualities at the experiment, a high brightness source and a beamline in which this brightness is conserved are required. Figure 1.1.1 illustrates the differences between a high brightness system and one with a lower brightness. Figure 1.1.2a shows the brightness expected from the planned SR-facility BESSY-II [1.6]. In addition, the flux curves for the source are shown (Fig. 1.1.2b).

Figure 1.1.1:

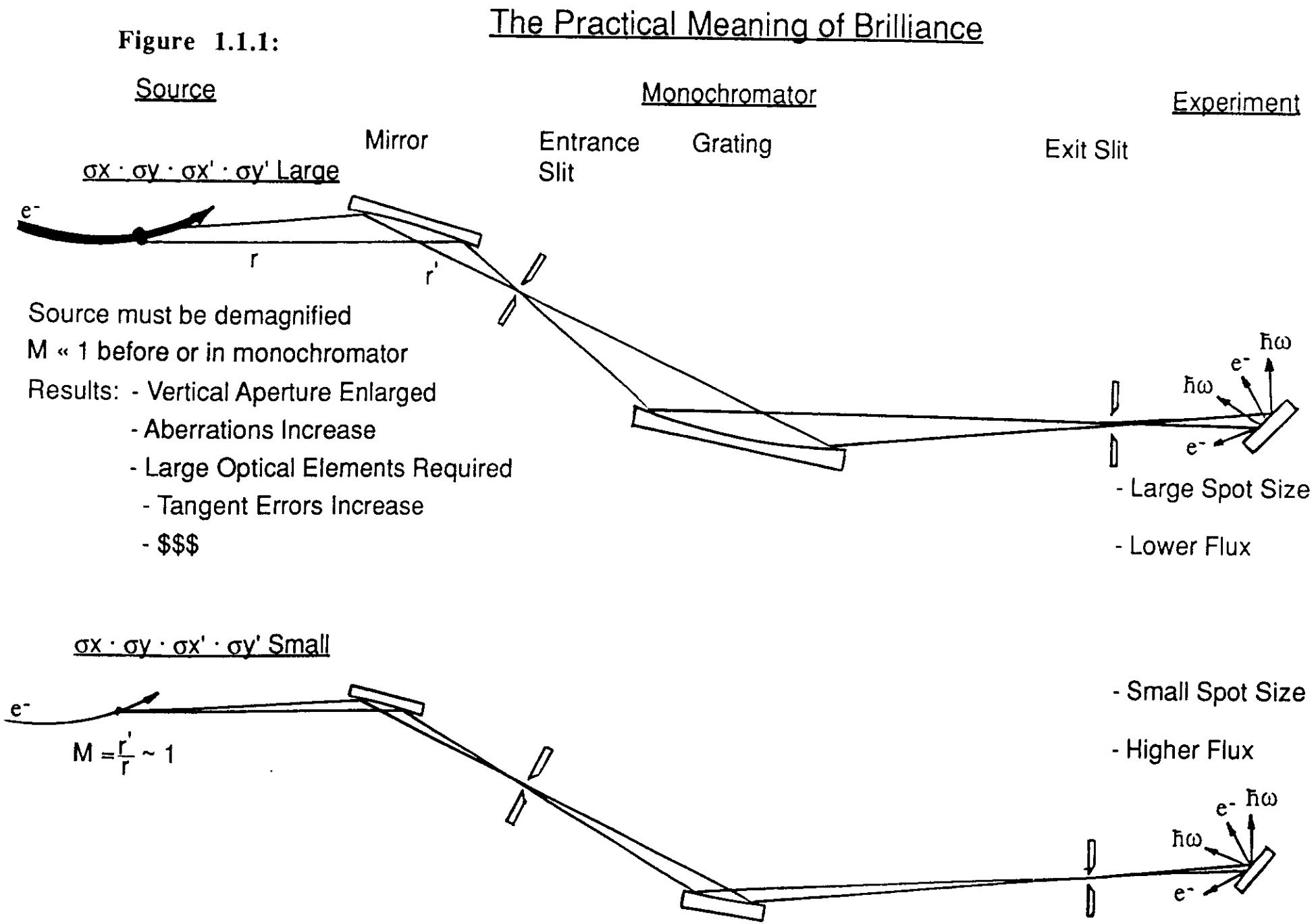
The Practical Meaning of Brilliance
Source
Monochromator
Experiment
Mirror
Entrance Slit
Grating
Exit Slit
σx · σy · σx' · σy' Large
e⁻
r
r'
Source must be demagnified
M « 1 before or in monochromator
Results: - Vertical Aperture Enlarged
- Aberrations Increase
- Large Optical Elements Required
- Tangent Errors Increase
- $$$
ħω
e⁻
ħω
e⁻
- Large Spot Size
- Lower Flux
σx · σy · σx' · σy' Small
e⁻
M = r'/r ~ 1
- Small Spot Size
- Higher Flux
e⁻
ħω
ħω
e⁻

Figure 1.1.1: The Practical Meaning of Brightness

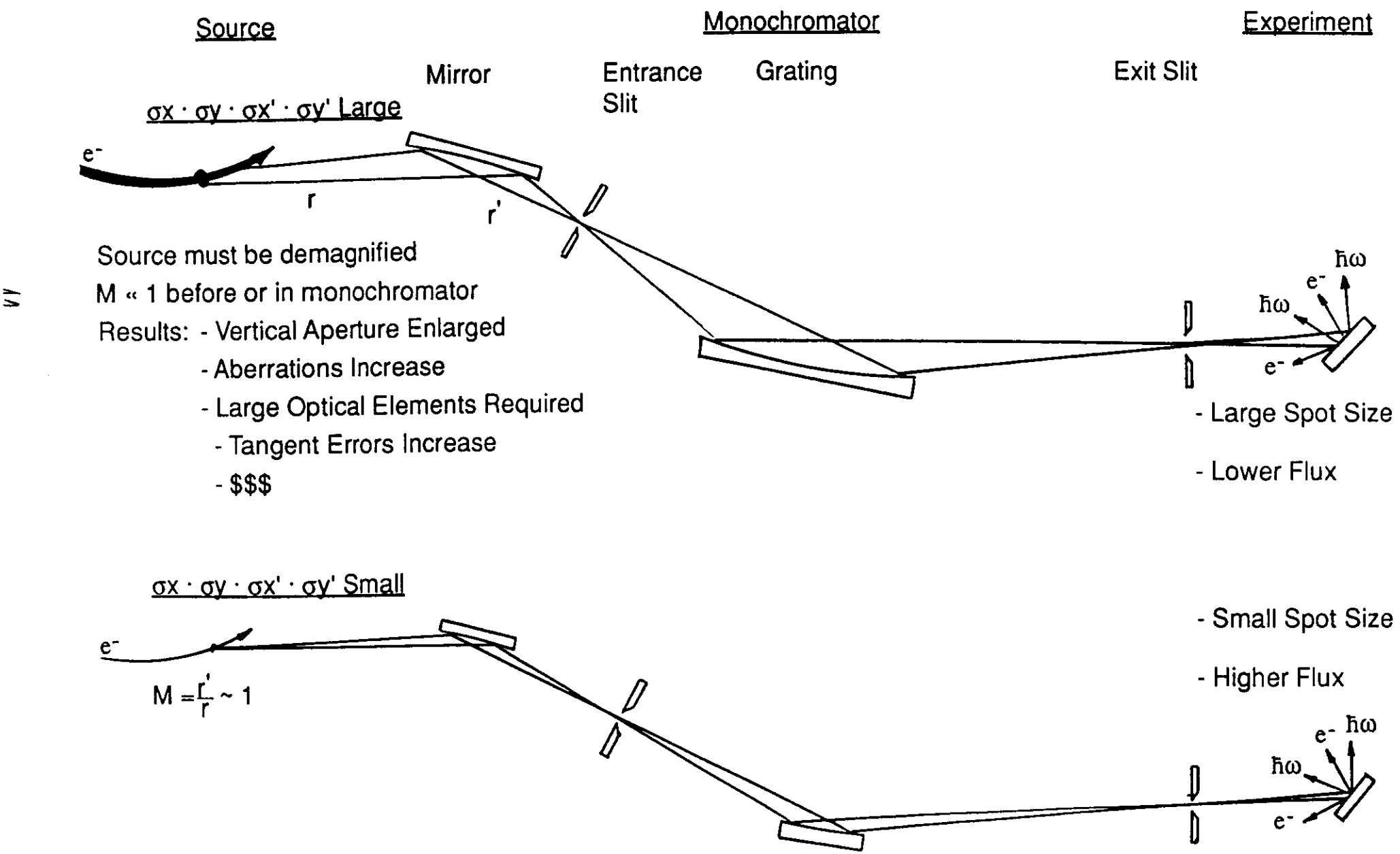

Figure 1.1.2: BESSY II: Brightness and Flux

A. Brilliance curves

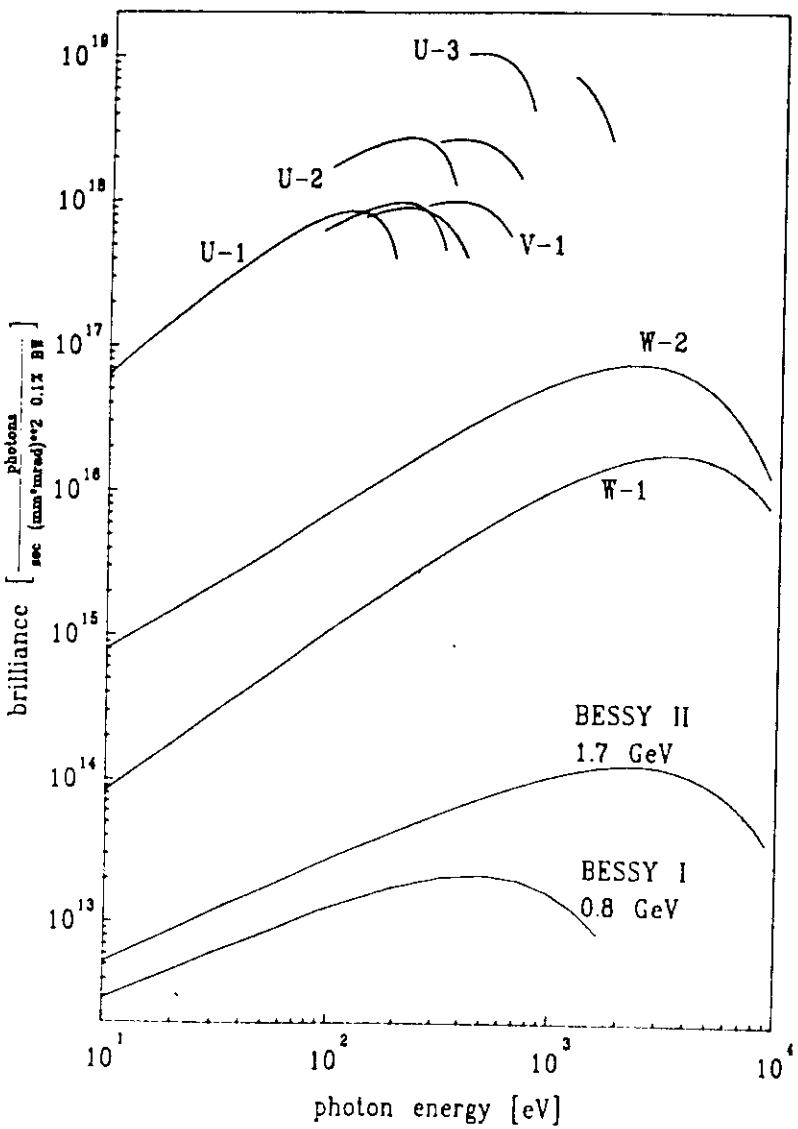

B. Flux curves

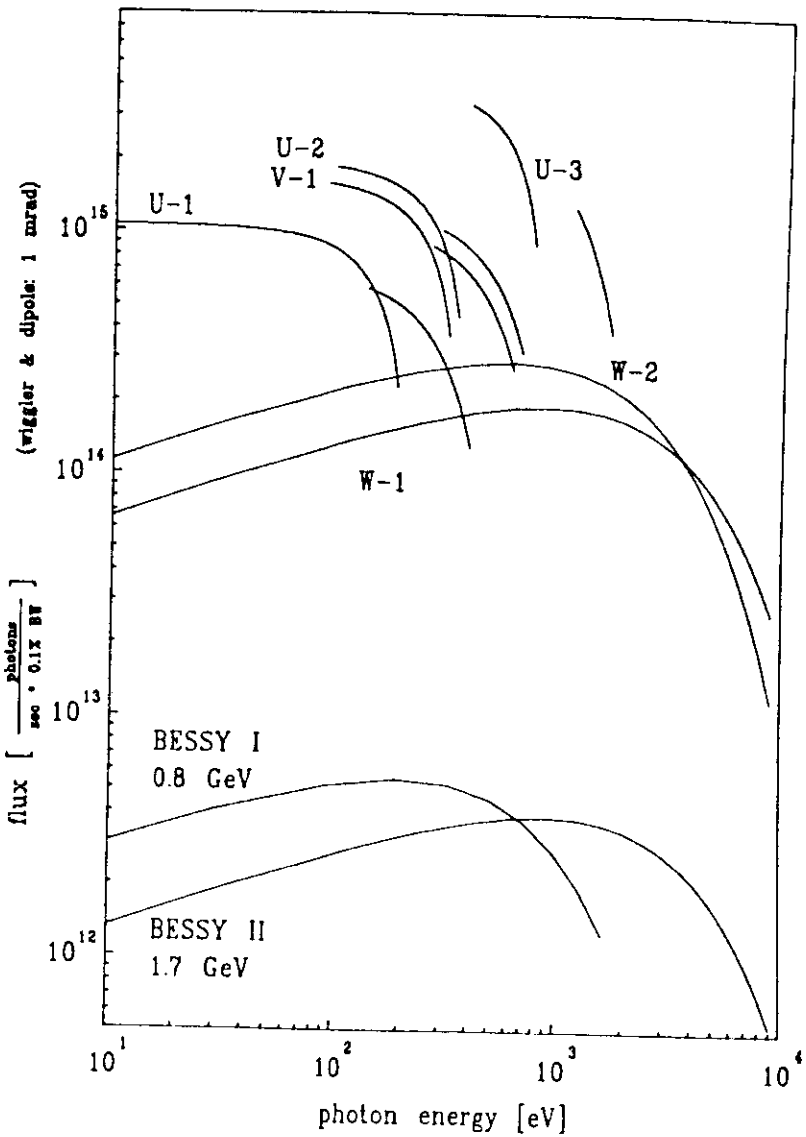

Fig. 1. (a) Brilliance curves for BESSY II (100 mA, 1.7 GeV) and BESSY I (300 mA, 0.8 GeV). (b) Flux curves for BESSY II and BESSY I as above. For complete details, see: "BESSY II, eine optimierte Undulator/Wiggler-Speicherring Lichtquelle für den VUV- und XUV-Spektralbereich."

Regardless of the source, dipole, wiggler or undulator, the vertical source size stems primarily from the horizontal emittance of the storage ring, the horizontal to vertical coupling factor and the vertical β-function and is generally much smaller than the horizontal source size, typically by a factor of between 3 and 10 (see Chapter 2). If great importance is ascribed to energy resolution (BW), then the dispersive plane of the beamline should be vertical. For this reason, we will direct our energies in particular towards conserving vertical brightness, in cases where energy resolution is to be optimized.

In order to illustrate some of the topics to be encountered in the subsequent chapers figures 1.1.3 - 1.1.4 are provided [1.7]. Figure 1.1.3 shows the spectral power distribution of undulator U-2.5 planned for BESSY-II. The total power of 130 watts corresponds to the brightness and flux curves shown in figure 1.1.2a and b. Also shown in figure 1.1.3 is the amount of power absorbed in the first two mirrors in the model beamline shown in figure 1.1.4a. For reasons to be given later (Chapter 5) the second of these mirrors is crucial for conserving vertical brightness in this beamline. Figure 1.1.4b shows schematically the deformation of this mirror resulting from the heat absorbed in it (bottom curve of figure 1.1.3). Although the subject of heat loading will not be dealt with explicitly in these "Notes", references hereto are given under chapter 8. In Table 1.1.1 one can find the various power loading relationships for wigglers and undulators: total power, maximum (axial) power/mrad(hor), maximum power/mrad^2, maximum power/mm(hor) and maximum power/mm^2. Examples of these power relationships are to be found in chapter 2 (figure 2.5.2, table 2.5.2).

Whether the deformation of optical elements is caused by heat loading as shown or by manufacturing limits (figure errors) brightness is degraded and some of the scientific potential of the high brightness source irretrievably lost. Thus, it is an exciting challenge for the designer of a beamline to keep all of the relevant parameters in mind and to optimize the entire system from the source to the experiment.

Table 1.1.1 Thermal Loading of Optical Elements by Wiggler and Undulator Radiation [1.8, 1.9]

($K = 0.934\ B_{max}\ \lambda_o$)

a) Total power

$$P(W) = 12.7\ E^2 < B^2 > L\ I$$

b) Max. power per mrad (hor)

$$P_a\ (W/mrad) = 4.33\ E^3\ B_{max}\ I\ N$$

c) Max. power per solid angle

$$P_b\ (W/mrad^2) = 5.38\ E^4\ B_{max}\ I\ N$$

d) Max. power per mm (hor)

$$P_c\ (W/mm) = \frac{P_a\ (W/mrad)}{Z}$$

e) Max. power per mm^2

$$P_d\ (W/mm^2) = \frac{P_b\ (W/mrad^2)}{Z^2}$$

E = GeV
B = T
L = cm = $N\lambda_o$
N = No. of periods
λ_o = cm
I = A
Z = m (distance from source)

Figure 1.1.3: Spectral Power Distribution of Undulator U - 2.5 [1.7]

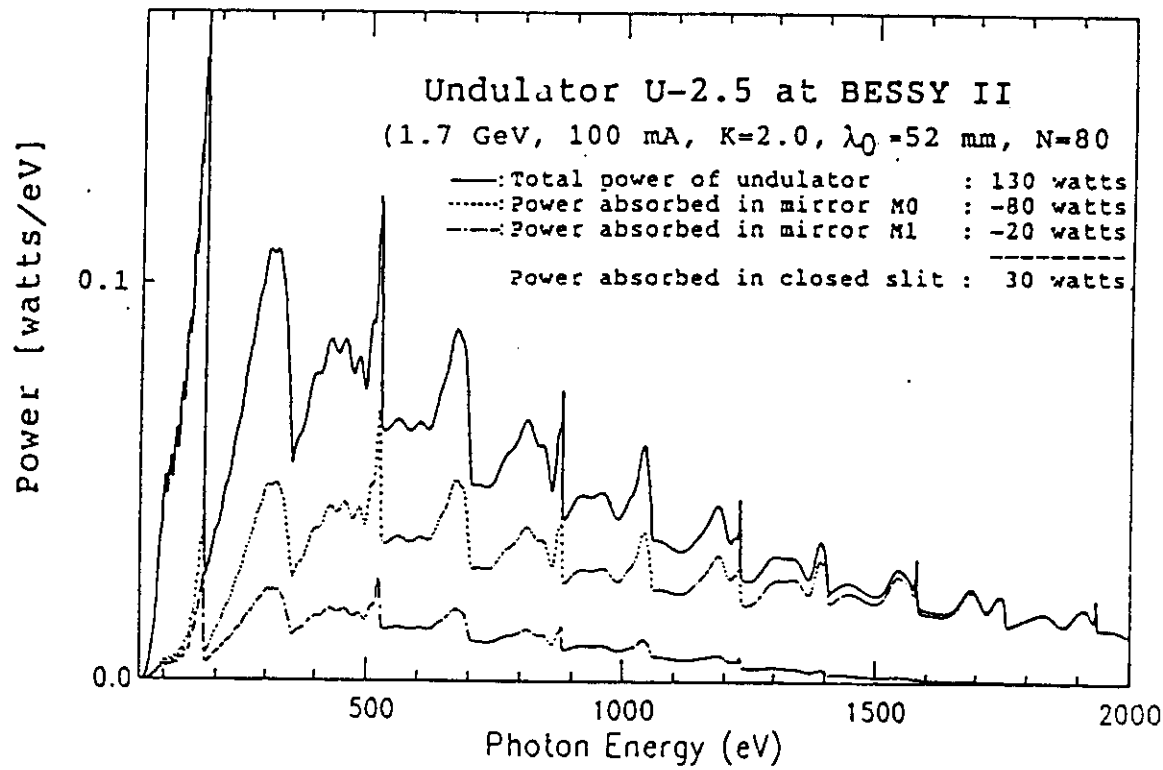

The spectral power distribution of undulator U-2.5 ($\lambda_0 = 52$ mm, N = 80) at BESSY II for 100 mA and K = 2. Also shown is the spectrum of the power absorbed in the mirror M0 and in M1.

Figure 1.1.4: Pre-Monochromator Optical System [1.7]

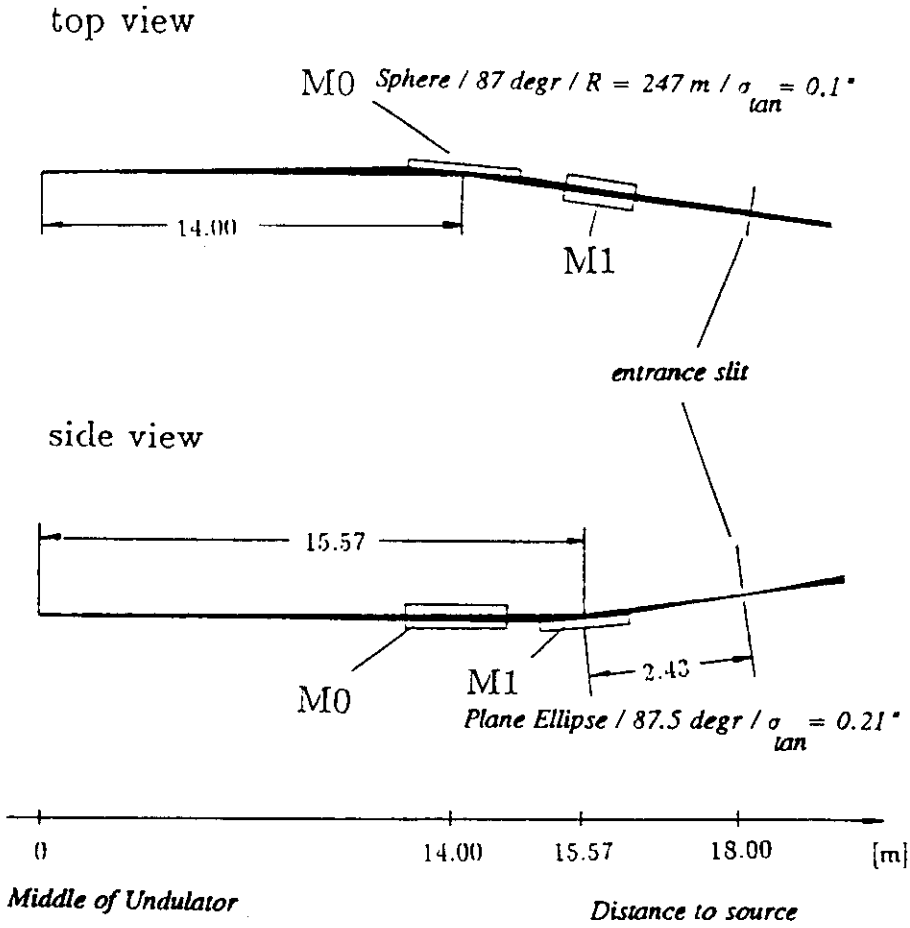

The premirror system showing the Kirkpatrick-Baez [11] arrangement used. The storage ring magnets take up most of the first 14 m of the beamline.

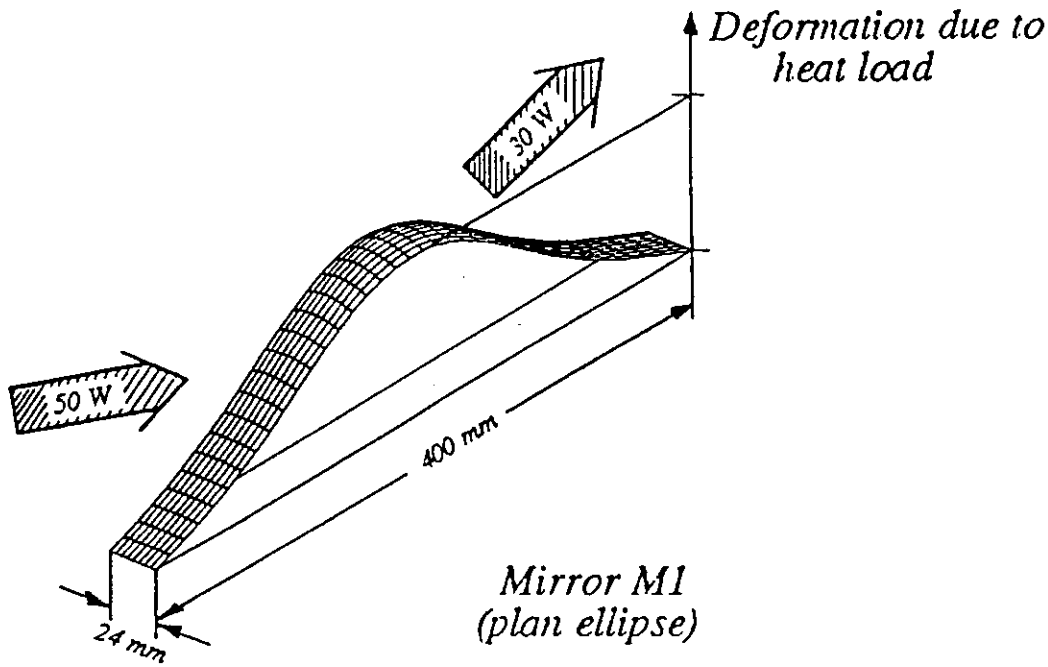

The mirror M1 showing schematically a possible effect of the 20 W of heat absorbed. The length and width shown were used for all the test cases.

1.2 Tools necessary

1.2.1 Design Tools

In order to design and optimize a beamline from the source to the experiment certain "tools" are highly desirable. With the availability of inexpensive, powerful computers along with the development and generally gratis distribution of various computer codes, one can maintain that the latter are indispensible. The amount of work required to familiarize oneself with, for example, a ray trace program is more than returned in the certainty it lends to the choice of optical elements and overall design. One cannot rely on intuition alone!

Similarly, computer codes are available which enable one to describe undulator sources in great detail and realism. Others are available to calculate the optical properties of reflectors from the optical constants. Still others will optimize the multitude of parameters in a monochromator for resolution.

Finally, it is possible to determine the effect of the power of the SR on the geometry of optical components and to develop cooling schemes to combat deformations due to heat. Such programs, called the finite element method (FEM) of analyses, are, however, much more difficult to use than the aforementioned ones and are generally available only at considerable cost.

The names and sources of several useful computer codes are given in the reference section (section 10).

1.2.2 Alignment tools

Once the components have been selected and optimized, they, their optical mounts and the vacuum vessels that house them should be examined with an eye towards aligning and adjusting them. Mirrored flats, fiducial marks, etc. can be provided by the manufacturer on mirrors and gratings in order to facilitate aligning them initially and maintaining alignment in routine operation. Windows, feedthroughs, adjustable apertures, moveable fluorescent screens, auxilliary optical components such as 90° prisms for peering into a beamline from the side should be brought into the design from the start.

The most common hardware "tools" which one employs to set up and align beamlines are the following:

Plumb line
50 m steel measuring tape
Machinists level
Vernier caliper
Red or green helium laser (low power) and adjustable tripod
Theodolyte and tripod
Levelling telescope and tripod
Autocollimator and tripod or stand
Various first surface mirrors, prisms, holders for same etc.

Other instruments are available for determining the profile and/or surface roughness of optical elements and although highly desirable are highly expensive.

1.3 Cost

The cost of a beamline varies widely, depending upon the pocketbook and the goals of the facility. There are all sorts of trade-offs one can make depending on the circumstances. Good optical components with poorly designed holders and vessels makes no sense. If the beamline is intended to be in operation with as little "down time" as possible, suitable alignment equipment and adjustments should be provided, including such things as SR position monitors. The use of optical elements which are particularly expensive and difficult to align such as ellipsoidal mirrors should be justified by the (realistic) performance expected. The attainment of high resolution demands particular expenses and complexities. Such resolution is not always required nor desirable.

Thus, cost includes not only the initial investment but also the set-up and maintainence costs as well.

1.4 Further remarks

1.4.1 Coordinate systems

There is no single generally accepted coordinate system for both storage ring geometry and optical geometry. Indeed, this statement holds for each area alone. In these notes we try to adhere to the convention that the vertical direction, i.e. perpendicular to the plane of the storage ring, is the "y" direction. In machine physics this is often designated as the "z" direction. The direction of propagation of electrons or photons is generally labled "s" by machine physicists, "r" in grating theory and in ray trace programs "z". For examples see figures 2.1.1, 4.2.1 and 5.4.1. The "right hand rule" for cartesian coordinate systems is often violated. In addition, in ray trace programs the coordinate system is usually rotated according to the deflection plane of mirrors and gratings, meridional and sagittal maintaining their designators (y or z and x respectively) throughout the optical system.

Thus, the reader being aware of this state of affairs should try to avoid being irritated or lead astray by it! One final point to this subject: in these "Notes" we try to adhere to the convention that a primed quantity refers to an angle and an unprimed quantity to a length. Thus σ' is (almost) always the standard deviation of an angle and σ that of a length. There are, however, a few exceptions, the main one being the definition of the arm lengths of an optical system, r and r' (chapters 4, 5).

1.4.2 Definition of errors

In the development presented in these "Notes", we will either (a) derive the expressions for uncertainties in terms of the Gaußian or normal error distribution or (b) assume that a given distribution obeys it. In some cases it may be clear that a particular distribution is non-Gaußian but for matters of convenience the approximation may be made that it is, without diminishing the quality of the results unacceptably. This is particularly true for ray trace calculations where some sort of distribution function is required for a realistic definition of the source, of random surface errors of mirrors and gratings, etc. In addition, the assumption of a Gaußian distribution makes the interpretation of measured or calculated data very easy: for a Gaußian distribution, the

Table 1.4.1: Some Characteristics of a Gaußian Distribution

For randomly distributed errors, the scatter of measured values of x_i about their average value, $\bar{x}$, obeys the relationship derived by Gauß:

$$P(x) = \frac{1}{\sigma\sqrt{2\pi}} e^{\frac{-(x-\bar{x})^2}{2\sigma^2}}.$$

The value of the standard deviation, σ, is determined as follows:

$$\sigma^2 = \frac{1}{n-1} \sum_{i=1}^{n} (x_i-\bar{x})^2$$

where n is the number of trials

and $\bar{x} = \frac{1}{n} \sum_{i=1}^{n} x_i$

σ^2 is known as the variance and its square root, the root mean square (r.m.s.) error or standard deviation, σ.

A plot of the distribution P(x) versus x looks like the following:

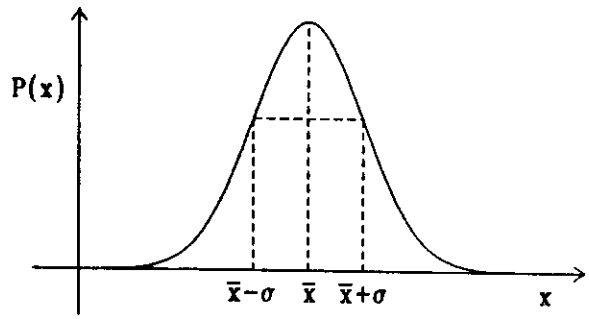

The following relationships between σ and the area under the curve are useful:

$\bar{x} \pm 1\,\sigma$	$\Rightarrow$	68.3 % of the area
$\bar{x} \pm \frac{2.35}{2}\sigma$	$\Rightarrow$	76.0 % of the area
$\bar{x} \pm 2\,\sigma$	$\Rightarrow$	95.4 % of the area
$\bar{x} \pm 3\,\sigma$	$\Rightarrow$	99.7 % of the area
$\bar{x} \pm \infty\,\sigma$	$\Rightarrow$	100 % of the area
$2.35\,\sigma$	$\Rightarrow$	Full width at half maximum of the curve (FWHM) sometimes designated as "Δ".

full width at half maximum (FWHM) is equal to 2.35 standard deviations (σ). In other cases we will be interested in the area under a distribution curve. We can utilize the fact that, again for a Gaußian distribution, 4 σ corresponds to 95 % of the area under the curve. See, for example, figures 2.5.3 a-d and tables 2.5.2 and 2.5.3 a-c. From the calculated data (figure 2.5.3 a-d) we can determine the asymptotic limit quite reliably and, taking 95 % of it, arrive at a σ value. The main characteristics of a Gaußian distribution are shown in table 1.4.1.

1.4.3 Disturbing effects of wiggler/undulator operation

The installation of a wiggler or undulator in a storage ring presents particular problems to the ring designers: the symmetry of the ring is broken, a variable perturbation of the electron optics is introduced and the coupling of the horizontal equations of motion of the electrons with the vertical ones is increased due to magnet field errors and inhomogenieties in the multipole structures. Examples of the effects of undulator operation on some characteristics of the storage ring are shown in figure 1.4.1. These were observed on the first wiggler/undulator installed at BESSY and result largely from a residual skew quadrupole component in the magnet structure leading to an increase in the vertical beam dimension with increasing K value (decreasing gap) i.e. an increased coupling factor. Similarly, the beam lifetime is reduced with decreasing gap, probably resulting from tune shifts into less stable parts of tune space. Finally, the position and angle of the electron trajectories are momentarily affected by gap changes reflecting the time constant of the feedback electronics/steerer magnet orbit correction system.

All of the above problems become more severe as K increases. This, along with the fact that the power emitted from a wiggler/undulator is proportional to K^2 suggests that an upper limit be set on K in order to set an upper limit on the problems created. Supporting this suggestion is the fact that at least 50 % of the relative contributions of the odd harmonics from 1 to 11 are achieved for K values between 0.5 and 2.0. This is shown in figure 1.4.2 in which the function $F_k(K)$ is plotted as a function of K. $F_k(K)$ is the Bessel function giving the relative contribution of the odd harmonics to central intensity of the total spectrum according to

Figure 1.4.1: Disturbing Effects of Undulator Operation on the Storage Ring [2.10]

A. Vertical beam size

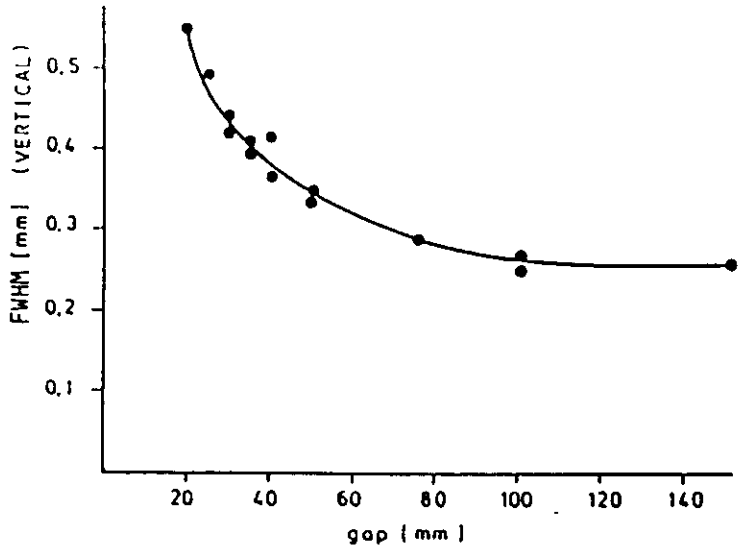

B. Beam lifetime

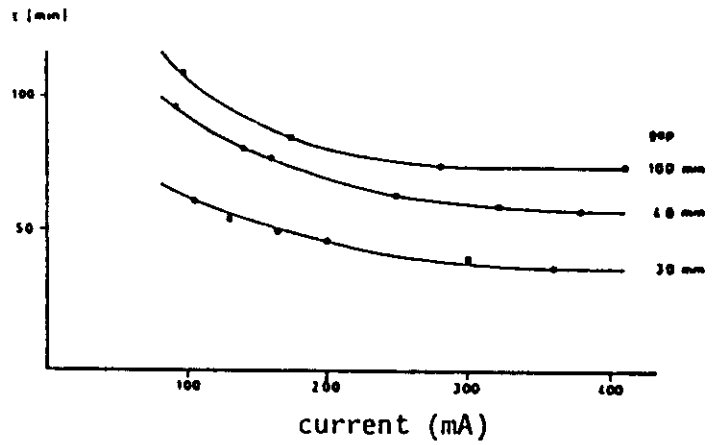

Lifetime vs. ring current for three W/U gaps

C. Beam position and angle measurements before, during, and after changing the gap.

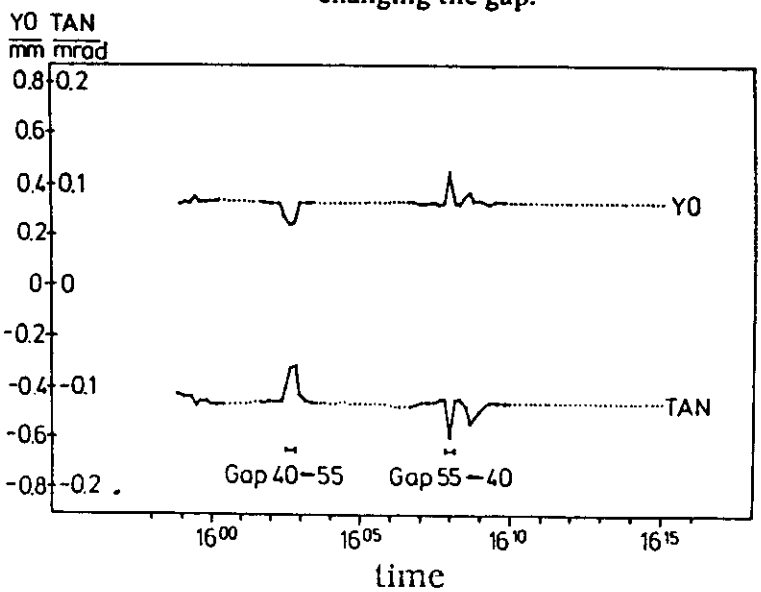

$$I_k(K) = 4.56 \times 10^6 N^2\gamma^2 I(A) F_k(K) \text{ photons/s·mrad}^2\text{·0.1 \% BW} \quad [2.1]$$

As seen in the figure, the higher the K value, the more unwanted harmonics are produced and with them unuseable power. This is also evident in measurements of the flux from an undulator as a function of K (figure 2.5.1b). In short, high K values increase the problems for the storage ring and heat loading of the optics without producing a commensurate increase in photon flux of the desired photons. An upper limit over which K can be continuously scanned combined with fixed, higher K values for which the storage ring can be tuned would appear to be a reasonable solution to the problem.

1.4.4 Spectral purity

A common problem in the VUV, soft x-ray portion of the spectrum is the transmission of higher orders of radiation by the monochromator according to the grating equation: $k\lambda = \frac{1}{N}(\sin\alpha + \sin\beta)$ (see chapter 4.2). Thus, for a given grating line density, N, and incident and diffraction angles, α and β, a family of $k\lambda$ pairs will be transmitted where k, the order of the radiation equals $\pm$ 1, $\pm$ 2, $\pm$ 3 etc. A typical spectrum from an undulator with a toroidal grating monochromator is shown in figure 1.4.3. The higher order contributions are plainly to be seen. In the visible portion of the electromagnetic spectrum these orders can be separated with the help of filters or prisms. At short wavelengths, prisms do not exist and few filters are available. The principal method of suppressing the higher order light takes advantage of the energy dependence of the reflectivity from mirrors, higher energies being reflected less well for a given angle of incidence. Thus, it is possible to design a monochromator such that the angles of incidence favor the desired wavelengths and partially suppress the undesired ones. It is also possible to build two mirror systems explicitly for the purpose of suppressing higher order light. References for this subject are given under chapter 7.

1.4.5 Thermal problems

Here we refer not to the deformation of the optical surface of a mirror or grating but rather to the change in position of a mirror or grating in the beamline or of a magnet in the storage ring itself. Figure 1.4.4 shows the

Figure 1.4.2: The Function $F_k(K)$ for Odd Harmonics of Undulator Radiation [2.1]

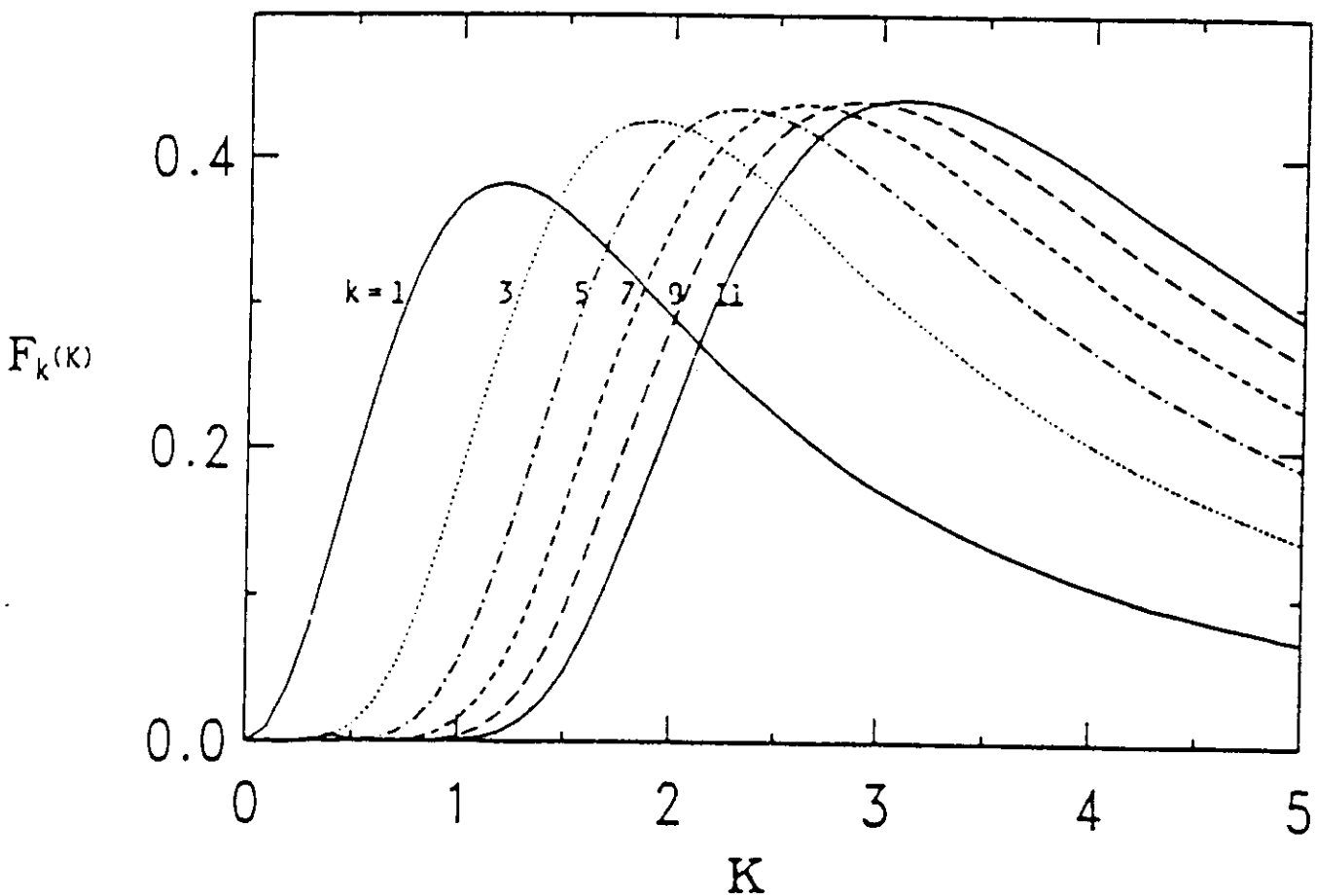

Figure 1.4.3: **Undulator Radiation: A Mixed Pleasure [2.11]**

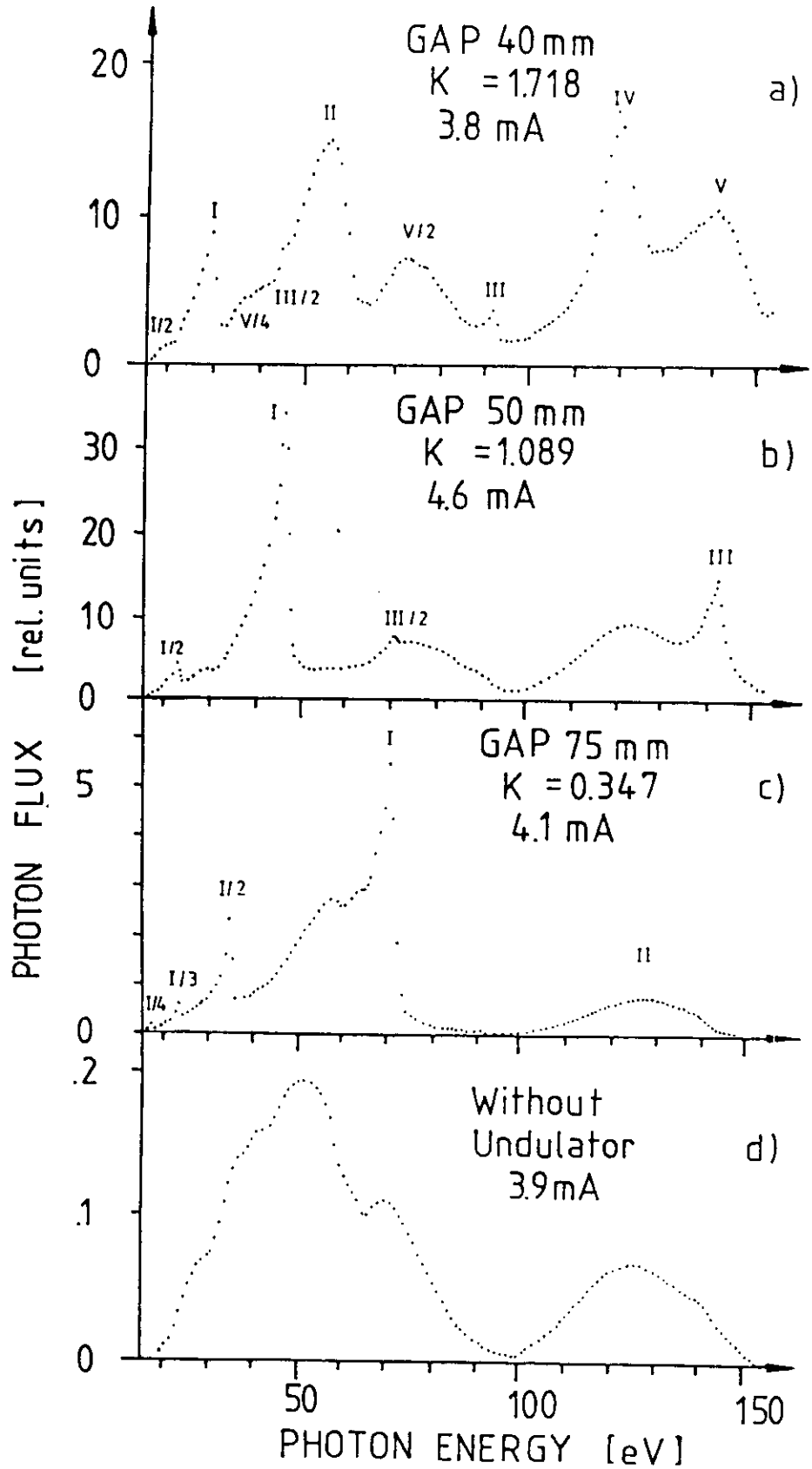

Fig. 8. Undulator spectra showing the presence of both higher harmonics (Roman numerals) and higher orders (Arabic numerals) [11]. "Without Undulator" is for a gap of 200 mm where the photon flux comes from the neighbouring dipole magnets.

measured photon intensity behind a 20 μm slit as a function of time. Also shown is the temperature of the mirror/mirror mount used to focus the SR on the slit. The unambiguous correlation between the two shows that the thermally regulated cooling water is periodically deadjusting the position of the mirror, and this despite a thermal regulation to ± 0.5° C. The period of the thermoregulator is 6.5 minutes (figure 1.4.4a). By putting a buffer reservoir in the cooling line before the water reaches the mirror, the water of 18°C ± 0.5°C is mixed producing a stable 18° ± 0.05°C or better regulation (figure 1.4.4b).

Similarly, the water cooling of magnets and consequently, of their support frames, can produce similar effects (figure 1.4.5). In these figures the position of the electron beam in a dipole magnet and the direction of the radiation emitted are shown as a function of time as measured with a SR-monitor system similar to that shown in figure 2.6.1. In the expanded scale of figure 1.4.5b one can clearly see the thermal cycle of the cooling water - with a period of about 3.3 minutes. In this case, the thermal "print through", although apparent, is harmless, being about 1 μrad peak to peak.

Figure 1.4.4: **Temperature Stability: Mirror Cooling**

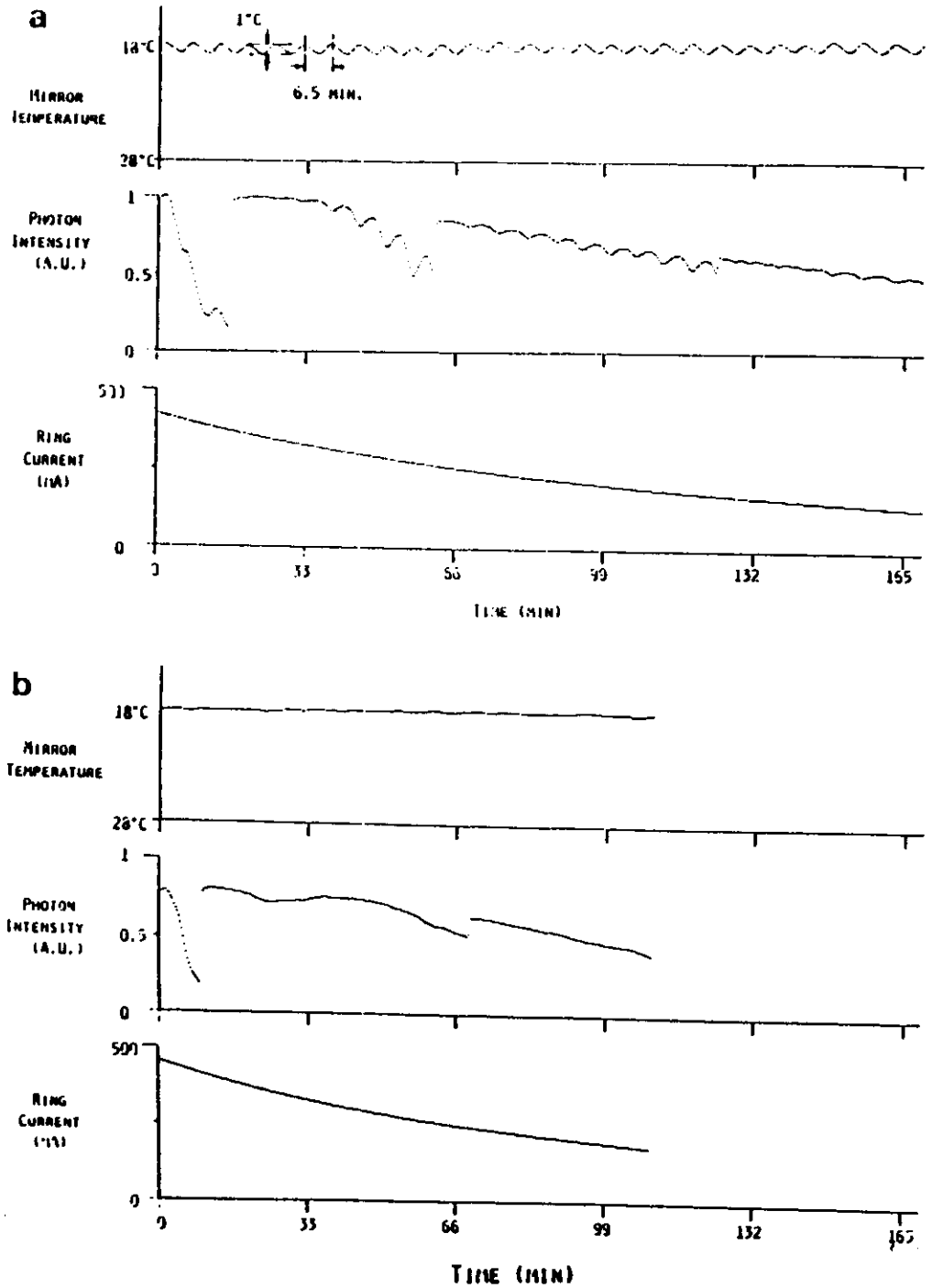

The variation in intensity through a 20 μm slit compared with the temperature of the focussing mirror used to illuminate it.

Cooling water regulated to (a) $\pm 0.5\,^{\circ}$C and (b) $< \pm 0.05\,^{\circ}$C, respectively.

Figure 1.4.5: Temperature Stability: Magnet Cooling

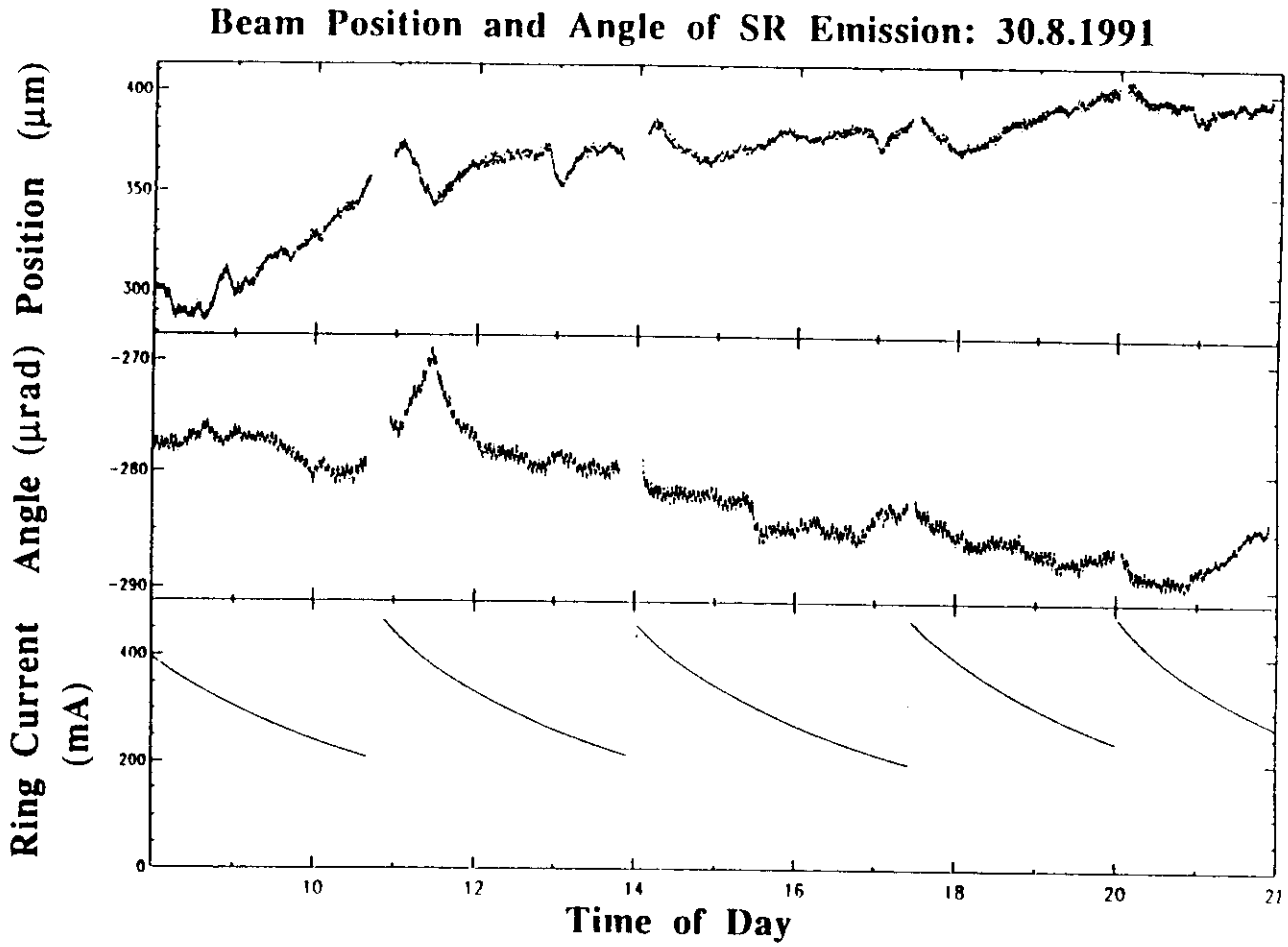

a) 8 Am - 10 PM

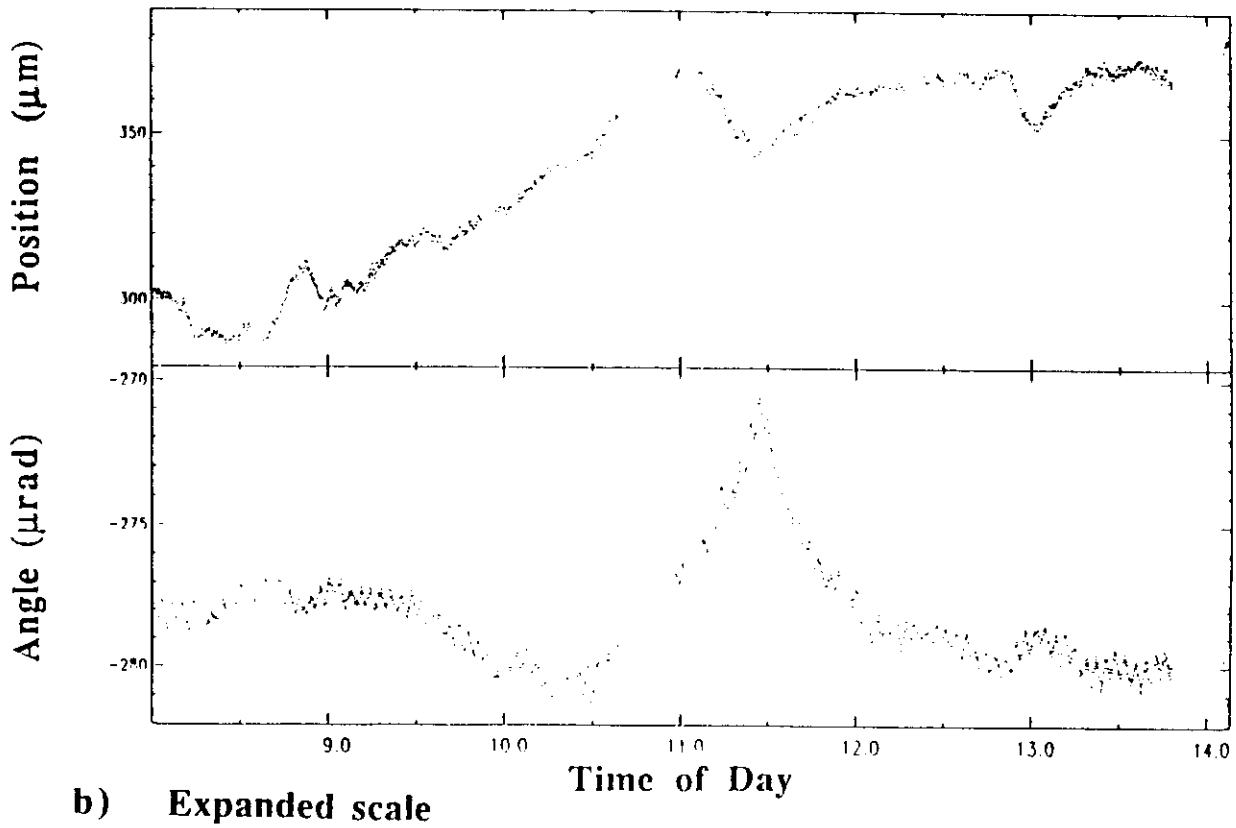

b) Expanded scale

2. SR-Source Characteristics

As seen in chapter 1, one of the primary advantages of SR is its inherent high brightness. The high brightness results from both the large flux of photons produced and from the small lateral size of the source and the fact that the electron acceleration vectors are projected into a small solid angle in the forward direction. The latter two quantities are expressed by the "emittance" of the storage ring and is an invariant of the storage ring and its operating parameters:

Emittance = $\varepsilon = \sigma_{el}\,\sigma_{el}'$

where σ_{el} = lateral extent of the electron beam

σ_{el}' = solid angle of the electron trajectories around the ideal trajectory.

With the help of the machine parameters it is easily possible to calculate σ_{el} and σ_{el}' as shown in this chapter. Since the two orthogonal lateral directions, x, in the plane of the ring, and y, perpendicular to it, are only weakly coupled it is useful to define a horizontal emittance, ε_x, and a vertical emittance, ε_y. Thus,

$$\varepsilon_y = C \cdot \varepsilon_x$$

where C corresponds to the coupling factor, also an invarient of the system. For storage rings designed explicity for the production of SR this coupling factor ranges between 0.01 and 0.1, and is a function primarily of the "goodness" of the alignment of the magnet fields in the ring. With perfect separation and alignment the coupling factor would be zero. The main contribution to misalignment comes from residual "skew-quadrupole" fields, expecially in insertion devices (I.D.'s): wigglers and undulators. Nevertheless, the vertical emittance can be kept much smaller than that in the ring plane making the vertical plane the logical one for dispersion in monochromators.

The definition of σ_{el}' given above should warn one that the definition of the radiation source is perhaps not so simple after all: for the design of the optical system, one needs the solid angle into which the photons are emitted. That may be quite different from σ_{el}'! We will define this

quantity simply by σ_{HSR}' and σ_{VSR}' where the latter is of prime importance for us.

Thus, σ_{VSR}' = r.m.s. solid angle in the vertical direction into which the SR is emitted.

With this in mind, we give in the following pages the relevant parameters and formulas for calculating or otherwise obtaining σ_x, σ_y, σ_{HSR}' and σ_{VSR}' necessary for obtaining the optical characteristics of a beamline. These parameters are essential as the starting point for a quantitative examination of the optical characteristics of a beamline using ray traces.

2.1 Electron Beam

The lateral dimensions of the electron beam, σ_x and σ_y, and the angular deviation of the individual electrons from the ideal orbit σ_x' and σ_y' vary along the orbit in the ring. To determine them a knowledge of the Twiss parameters, $\alpha(s)$, $\beta(s)$ and $\gamma(s)$ as well as of the emittance, ε, the coupling factor, C, the dispersion, $\eta(s)$, and the momentum or energy spread, $\frac{\delta p}{p_o}$ or $\frac{\delta E}{E_o}$ respectively is required. The coupling factor mentioned above relates the vertical emittance to the horizontal and usually lies between 0.01 and 0.1. Similarly, the vertical dispersion is coupled to that in the horizontal plane and can only be determined on an operating ring. This latter coupling is not independent of "s".

The Twiss parameters are defined as follows:

$\beta_x(s)$, $\beta_y(s)$ = horizontal and vertical betatron functions

$$\alpha_x(s) = -\frac{1}{2}\frac{d\beta_x(s)}{ds} \quad ; \alpha_y(s) = -\frac{1}{2}\frac{d\beta_y(s)}{ds}$$

$$\gamma_x(s) = \frac{1 + \alpha_x(s)^2}{\beta_x(s)} \quad ; \gamma_y(s) = \frac{1 + \alpha_y(s)^2}{\beta_y(s)}$$

The betatron functions reflect the focussing characteristics of the magnet lattice and are generally available for a given ring in the form shown in

figure 2.1.1. As seen there they are relatively constant in the straight sections but can vary strongly in the dipole magnets. The horizontal dispersion, $\eta_x(s)$, is also shown in figure 2.1.1.

The values of the electron beam characteristics are obtained from the following relationships:

$$\sigma_x(s) = \sqrt{\varepsilon_x \, \beta_x(s) + \left[\eta_x(s) \left(\frac{\delta p}{p_o}\right)\right]^2}$$

$$\sigma_x'(s) = \sqrt{\varepsilon_x \, \gamma_x(s) + \left[\eta_x'(s) \left(\frac{\delta p}{p_o}\right)\right]^2}$$

and analogous expressions for $\sigma_y(s)$, $\sigma_y'(s)$.

Based on the experiences won on storage rings of the second generation, it is possible to make some assumptions which simplify the calculations [1.6b, 2.8]:

$C \approx 0.04$

$\eta_y(s) \approx 0, \eta_y'(s) \approx 0$

$\frac{\delta p}{p_o} \approx 3 \times 10^{-3}$ for normal multibunch operation. For very low currents it can be much smaller: $\approx 5 \times 10^{-4}$ [2.9].

2.1.1 Electron beam characteristics in the straight sections

In the straight sections of the storage ring (fig. 2.1.1)

$\eta_x(s) = \eta_x'(s) = 0, \eta_y(s) = \eta_y'(s) = 0$ (general design goal)

$\alpha_x(s) \approx 0 \, , \alpha_y(s) \approx 0$ (exactly true only at center of straight)

$\gamma_x(s) = \frac{1}{\beta_x(s)}$; $\gamma_y(s) = \frac{1}{\beta_y(s)}$

Figure 2.1.1: **Beta Function and Dispersion for the Proposed BESSY II TBA 10 Lattice [1.6 b]**

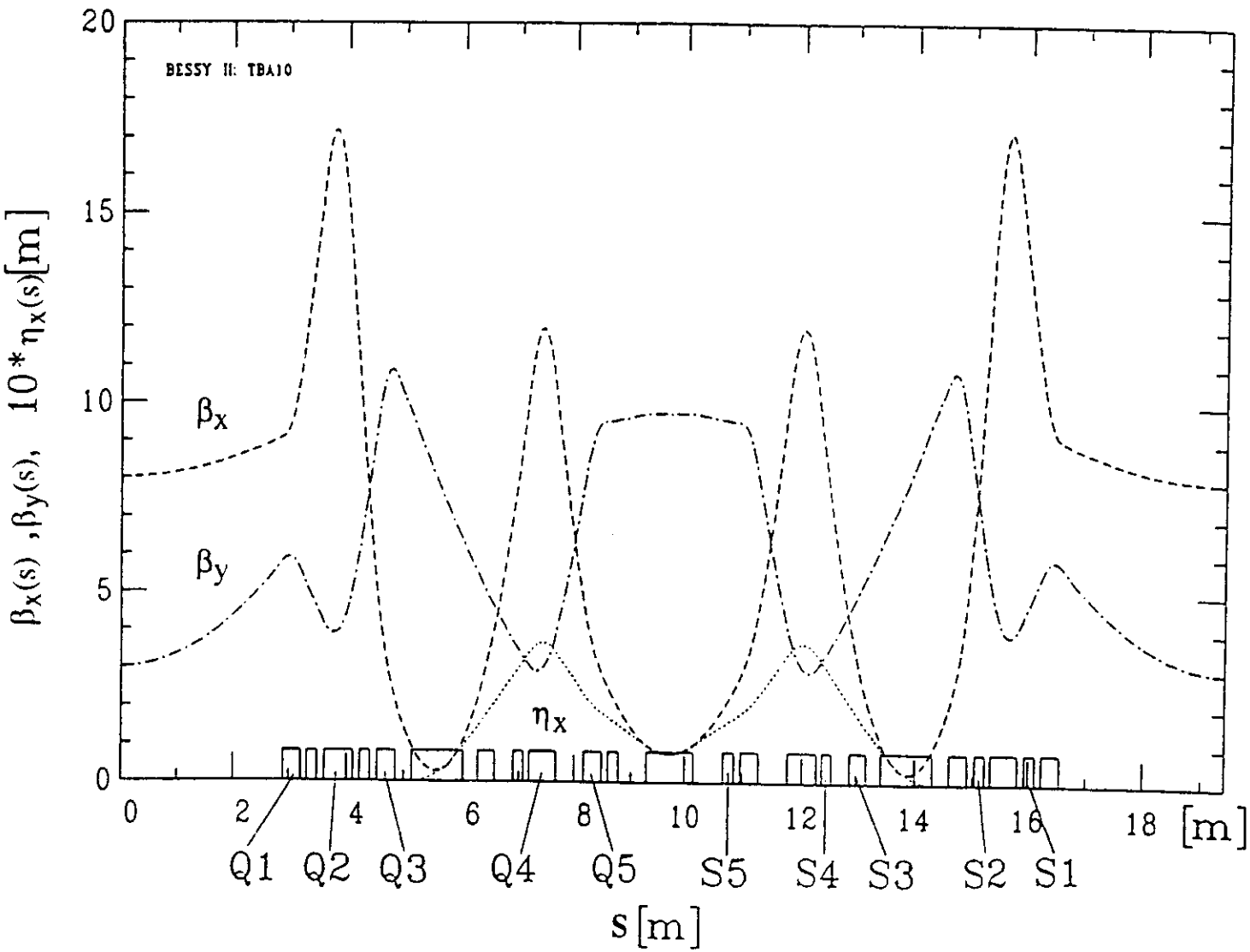

and finally

$$\sigma_x(s) = \sqrt{\varepsilon_x \beta_x(s)} \quad ; \sigma_x'(s) \approx \sqrt{\frac{\varepsilon_x}{\beta_x(s)}}$$

$$\sigma_y(s) = \sqrt{\varepsilon_y \beta_y(s)} \quad ; \sigma_y'(s) \approx \sqrt{\frac{\varepsilon_y}{\beta_y(s)}}$$

For long undulators, that is for undulators that essentially take up the full length of the straight section, the parabolic form of the betatron functions should be taken into consideration i.e. α_x and α_y can deviate significantly from zero.

2.1.2 Electron beam characteristics in the dipole magnets

As seen in figure 2.1.1, the betatron functions and the horizontal dispersion vary strongly with "s" in the curved sections of the storage ring. For an accurate calculation of the electron beam characteristics all the Twiss parameters must be evaluated and the full formulas used. Also to be seen in figure 2.1.1 is the fact that the β_x values may well exhibit a minimum in the middle of a dipole magnet making $\alpha_x \equiv 0$ at that point while just before or after the middle point, 6° for the lattice shown, α_x becomes very significant, characteristic of strongly focussed storage ring lattices. In order to examine the variation of the various Twiss parameters with "s" and their effect on the electron beam characteristics, we have tabulated them in table 2.1.1 for four points in the storage ring [1.6b]. Also shown for all four points are the results obtained using only the emittance and the betatron function for the calculations.

As will be seen in the ensuing sections, the σ_x, σ_y values obtained here are the relevant ones for ray trace calculations while the σ_x' and σ_y' values are often considerably smaller than the corresponding σ_{HSR}' and σ_{VSR}' values in which case they can be neglected. Their relative magnitudes must be examined case for case.

Table 2.1.1 Calculation of the Electron Beam Characteristics at Different Points in the Ring+

Location	i	β_i(m)	α_i	γ_i(m^{-1})	η_i(m)	η_i'	Exact σ_i(mm)	Exact σ_i'(mrad)	Approximate* σ_i(mm)	Approximate* σ_i'(mrad)
Middle of straight	x	8	0	1/8	0	0	0.219	0.027	0.219	0.027
	y	3	0	1/3	0	0	0.027	0.009	0.027	0.009
Middle (6°) of Dipoles 1 + 3	x	0.25	0	1/0.25	0.024	0.088	0.082	0.306	0.039	0.155
	y	7.9	+1.8	1/1.9	-	-	0.044	0.011	0.044	0.006
Middle (6°) of Dipole 2	x	0.78	0	1/0.78	0.078	0	0.243	0.088	0.068	0.088
	y	9.6	0	1/9.6	-	-	0.048	0.005	0.048	0.005
9° in Dipole 1	x	0.56	-0.94	1/0.30	0.056	0.19	0.178	0.587	0.058	0.104
	y	7.0	+1.7	1/1.8	-	-	0.041	0.012	0.041	0.006

+ For $\varepsilon = \varepsilon_x = 6 \times 10^{-9}$ m·rad; C = 0.04, $\eta_y = 0$, $\delta p/p_o = 3 \times 10^{-3}$ and data of Fig. 2.1.1 [1.6b]

* Approximately: $\sigma_i(s) = \sqrt{\varepsilon_i \beta_i(s)}$; $\sigma_i'(s) = \sqrt{\varepsilon_i/\beta_i(s)}$; i = x, y

2.2 Dipole Magnet

a) Vertical opening angle of the radiation [2.1]

$$\sigma'_{VSR}\,(\text{mrad}) = \frac{570}{\gamma}\left(\frac{\lambda}{\lambda_c}\right)^{0.43}$$

$$\text{for} \quad 0.2 < \frac{\lambda}{\lambda_c} < 100$$

$$\lambda_c\,(\text{Å}) = 5.59\,\rho/E^3 = 186/BE^2$$

$$\gamma = 1957\,E$$

$$\rho\,(\text{m}) = 33.35\,E/B$$

E = GeV
B = kG
ρ = m
I = Amp

b) Horizontal opening angle of the radiation, θ_{HSR}, is defined by the geometry of front end, and can be up to 100 mrad and more. This is not an r.m.s. quantity and is hence defined as θ instead of σ.

c) Electron beam dimensions: see section 2.1.2

Typical values of electron beam characteristics are given in table 2.1.1 for BESSY II.

d) Power emitted (total) (kW) $= 88.5\,IE^4/\rho$
$= 2.65\,E^3IB$

e) Power (Watt/s·mrad·1 % BW) $= 5.95 \times 10^{-15}\left(\frac{\gamma^4 I}{\rho}\right) G_2$ watt/s

The function G_2 is shown in figure 2.2.1a [2.1].

Figure 2.2.1: Functions G_2 ($\lambda/\lambda c$) and F ($\lambda/\lambda c$) [2.1]

S. Krinsky et al.

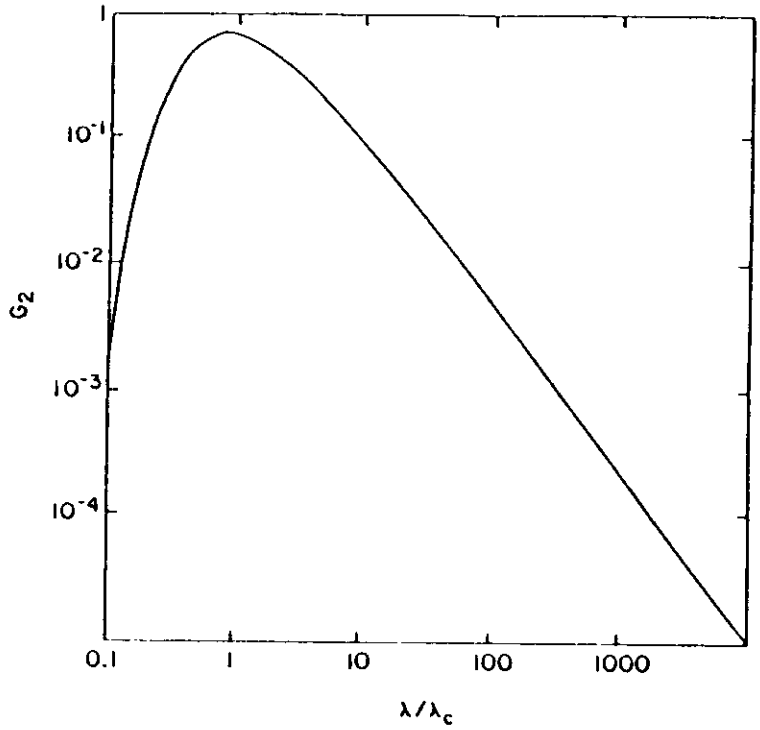

a) Function $G_2(\lambda/\lambda_c)$ of eq. (9) for the radiated power.

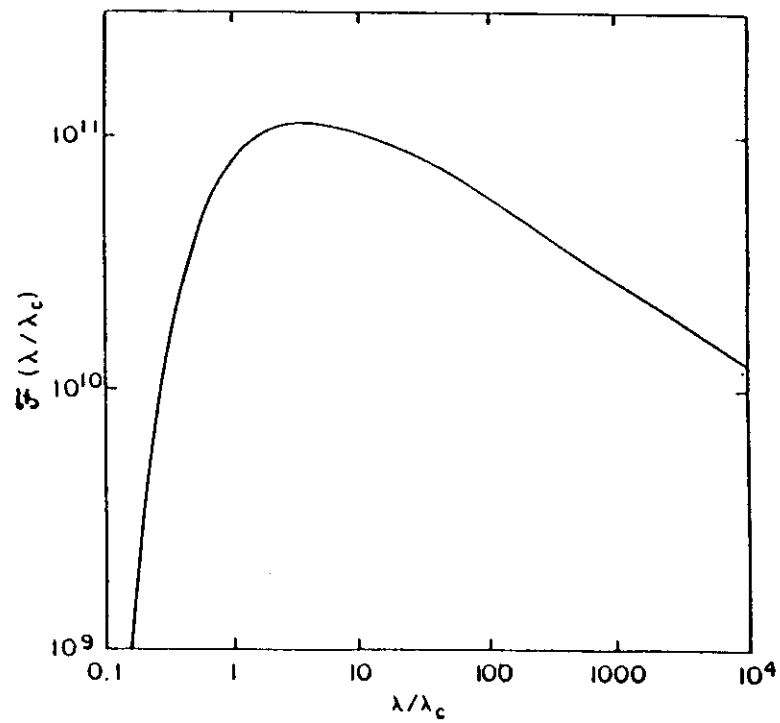

b) Function $\mathcal{F}(\lambda/\lambda_c)$ of eq. (11) for the photon flux integrated over all vertical angles ψ.

$$G_2 \equiv \left(\frac{\lambda_c}{\lambda}\right)^2 \int_{\frac{\lambda c}{\lambda}}^{\infty} K_{5/3}(\eta)\, d\eta \quad ; \quad G_{max} \cong \frac{2}{3}\lambda_c$$

f) Flux distribution (Photon/mrad·1 % BW)

$N = \gamma I F(\lambda/\lambda c)$ where $F(\lambda/\lambda c)$ is shown in figure 2.2.1b [2.1].

g) Polarisation:
Plane polarisation: see figures 2.2.2a, b
Circular polarisation: see figure 2.2.2c

2.3 Wavelength shifter (3 poles)

Similar to a dipole magnet with the corresponding

B or ρ (see 2.2 above)

2.4 Multipole wiggler (N = No. of periods)

see figure 2.4.1

Magnet field strength parameter, K

$$K = \delta\gamma = 0.934\, B\, \lambda_o$$

B = T
λ_o = cm
δ = Deflection angle of the electron path to the closed orbit.
γ = 1957 E [GeV]

a) Vertical opening angle of the radiation

$\sigma'_V = [\sigma'^2_y + \sigma'^2_{VSR}(Dipole)]^{1/2}$ see 2.2 a) and c) above

b) Horizontal opening angle of the radiation

Figure 2.2.2: Polarization Characteristics of SR

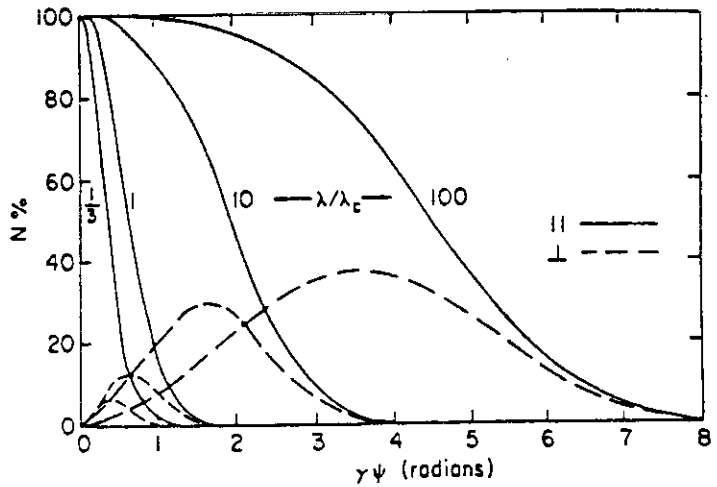

Fig. 3. Dependence on the vertical angle ψ of the intensities of the parallel (solid line) and perpendicular (dashed line) polarization components of the photon flux. The individual curves, plotted for $\lambda/\lambda_c = \frac{1}{3}$, 1, 10, and 100, are individually normalized to the intensity in the orbital plane ($\psi = 0$) at the respective λ/λ_c value. Note that the abscissa, ψ multiplied by the electron energy γ, makes these curves universal. **[2.1]**

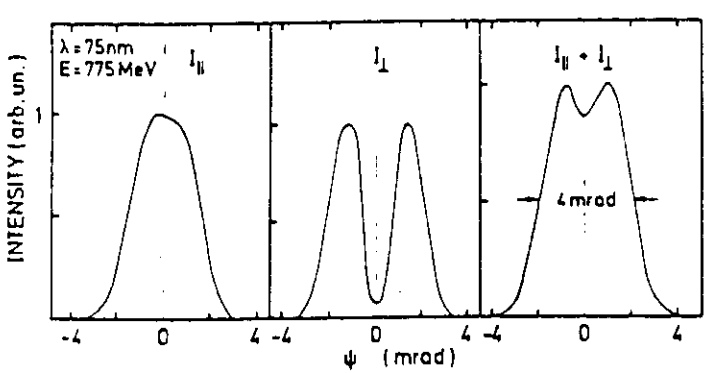

FIG. 9. Relative azimuthal intensity of the components, linearly polarized parallel and perpendicular with respect to the storage ring plane, and their sum measured at 75 nm. **[2.9]**

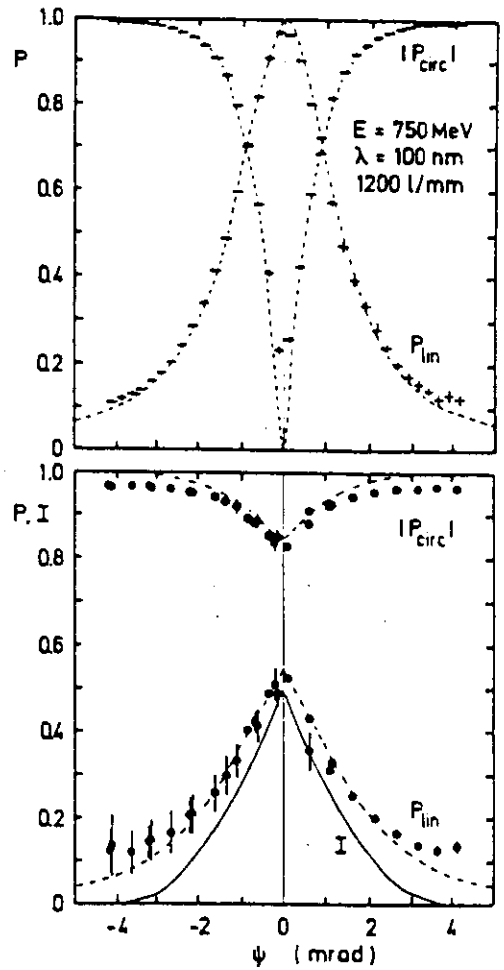

FIG. 10. Azimuthal dependence of the degree of the linear and circular polarization of 100-nm radiation. (a) Differential measurement with a vertical opening of 0.25 mrad (horizontal error bar).[37] (b) integral measurement with a slit from ψ to $\pm$ 5 mrad (error bars).[37] Full curve: ratio of the corresponding measured intensity of the radiation to the total radiation from $-$ 5 to $+$ 5 mrad. The dashed curves indicate the calculated polarization of the incident beam. **[2.9]**

Figure 2.4.1: Layout of a Wiggler, Undulator

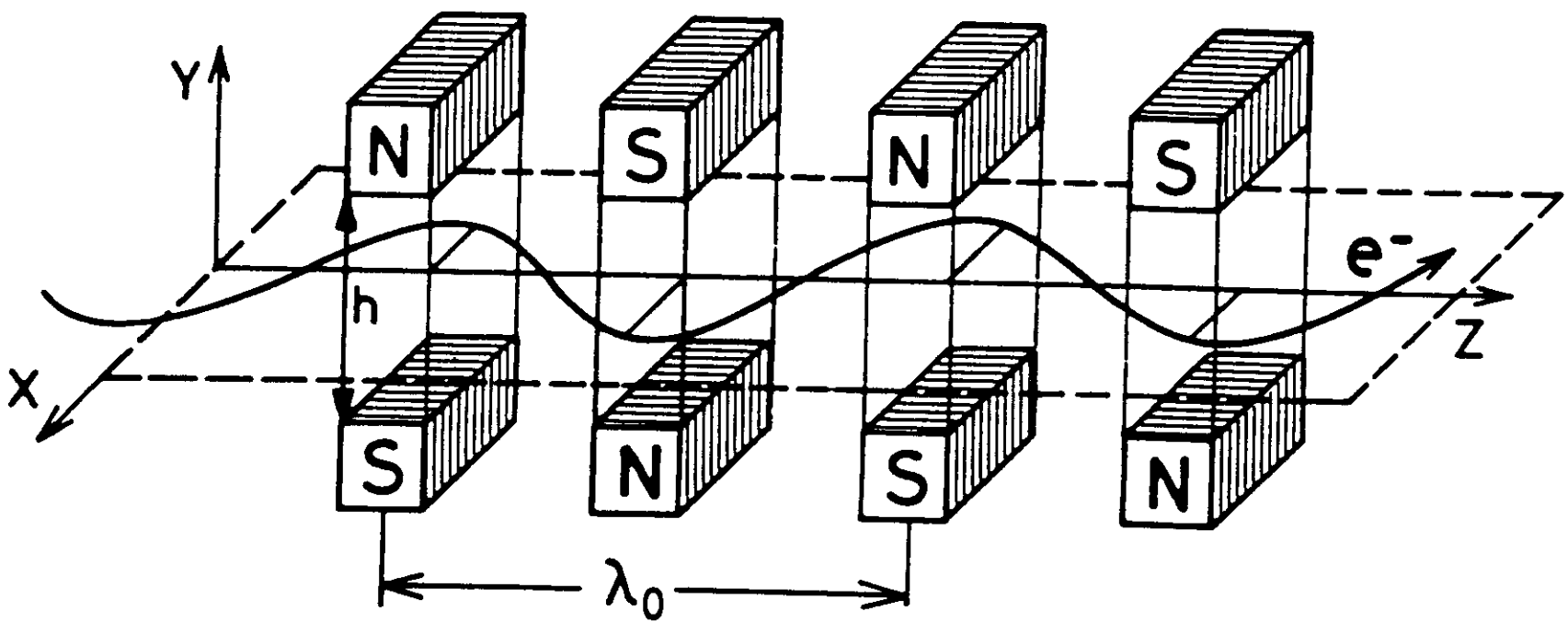

$$\sigma'_{HSR} \cong K/\gamma = \frac{0.934\ B\lambda_o}{\gamma}$$

c) Vertical source size [2.13]

$$\sigma_{vert} = \left[\sigma_y^2 + \left(\frac{\sigma_y'^2}{3} + \frac{\Delta\theta^2}{9} \right) \left(\frac{L}{2} \right)^2 \right]^{1/2}$$

$$L(cm) = N\ \lambda_o$$

and $\Delta\theta$ = the half opening angle of the optical system.

(Optimally $\frac{L\sigma'_R}{2} \leq \sigma_y$ and $\frac{L}{2} \geq \beta_y$, see 2.2 c)

d) Horizontal source size (zero dispersion [2.13])

$$\sigma_{hor} = \left[\sigma_x^2 + x_o^2 + \left(\frac{\sigma_x'^2}{3} + \frac{\Delta\theta^2}{9} \right) \left(\frac{L}{2} \right)^2 \right]^{1/2}$$

where $\Delta\theta$ = the half opening angle of the optical system

and $x_o = \frac{K}{\gamma} \cdot \frac{\lambda_o}{2\pi}$ (see "e" below)

e) Separation, $2x_o$, between the transverse source points:

where $x_o = \frac{K}{\gamma} \frac{\lambda_o}{2\pi}$

f) Total power

$$P_{tot}\,(W) \approx 1.9 \times 10^{-6}\ N\gamma^2 K^2 I/\lambda_o$$

$$\text{or } P_{tot}\,(W) = 12.7\ E^2 < B^2 > LI$$

2.5 Undulator: $0 < K \lesssim 2$

see figure 2.4.1

$$K = \delta\gamma = 0.934\, B\lambda_o \qquad \text{as above (sect. 2.4)}$$

$$P\,(\text{Watt}) = 1.9\times10^{-6} N\gamma^2 K^2 I/\lambda_o$$

2.5.1 Vertical opening angle, odd harmonics

In order to eliminate unwanted undulator radiation, the vertical opening angle can be reduced from its nominal value of $1/\gamma$ by the square root of the bandwidth $(kN)^{-1/2}$.

$$\text{i.e. } \frac{\Delta\lambda}{\lambda} \approx \frac{1}{kN}$$

$$\text{Thus } \sigma_{k'VERT} = \frac{1}{\gamma(kN)^{1/2}} \text{ for odd harmonics.}$$

2.5.2 Vertical opening angle, even harmonics

As seen in table 2.5.2 a-c and in figure 2.5.1 c, the even harmonics are broader than the odd ones, both in their spectral distribution and in their spatial distribution. Only with the help of detailed calculations in which the emittance and beta functions of the electron beam are taken into account can one determine how large the acceptance of a monochromator should be made in order to accept much or most of the even harmonics (2.4, 2.7). Such calculations and plots are given in this chapter.

Nevertheless, the vertical opening angle is smaller than that in the horizontal direction as dictated by the intrinsically higher brightness vertically. For the undulators planned for BESSY II the calculations indicate that the vertical opening angle for the even harmonics can be 30 - 40 % smaller than the horizontal opening angle without sacrificing flux significantly. See table 2.5.3 for relevant data.

Figure 2.5.1: Typical Undulator Spectra [2.10, 2.11]

a)

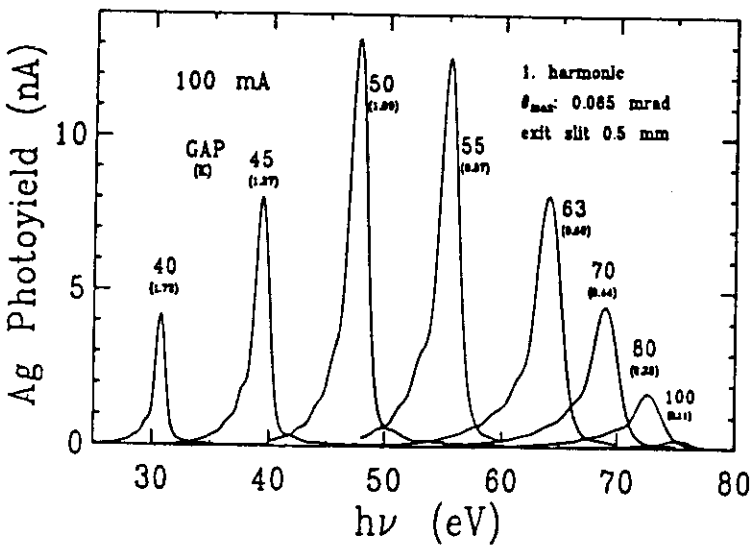

Spectra taken with the 800-line/mm grating. (a) First harmonic as a function of gap.

b)

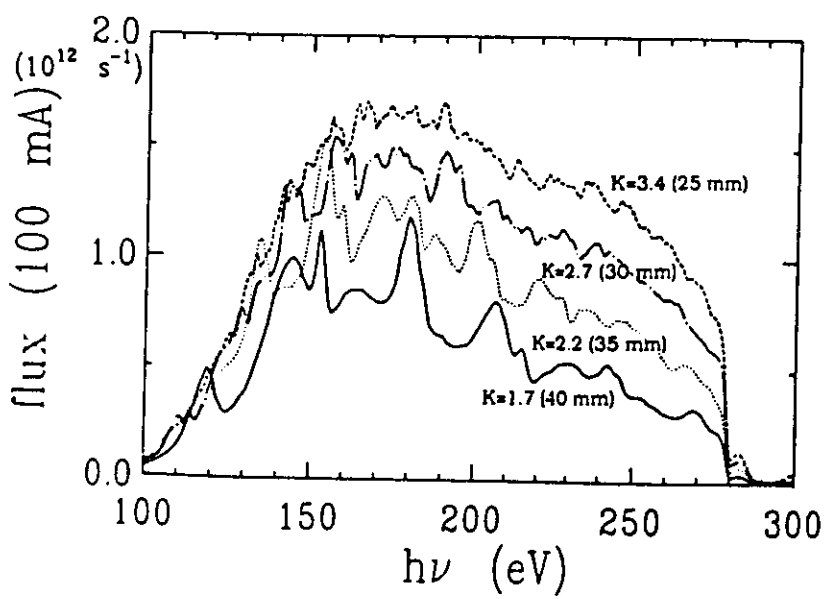

Measured intensities with the W/U and TGM-5 for various values of K. The gap in mm is also given. 100 mA ring current. The acceptance is $\sigma_h = \sigma_v = 125$ μrad.

Spectra taken at higher energies.

c)

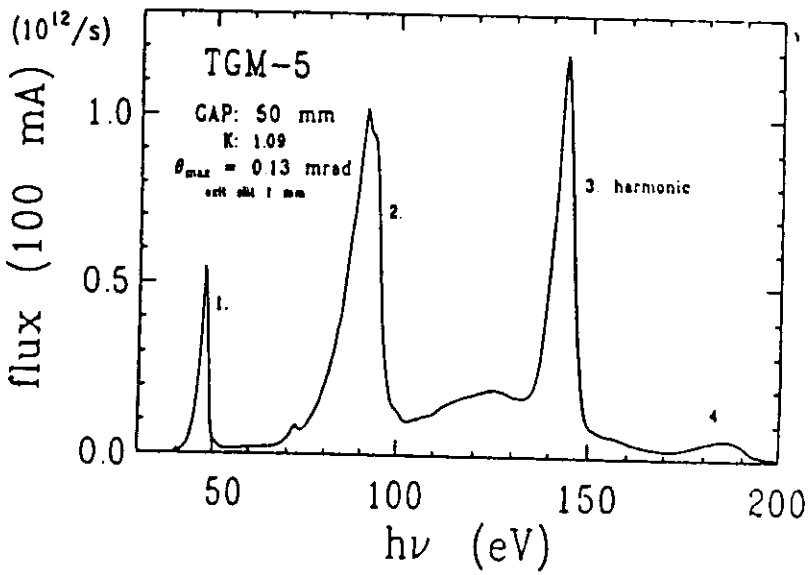

With the 1100-line/mm grating and pinhole.

d)

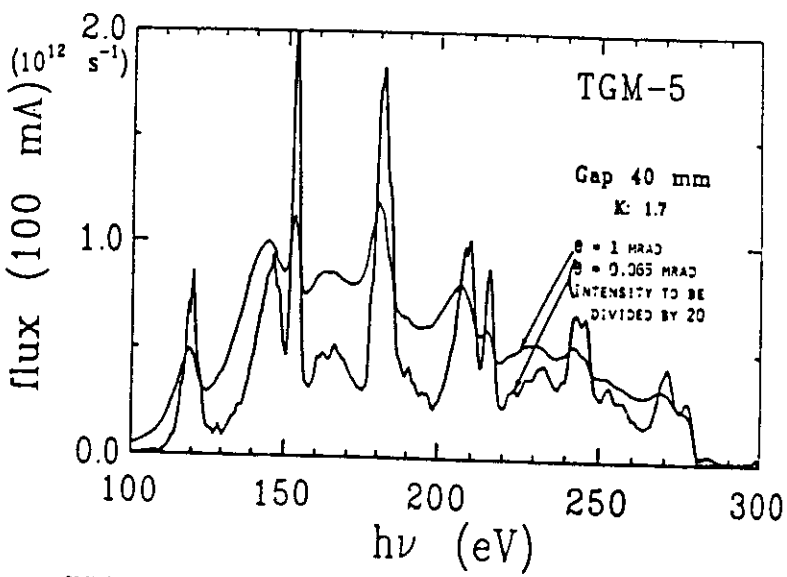

With the 1500-line/mm grating and two acceptances.

2.5.3 Horizontal opening angle, odd harmonics

For odd harmonics, the opening angle depends on both k and K:

$$\sigma'hor \approx \left(\sigma'el^2 + \sigma_k'HOR\,(K)^2\right)^{1/2}$$

where

$$\sigma_k'HOR\,(K) \approx \frac{1}{\gamma}\sqrt{\frac{1 + \frac{K^2}{2} + \ldots}{2\,kN}} = \sqrt{\frac{\lambda}{L}} \qquad \text{for} \quad \varepsilon_x = 0$$

$$\lambda = \frac{\lambda_o}{2\,k\gamma^2}\left(1 + \frac{K^2}{2} + \gamma^2\theta^2 + \ldots\right)$$

λ_o	= period length of the undulator
λ	= wavelength of the k^{th} harmonic
$\Delta\lambda$	= bandwidth of the k^{th} harmonic
L	= length of undulator = $N \cdot \lambda_o$
k	= harmonic = 1, 3, 5, ...
θ	= observation angle relative to the closed orbit

Typical values of $\sigma_k'(K)_H$ for odd harmonics are given in table 2.5.1 for BESSY I and BESSY II.

For better values of the horizontal opening angle, calculations with the real emittance should be carried through. This has been done below for several cases. The opening angles for the even harmonics can only be obtained with the help of computer programs such as SMUT [2.3] or URGENT [2.6]. The results of such calculations for typical undulators on a 1.7 GeV storage ring are shown in tables 2.5.2, 2.5.3 a-c, 2.5.4, 2.5.5 and figures 2.5.1 a-d, 2.5.2 and 2.5.3 a-c.

Table 2.5.1: Angular Divergences of $\sigma_{k'HOR}$ (K) (Odd Harmonics)

Angular divergence of the kth harmonic as compared with the divergence of the electron beam in the straight section.

BESSY: 755 MeV

$\varepsilon_x = 4.6 \times 10^{-8}$ π·m·rad; $\beta_x = 3.2$ m/rad
$\varepsilon_y = 3.5 \times 10^{-9}$ π·m·rad; $\beta_y = 15.5$ m/rad
$\sigma_{x'} = 0.12$ mrad (Section 2.1.1)
$\lambda_o = 70$ mm; N = 35

		k = 1	k = 9
K	0.5	0.086 mrad	0.029 mrad
	2.0	0.140 mrad	0.047 mrad

BESSY II: 1.7 GeV

$\varepsilon_x < 6.5 \times 10^{-9}$ π·m·rad; $\beta_x \leq 8$m/rad
$\varepsilon_y < 6.5 \times 10^{-10}$ π·m·rad; $\beta_y \leq 3$ m/rad
$\sigma_{x'} = 0.029$ mrad (Section 2.1.1)
$\lambda_o = 52$ mm; N = 80

N = 80		k = 1	k = 9
K	0.5	0.025 mrad	0.008 mrad
	2.0	0.041 mrad	0.014 mrad

Figure 2.5.2: **Angular Distribution of the Power from W-2 and U-3 [1.6 b]**

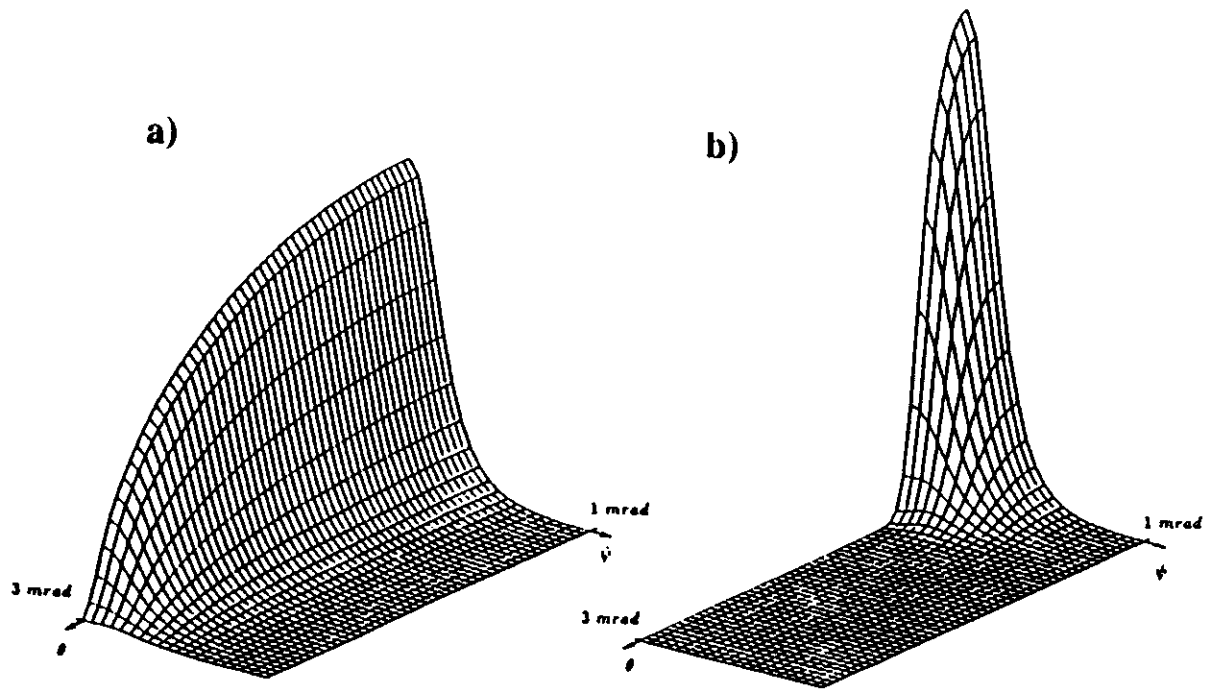

a) Angular distribution of the power for W-2/BESSY II (1.7 GeV) with 100 mA. The peak power is 371 Watt/mrad^2. K = 9.7

b) Angular distribution of the power for U-3/BESSY II as above. The peak power is 552 Watt/mrad^2. K = 1.6

Figure 2.5.3: **Undulator Flux Versus Pinhole Area**

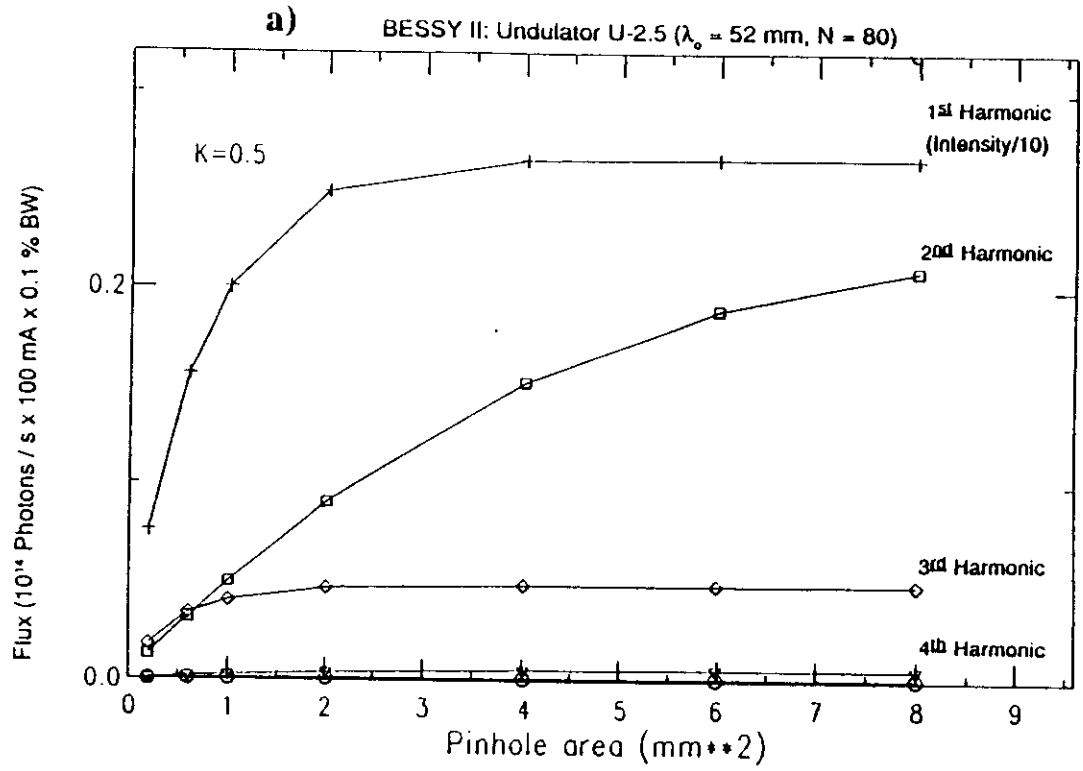

Peak intensities of the 1st to 5th Harmonic versus Pinhole size.
Pinhole is 10 m from the middle of the undulator.

θ (μrad)	56	98	126	149	169

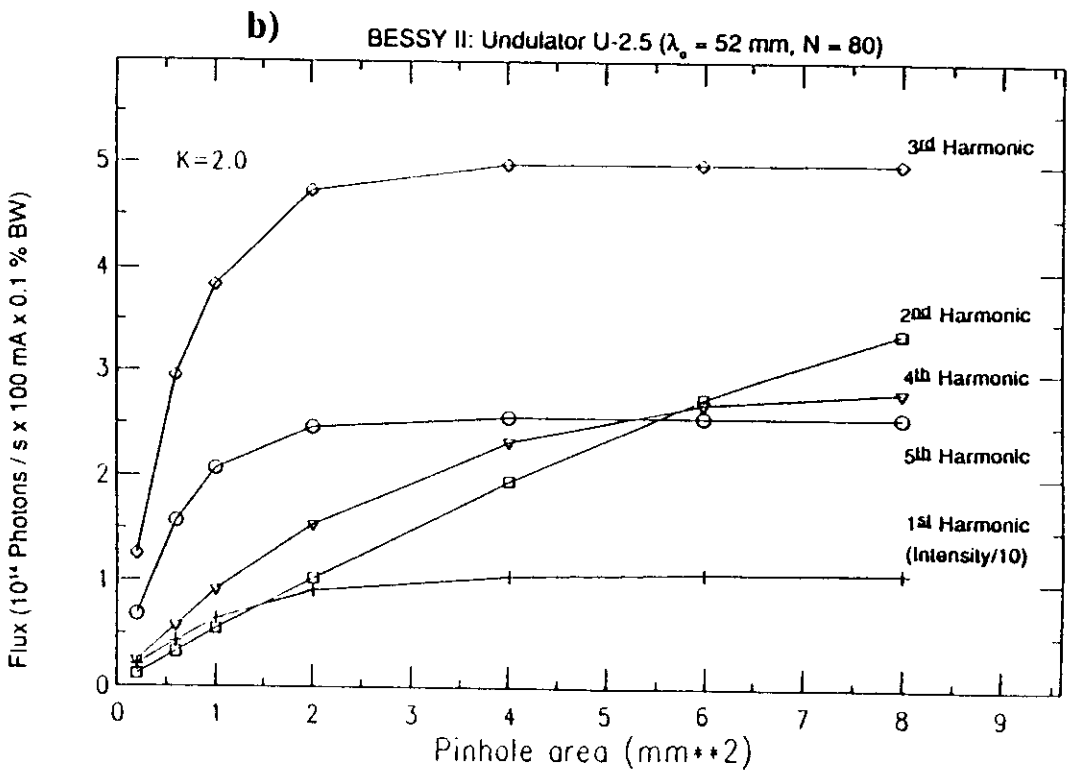

Peak intensities of the 1st to 5th Harmonic versus Pinhole size.
Pinhole is 10 m from the middle of the undulator.

θ (μrad)	56	98	126	149	169

Figure 2.5.3: Undulator Flux Versus Pinhole Area

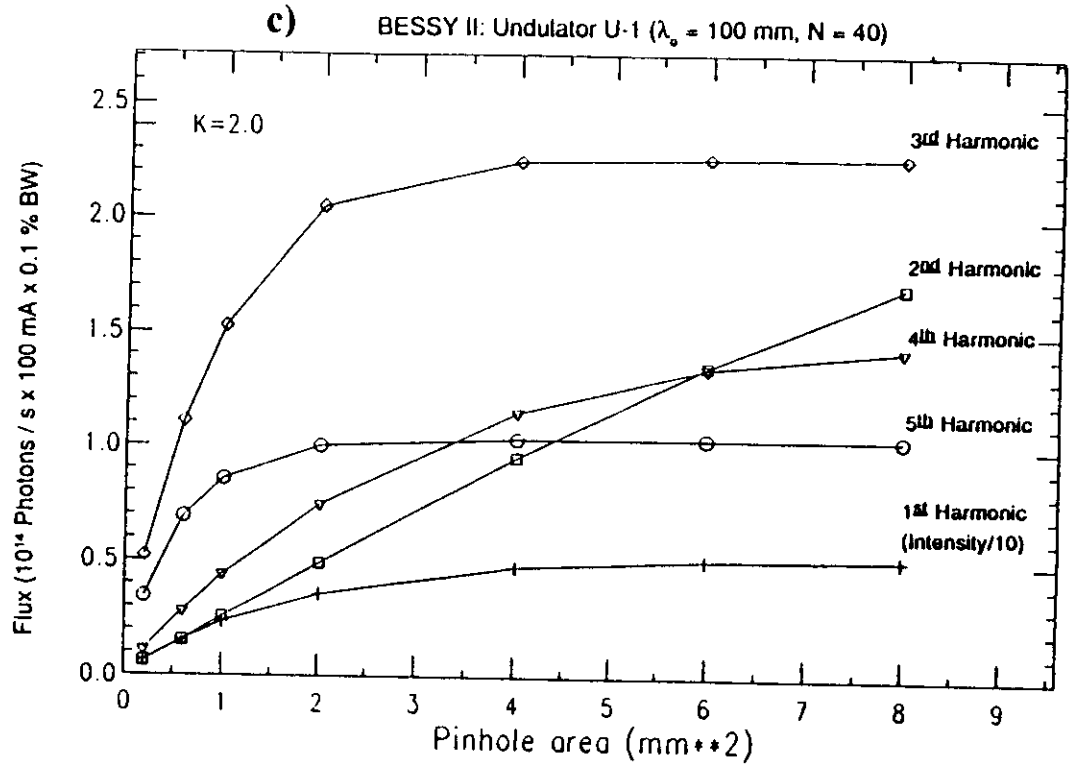

Peak intensities of the 1st to 5th Harmonic versus Pinhole size.
Pinhole is 10 m from the middle of the undulator.

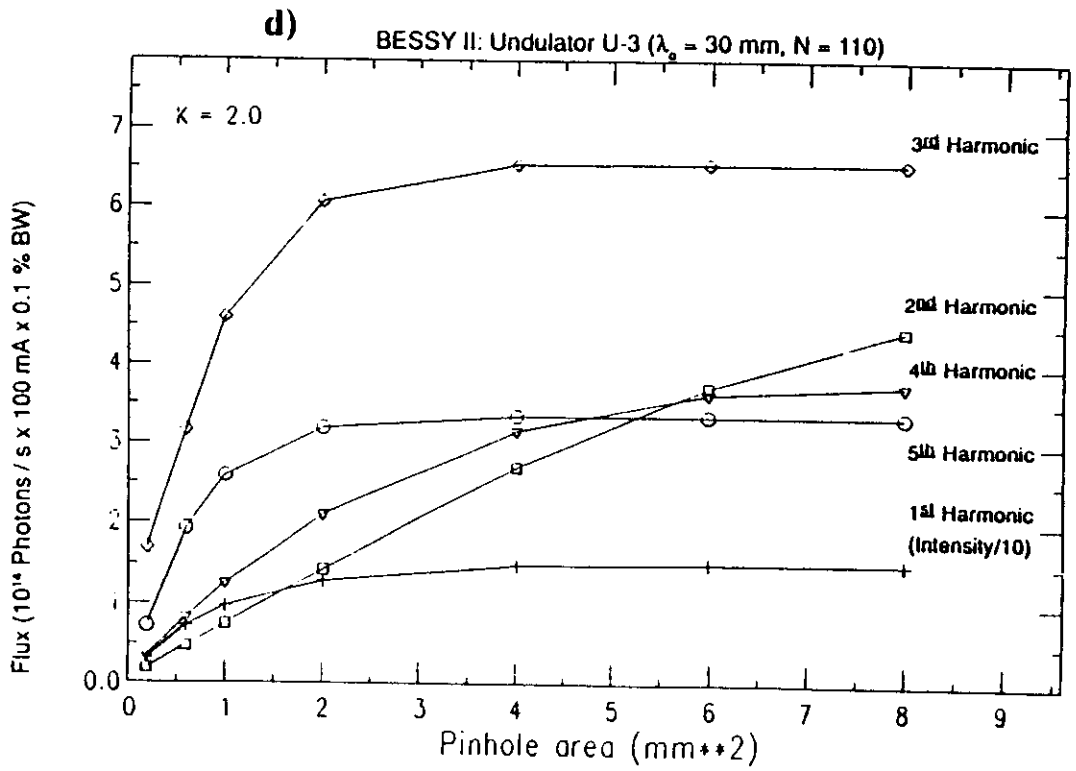

Peak intensities of the 1st to 5th Harmonic versus Pinhole size.
Pinhole is 10 m from the middle of the undulator.

Table 2.5.2: Radiative Power And Beam Divergence of the B-II Undulators*

1)	U-1 (λ_0 = 100 mm, N = 40)	K = 0.5	K = 2.2
	Total power (W)	2.1	41
	Axial power (W/mrad^2)	15.6	84
	θ_h (mrad)/L_h (mm)+	0.31/6.2	0.72/14.4
	θ_v (mrad)/L_v (mm)+	0.50/10.0	0.50/10.0
2)	U-2.5 (λ_0 = 52 mm, N = 80)	K = 0.5	K = 2.2
	Total power (W)	8	156
	Axial power (W/mrad^2)	60	322
	θ_h (mrad)/L_h (mm)+	0.26/5.2	0.78/15.6
	θ_v (mrad)/L_v (mm)+	0.50/10.0	0.50/10.0
3)	U-3.0 (λ_0 = 30 mm, N = 110)	K = 0.5	K = 1.6
	Total power (W)	19.2	197
	Axial power (W/mrad^2)	143	552
	θ_h (mrad)/L_h (mm)+	0.30/6.0	0.60/12.0
	θ_v (mrad)/L_v (mm)+	0.50/10.0	0.55/11.0
4)	W-2 (λ_0 = 100 mm, N = 40)		K = 9.7
	Total power (W)		789
	Axial power (W/mrad^2)		371
	θ_h (mrad)/L_h (mm)+		2.94/58.8
	θ_v (mrad)/L_v (mm)+		0.55/11.0

* for 100 mA ring current and 1.7 GeV

\+ Half opening angle for ca. 95% of the power delivered (ca. 2 σ-value). The equivalent opening in mm is given for a distance of 10 m from the middle of the undulator.

Table 2.5.3 a: Undulator U - 1 (λ = 100 mm, N = 40)

Energy, Flux and Opening Aperture^{+} of the First Five Harmonics* for K=0.5 and 2.0

	K = 0.5	K = 2.0
1st Harmonic, Energy (eV):	239	90
-Flux (photons/sec)	1.2×10^{14}	4.8×10^{14}
-Opening Aperture (R(mm))$^{+}$	1.2	1.2
2nd Harmonic, Energy (eV):	431	164 (172)#
-Flux (photons/sec)	1.2×10^{13}	2.5×10^{14} (1.7×10^{14})
-Opening Aperture (R(mm))$^{+}$	1.6	3.2 (1.6)
3rd Harmonic, Energy (eV):	728	273
-Flux (photons/sec)	2.3×10^{12}	2.2×10^{14}
-Opening Aperture (R(mm))$^{+}$	0.8	1.2
4th Harmonic, Energy (eV):	932	353
-Flux (photons/sec)	2.8×10^{11}	1.4×10^{14}
-Opening Aperture (R(mm))$^{+}$	1.2	1.6
5th Harmonic, Energy (eV):	1214	457
-Flux (photons/sec)	4.3×10^{10}	1.0×10^{14}
-Opening Aperture (R(mm))$^{+}$	0.8	0.8

* For 100 mA ring current and 0.1% BW. Calculation used the beam parameters of BESSY II.

$^{+}$ The opening aperture is defined as the radius, R, of a circular aperture at 10 m from the source through which 95% of the radiation passes.

Case where the radius of the aperture is R/2 where R is defined above (only important for second harmonic).

Table 2.5.3 b: Undulator U - 2.5 (λ = 52 mm, N = 80)

Energy, Flux and Opening Aperture+ of the First Five Harmonics* for K=0.5 and 2.0

	K = 0.5	K = 2.0
1st Harmonic, Energy (eV):	464	174
-Flux (photons/sec)	2.6×10^{14}	1.0×10^{15}
-Opening Aperture (R(mm))+	1.2	1.2
2nd Harmonic, Energy (eV):	843	326(332)#
-Flux (photons/sec)	2.1×10^{13}	$4.0 \times 10^{14}(3.4 \times 10^{14})$
-Opening Aperture (R(mm))+	1.6	3.2(1.6)
3rd Harmonic, Energy (eV):	1400	526
-Flux (photons/sec)	4.7×10^{12}	5.0×10^{14}
-Opening Aperture (R(mm))+	0.8	1.2
4th Harmonic, Energy (eV):	1792	682
-Flux (photons/sec)	5.7×10^{11}	2.8×10^{14}
-Opening Aperture (R(mm))+	1.4	1.6
5th Harmonic, Energy (eV):	2344	878
-Flux (photons/sec)	1.0×10^{11}	2.5×10^{14}
-Opening Aperture (R(mm))+	0.8	0.8

* For 100 mA ring current and 0.1% BW. Calculation used the beam parameters of BESSY II.

+ The opening aperture is defined as the radius, R, of a circular aperture at 10 m from the source through which 95% of the radiation passes.

Case where the radius of the aperture is R/2 where R is defined above (only important for second harmonic).

Table 2.5.3 c: Undulator U - 3 (λ = 30 mm, N = 110)

Energy, Flux and Opening Aperture[+] of the First Five Harmonics[*] for K=0.5 and 2.0

	K = 0.5	K = 2.0
1st Harmonic, Energy (eV):	806	302
-Flux (photons/sec)	3.6×10^{14}	1.5×10^{15}
-Opening Aperture (R(mm))[+]	0.9	1.2
2nd Harmonic, Energy (eV):	1483	572 (578)[#]
-Flux (photons/sec)	2.7×10^{13}	4.9×10^{14} (4.4×10^{14})
-Opening Aperture (R(mm))[+]	1.6	3.2 (1.6)
3rd Harmonic, Energy (eV):	2427	910
-Flux (photons/sec)	6.7×10^{12}	6.5×10^{14}
-Opening Aperture (R(mm))[+]	0.8	1.2
4th Harmonic, Energy (eV):	3126	1185
-Flux (photons/sec)	7.8×10^{11}	3.8×10^{14}
-Opening Aperture (R(mm))[+]	1.4	1.6
5th Harmonic, Energy (eV):	4076	1520
-Flux (photons/sec)	1.2×10^{11}	3.2×10^{14}
-Opening Aperture (R(mm))[+]	0.8	0.8

[*] For 100 mA ring current and 0.1% BW. Calculation used the beam parameters of BESSY II.

[+] The opening aperture is defined as the radius, R, of a circular aperture at 10 m from the source through which 95% of the radiation passes.

Case where the radius of the aperture is R/2 where R is defined above (only important for second harmonic).

Table 2.5.4: Comparison of Divergence of Power and Flux [1.6 b]

BESSY II (1.7 GeV)

Comparison of the total emitted power of an undulator with the flux of the first five harmonics as a function of the hard edge half opening angle, θ, of an aperture.

	θ (μrad)	P+	F* 1.	2.	3.	4.	5.
	40	0.007	0.24	0.05	0.42	0.09	0.59
U-1	80	0.06	0.68	0.19	0.90	0.53	
(K = 2.0)	160	0.16		0.68			
λ_0 = 100 mm	320	0.50		0.95			
N = 40	640	0.92					
	40	0.007	0.34	0.07	0.50	0.16	0.51
U-2.5	80	0.06	0.84	0.25	0.95	0.53	0.96
(K = 2.0)	160	0.16		0.84		0.98	
λ_0 = 52 mm	320	0.50		0.95			
N = 80	640	0.92					
	40	0.008	0.40	0.08	0.42	0.18	0.49
U-3	80	0.07	0.83	0.29	0.92	0.53	0.95
(K = 1.6)	160	0.20		0.90		0.97	
λ_0 = 30 mm	320	0.59		0.95			
N = 110	640	0.95					

+ P = fraction of total power emitted

*F = fraction of the total flux of the harmonic. If F ≥ 0.99 no entry is made.

Table 2.5.5: Source Characteristics for the Undulators at BESSY II

1. Characteristics of the electron beam in the straight sections

γ = 3327 (E = 1.7 GeV)
$\varepsilon_x = 6 \cdot 10^{-9}\pi$. m . rad
$\varepsilon_y = 0.1\ \varepsilon_x$
β_x = 8 m/rad
β_y = 3 m/rad
σ_x = 220 µm
σ_y = 42 µm
σ_x' = 27 µrad ⎫ not relevant
σ_y' = 14 µrad ⎭ see below

2. Depths of source: An average length of 4100 mm is used.

3. Divergence of undulator radiation:

A pinhole of diameter 3.2 mm located 10 m from the middle of the undulators transmits 95% of the flux of the 1st, 3rd, 4th, and 5th harmonics of the planned undulators. For the 2nd harmonic a diameter of 6.4 mm is required (see Table 2.5.4). Thus,

$$\sigma_{k'\,VERT} = 55\text{-}110\ \mu\text{rad}\ (70\%\ \text{of}\ \sigma_{k'\,HOR})$$

$$\sigma_{k'\,HOR} = 80\text{-}160\ \mu\text{rad}$$

4. Minimum distance between middle of undulator and first optical element: 12000 mm.

2.6 Determination of the direction and position of SR

The alignment of a beamline starts with the determination of the optical axis of the SR itself. Electron beam position monitors installed in the storage ring are essential for stable ring operation but are sufficient neither for checking the stability of the SR position/angle nor for aligning the beamline. Before the beamline is set up, but after completion of the front end, the fan of visible SR passing through a window flange can be used to determine the horizontal area into which the tangents to the electron orbit fall. The exact positions of the tangents can be determined by the shadow method: a plumb line is suspended near the front end and its shadow is observed further back. **Note: This can only be done with low currents in the ring and with approval of the radiation safety officer.** Higher currents can produce dangerous amounts of radiation and the heat of the SR can crack the window. The location of the observed SR axis or fan can be marked on the floor with surveying studs, for example.

In designing a beamline for dipole radiation it is generally possible to use some of the SR just outside of the primary area for monitors. Most commonly plate or wire monitors are located just above and below the meridional plane and the difference signal used to detect changes in the height of this plane. By employing two sets of monitors in the beamline, the second at about twice the distance of the first from the source, the angle of emission of SR from the electron beam can be determined (see figure 2.6.1 [6.14]. The horizontal direction of the tangent to the bending radius is easily determined by placing a vertical wire early in the beamline and scanning through the position of its shadow at double the distance [6.11]. If the wires are fine enough, the horizontal source size can also be determined. It is strongly recommended that SR-position monitors for both the vertical and horizontal directions be installed as standard procedure in a beamline behind every front end. Diagnosing problems on the beamline is much more straightforward with than without them. The first goal of troubleshooting is to determine where the problem is located: in the storage ring, in the monochromator/beamline or at the experiment.

In addition to electronic SR-monitors in the beamline it is useful to have stratigically placed, moveable ground glass screens: in front of the entrance and exit slits for example using a phosphor (e.g. ZnS) where/when necessary to detect

Figure 2.6.1: **Determination of the Direction and Position of SR [6.14]**

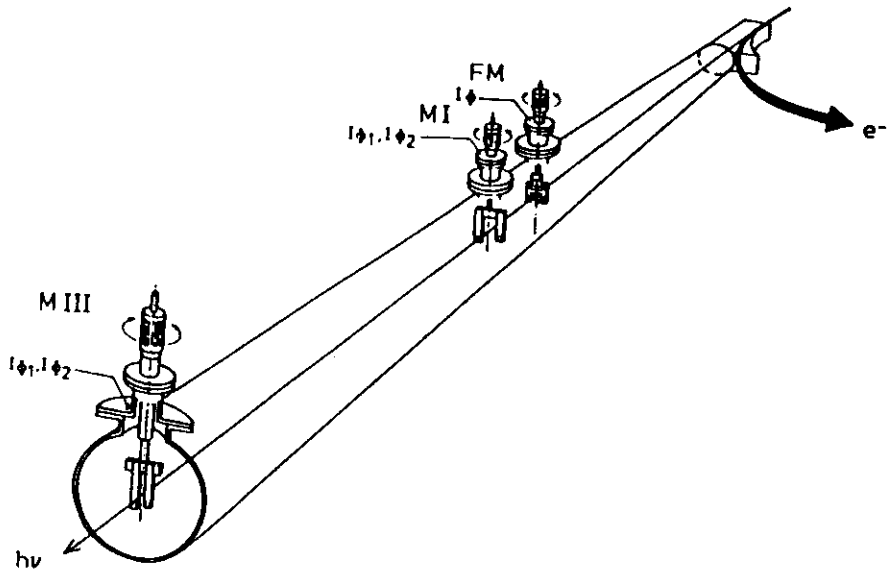

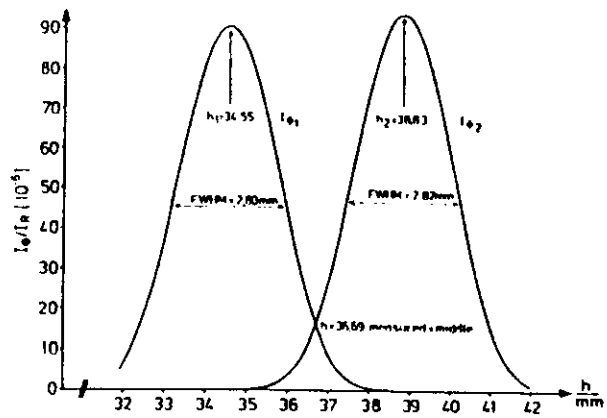

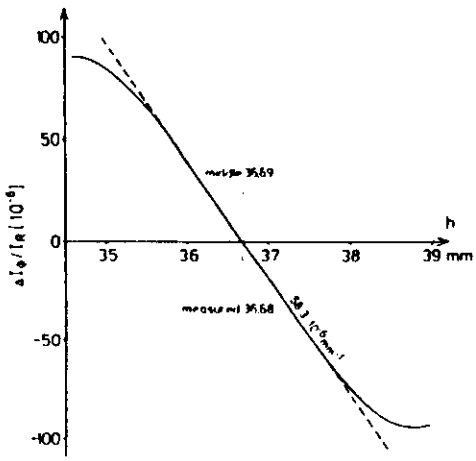

otherwise invisible undulator radiation. "Seeing is believing" and avoids spurious effects that occasionally crop up in electronic systems.

The above methods of locating and viewing the SR fan in a beamline are only of limited use in an undulator beamline. Photoemission from suitably designed four blade monitors (see reference 6.10 and figure 2.6.2 for example) along with a feedback circuit to steerer magnets to regulate the direction of the electron beam [6.5 - 6.9] are essential for high brightness undulators: the acceptance of a monochromator for undulator radiation is generally much smaller than that for dipole radiation. Since undulators tend to steer the electron beam with increasing K values, a high brightness undulator/monochromator would tend to be self-defeating without controlling monitors and feedback loops.

There are two fundamental differences between monitoring dipole radiation and monitoring undulator radiation:

a) For electrons of energy 700 MeV and higher, undulator radiation is not visible to the eye.
b) The neighboring dipole magnets, which bound the straight section containing the undulator, produce copious amounts of both visible and short wavelength light.

Thus, what one sees in an undulator beamline is not undulator radiation at all, but is instead dipole radiation from sources far removed from the undulator. Photoelectric devices also "see" the dipole radiation and can yield misleading results. The nature of the undulator radiation must be exploited in order to separate the two types of radiation:

c) Undulator radiation is strongly collimated in both transverse directions.
d) Undulator radiation consists of discrete lines or peaks whose energy maximum lies on the optical axis of the undulator itself (see chapter 2.4).

The four blade monitor mentioned above [6.10] effectively exploits the first of these two characteristics of undulator radiation.

The latter characteristic (d above) is generally used to locate the undulator axis with the highest accuracy and certainty. A moveable pinhole of dimensions of the order of those of the electron beam is positioned on what is thought to be the undulator axis. An energy scan is then made on the monochromator. The

Figure 2.6.2: **An Example of a 4 Blade Detector for Undulator Radiation [6.10]**

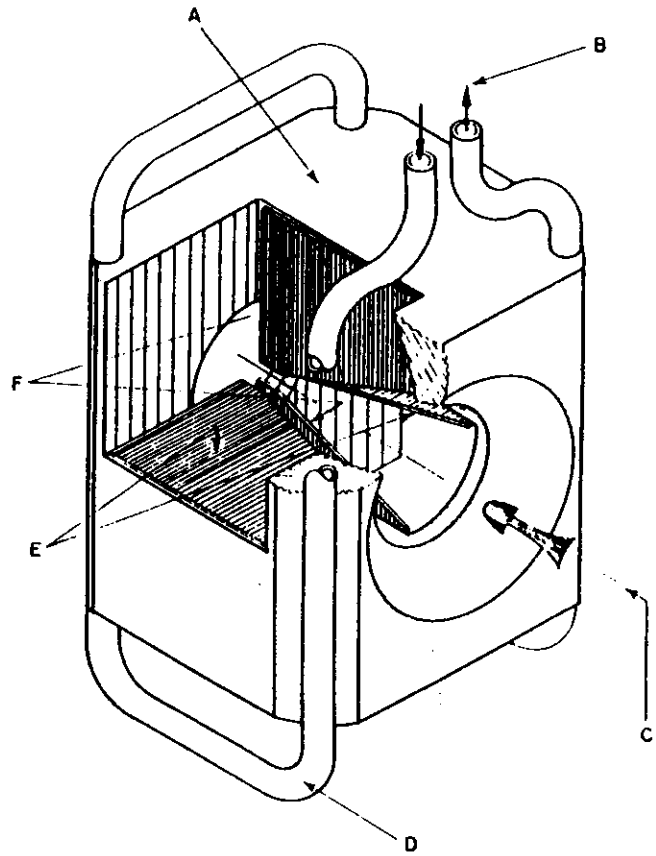

FIG. 2. Phantom view of the monolith showing the blades and the cooling tubes. A—copper monolith, B—cooling water flow, C—direction of photon beam, D—cooling water tubes, E—horizontal blades, and F—vertical blades.

pinhole is moved slightly (laterally) and the energy scan repeated. By systematically searching the area with the pinhole, the exact location of the undulator axis can be determined. It is the location which produces a spectrum of the first harmonic, for example, of the undulator spectrum which is shifted to the highest energy relative to the other spectra, of the first harmonic.

Such moveable pinholes or apertures are essential in an undulator beamline. They serve not only to set up the beamline initially but also to check the stability of the electron beam in the undulator against time or K value, for example. They can also be used as a fairly good check of the general alignment of the beamline in that the visible dipole radiation passing through a pinhole which is known to lie on the undulator axis simulates the path of the invisible undulator radiation quite well.

It is hoped that the reader is now so convinced of the necessity of SR and undulator radiation monitors in beamlines that he is willing to put the time and effort into planning and installing them.

3. Requirements of the Optical System

In this section the boundary conditions for the designer are established: energy range, resolution, polarisation of the radiation and coherence are just a few of the more obvious ones. The decisions to be made here must be consonant with (a) the goals of the beamline user and (b) reality. The beamline designer is perhaps more concerned with the latter. It is essential that one or more of the future users of the beamline be involved in the design at this stage.

If for example the beamline is to be dedicated to one application or to one type of research, it is possible to optimize it in ways which differ from a general purpose beamline. For example, for near edge spectroscopy at the carbon, nitrogen and oxygen K-edges, three gratings can be chosen for best resolution at 284, 400 and 540 eV respectively and over the range of 60 - 80 eV above them. As a second example, monochromators for circularly polarized radiation from dipole magnets have been reported in the literature, using off-plane radiation from the storage ring and requiring two optical paths through the monochromator [4.23, 4.24, 4.25].

High flux designs where resolution plays a secondary role can also be designed. One application is as a wavelength "filter" for a subsequent zone plate system for x-ray microscopy. The possibilities are too numerous to list. The solution is, as stated above, to get the users involved at this stage. By this means, new types of monochromators for new types of experiments will be conceived and both the users and the beamline designers will be more satisfied.

3.1 Critical Aspects of Sources and Monochromators for Synchrotron Radiation (10 - 1000 eV)

1. ***The light source is fixed (point or point on an axis). The experiment is also fixed in general (points, axis/point). The optical system must connect these two points, axis/points.*** For fixed experiments resolution and/or transmission may suffer from the use of additional optical elements.

2. ***SR-Sources (Dipole, Wiggler, Undulator) are highly collimated and of small size (i. e. brilliant).*** This makes possible optical designs of high transmission and high resolution.

3. ***The vertical source size and, for a dipole or wiggler source, the opening angle of the radiation is much smaller than in the horizontal plane.*** Hence, vertical dispersion is desirable. For dipole and wiggler radiation, anamorphotic optics are required to illuminate the grating in both directions.

4. ***The source position and axis must be highly stable.*** Dynamic feedback loops between beamline monitors and steering magnets are required for undulators.

5. ***The ring current is not a reliable measure of the intensity of the SR behind the exit slit.*** The latter should be monitored.

6. ***The SR is linearly polarized in the plane of the storage ring. For low energies (< 50 eV) the "p" and "s" reflectivities are very different.***

7. ***The reflectivity and the transmission of all optical materials in the 10 - 1000 eV range are poor.*** Hence, windowless, grazing incidence optical designs are required.

8. ***In the 10 - 1000 eV range higher order radiation is a problem.*** It should be determinable and/or suppressed.

9. ***The optical elements, in particular the first one, are subject to radiation damage and/or heat loading. The heat loading from wigglers and undulators produces bends and local bumps on mirrors and gratings.*** Cooling is required but problematic.

10. ***Ultrahigh vacuum conditions ($P \leq 1 - 2 \times 10^{-9}$ mbar) are required:*** (1) to be compatible with the vacuum requirements of the storage ring, (2) to avoid contamination of the optical surfaces, especially with carbon and (3) to be compatible with the vacuum requirements of the experiment in many cases.

4. Gratings and Monochromators

On the basis of the goals set by the beamline user and the beamline designer in chapter 3, the designer can now forge ahead with the detailed decisions aimed at achieving those goals. Here is where a detailed knowledge of the source (chapter 2) and of optics are coupled to produce an optimal solution to the goals at hand.

In this chapter some basic aspects of diffraction gratings are discussed and the relationship between optical aberrations and resolution developed. In addition, several equations and approximations are derived or stated which should be of use to the designer. Special emphasis is given to spherical gratings but most of the development is equally applicable to plane gratings. The desirable characteristics of the "ideal" high resolution monochromator for the energy range 90 - 800 eV are given in table 4.0.1.

At the present time (1992) there are several developments that are very promising but which have as yet not been proven in operation. In particular the following should be mentioned:

a) Variable line spacing gratings, both plane and concave
b) Multilayers
c) Multilayer gratings
d) Conical diffraction

These topics will be taken up here at some future date.

Table 4.0.1: The "Ideal" High Resolution Monochromator for Energies 90 - 800 eV

1) Focussed for all λ ($F_{20} \equiv 0$)
2) Coma corrected for all λ ($F_{30} \equiv 0$)
3) Other aberrations minimized
4) Large energy range without grating change
5) Grating always on "blaze"
6) Higher orders suppressed
7) Fixed entrance and exit slits
8) Fixed entrance and exit directions
9) Perfect matching to source
10) Performance unaffected by heat load
11) High transmission
    - Number of optical elements
    - Quality of optical elements
12) Possible to align!
13) Possible to pay for!

4.1 On the optimization of grazing incidence monochromators. Zero order layout:

Decisions, decisions, decisions!

- Energy range and resolution: number of gratings to be used
- Whether or not an entrance slit is to be used.
- The size of the monochromator (r, r'): (see Fig. 4.2.1 for definitions) determined by space available, source brightness, resolution desired, etc.
- Means of reducing heat loading problems.
- The grating type: plane, spherical or some other, e.g. "corrected" gratings (variable line spacing).
- Deflection angle, α - β, is chosen on the basis of the maximum photon energy, E_{max}, to be transmitted with (say) 50% reflectance. If possible, α - β should increase with increasing energy.
- Means and location of sagittal focussing.
- Means of suppression of higher order light.
- Optical aberrations are minimized: strongly dependent on α_{max} and grating length:

a) α_{max} (β_{max} if k = -1) is determined by

$$\frac{\lambda_2}{\lambda_1} = \frac{\sin\phi_2}{\sin\phi_1} \text{ where } \phi = \frac{\alpha + \beta}{2}$$

(ϕ_2 - ϕ_1 = angular scanning range of grating for the wave length range λ_1 - λ_2)

b) Grating length $\cong$ 2 r sin m/sin θg;
θg = 90° - α = grazing angle of incidence
$\pm$ m = vertical acceptance
r = distance between entrance slit and grating

From here on, things get complicated. Detailed calculations and ray traces are necessary.

4.2 Geometric Aberration Theory of Straight Ruled, Constant Spacing Diffraction Gratings

For a diffraction grating, light coming from point A (see figure 4.2.1) and impinging on an arbitrary point P (ξ, w, l) on a grating will contribute to an image at B only if the light path function is fulfilled:

$$F = AP + PB + Nk\lambda w \qquad (1)$$

where N is the line density
k is the order of diffraction $\pm 1, \pm 2$ etc.
λ is the wavelength of the light being diffracted
and w is the position in the dispersion plane.

Thus, the rays of light coming from A will arrive at B with the same phase, yielding constructive interference and hence, an image. According to Rayleigh's criterion for constructive interference, $\Delta F \leq \lambda/4$. That is, there is a certain bandpass associated with the light path function, a fact which we will not pursue here any further.

According to Fermats' principle of least time, the conditions for focussing A at B are given by

$$\partial F/\partial w = 0 \quad \text{(meridional focus)} \qquad (2)$$

$$\text{and} \quad \partial F/\partial l = 0 \quad \text{(sagittal focus)} \qquad (3)$$

These three equations provide the basis for determining the optical properties of a given diffraction grating. More subtly, they can be used to decide on the characteristics of the diffraction grating, in particular, the shape of the surface and the groove density N in order to optimize the performance of the entire system. With regard to the latter point, various authors have determined that certain optical properties can be improved, or aberrations reduced, if N is variable across the surface of the grating [4.3 and references therein, 4.11, 4.16]. This possibility will not be developed here, and we restrict ourselves to straight ruled, constant spacing diffraction gratings. Our goal here is to develop the relationship between the geometry of the optical system and the dispersion, $\Delta\lambda$, resulting from this geometry, the aberration dispersion.

Figure 4.2.1: Grating Definitions

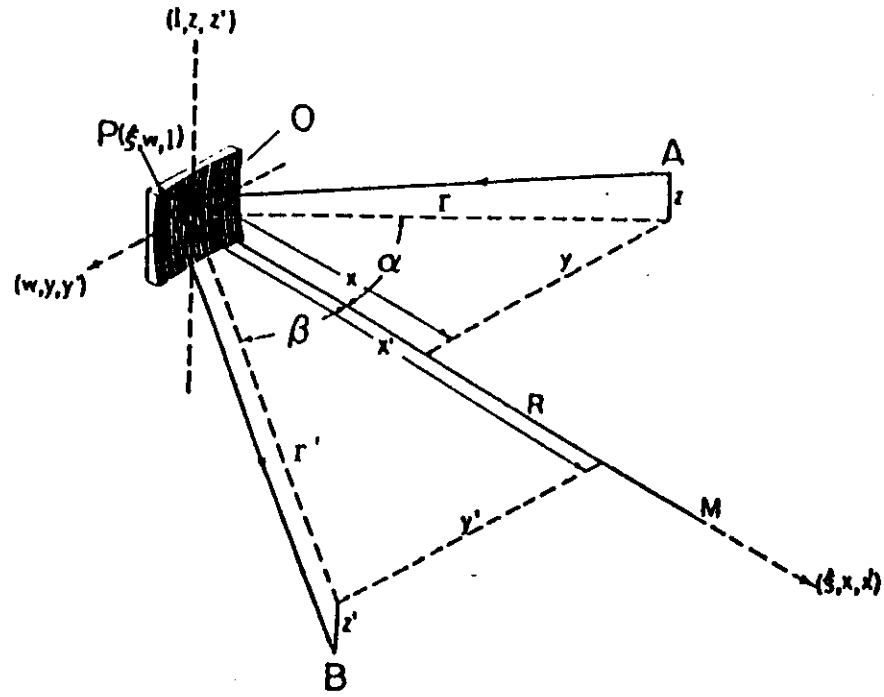

a) Coordinate systems [taken from Reference 4.1]

Whereas Beutler [4.1] uses the notation ξ, w, l for the grating and x, y, z, x', y', z' for the object and image respectively, Haber [4.2] uses x, y, z for the grating and x_a, x_b, x_c, x_b, y_b and z_b for the object and image. We use the Beutler notation as do references 4.3 and 4.10.

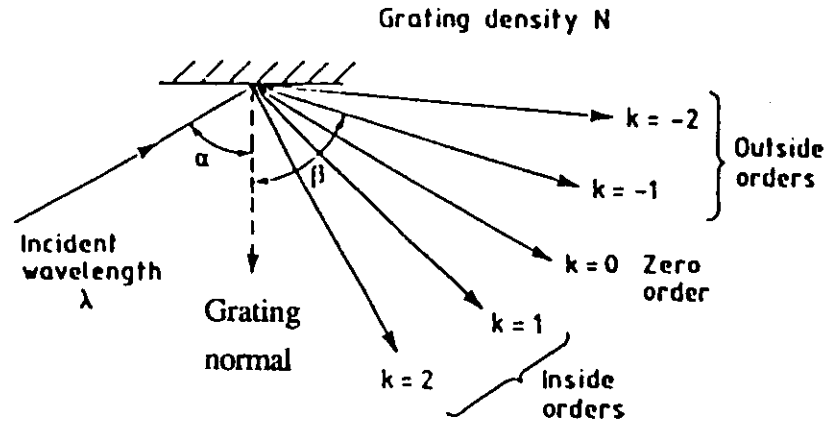

b) Grating orders [taken from Reference 3.4]. Note the sign convention for the angle β:

$\beta > 0$	when on the same side of the grating normal as α
$\beta < 0$	when on the opposite side of the grating normal

The equations 1-3 above only gain a practical meaning if we define the surface under study. For the purpose at hand, it is most convenient to use a polynominal for the surface P (ξ, w, l):

where
$$\xi = \sum_{i=o}^{\infty} \sum_{j=o}^{\infty} a_{ij} w^i \mu^j$$

and

$$a_{00} = a_{10} = 0; \; j = \text{even}$$

as dictated by the choice of origin and the fact that the xy plane is a symmetry plane. We should like to point out here that this is not the usual way of defining surfaces and that, in the past, a considerable amount of work was required to achieve the series expansions from the familiar expressions (see for example references 4.1 and 4.2). We have obtained the coefficients with the help of a computer code [4.18] the results of which are given in table 4.2.1 for various surfaces (see figure 4.2.2).

Then,

$$\langle AP \rangle = [(x - \xi)^2 + (y - w)^2 + (z - l)^2]^{1/2}$$

$$\langle PB \rangle = [(x' - \xi)^2 + (y' - w)^2 + (z' - l)^2]^{1/2}$$

From figure 4.2.1 it can be seen that the following substitutions can be made:

$$x = r \cos \alpha \; , \; y = r \sin \alpha$$
$$x' = r' \cos \beta \; , \; y' = r' \sin \beta$$

and that
$$\frac{z}{r} = -\frac{z'}{r'}$$

where the signs of α and β are opposite if points A and B lie on opposite sides of the xz-plane. The grating dimensions are $\pm w_o$ in the y (dispersive) direction and $\pm l_o$ in the sagittal direction. The origin is in the middle of the grating. In the development of the geometric relations relating A, P and B, the variables x, y, x', y' for A and B are eliminated as shown above and for a given surface geometry, P, ξ can be expressed

Figure 4.2.2: **Three Geometries [3.4, 5.7]**

Toroid

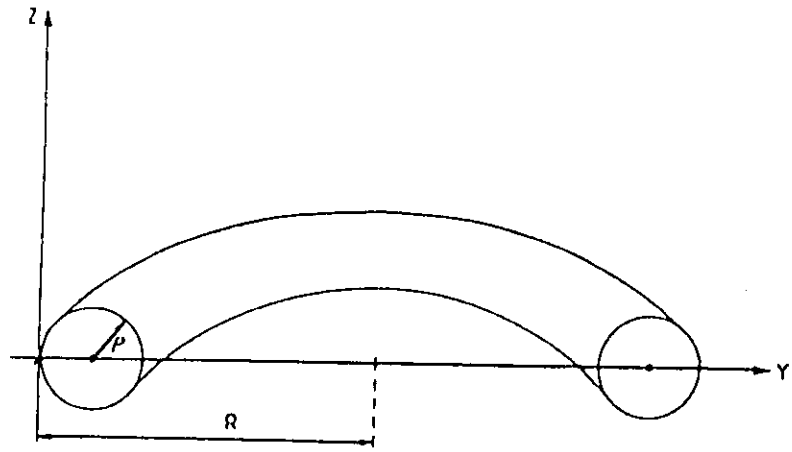

(a)

Parabola

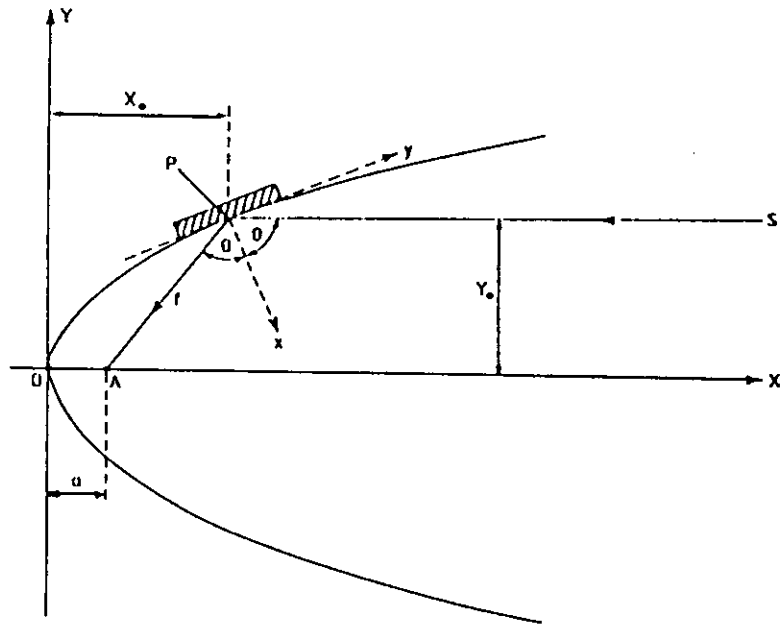

Ellipse

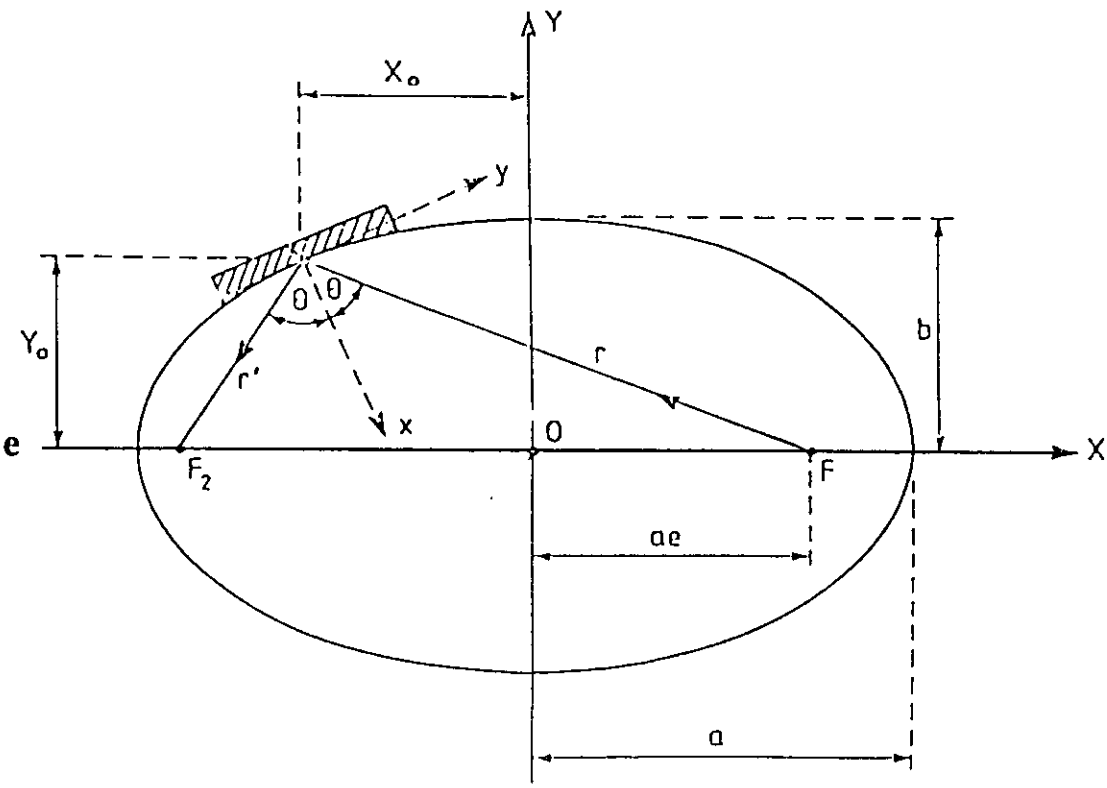

Table 4.2.1 The a_{ij} coefficients for various surfaces [4.18].
see figure 4.2.2 for definitions of terms.

Toroid Note: For a sphere, $\rho = R$

$$a_{02} = \frac{1}{2\rho} \qquad a_{20} = \frac{1}{2R} \qquad a_{22} = \frac{1}{4R^2\rho}$$

$$a_{40} = \frac{1}{8R^3} \qquad a_{04} = \frac{1}{8\rho^3}$$

Ellipsoid Note: $f = \left[\frac{1}{r} + \frac{1}{r'}\right]^{-1}$

$$a_{02} = \frac{1}{4f\cos\theta} \; ; \quad a_{20} = \frac{\cos\theta}{4f} \; ; \quad a_{04} = \frac{b^2}{64f^3\cos^3\theta}\left[\frac{\sin^2\theta}{b^2} + \frac{1}{a^2}\right]$$

$$a_{12} = \frac{\tan\theta(e^2 - \sin^2\theta)^{1/2}}{8f^2\cos\theta} \; ; \quad a_{30} = \frac{\sin\theta}{8f^2}(e^2 - \sin^2\theta)^{1/2}$$

$$a_{40} = \frac{b^2}{64f^3\cos\theta}\left[\frac{5\sin^2\theta\cos^2\theta}{b^2} - \frac{5\sin^2\theta}{a^2} + \frac{1}{a^2}\right]$$

$$a_{22} = \frac{\sin^2\theta}{16f^3\cos^3\theta}\left[\frac{3}{2}\cos^2\theta - \frac{b^2}{a^2}\left(1 - \frac{\cos^2\theta}{2}\right)\right]$$

Paraboloid

$$a_{02} = \frac{1}{4f\cos\theta} \; ; \quad a_{20} = \frac{\cos\theta}{4f} \; ; \quad a_{04} = \frac{\sin^2\theta}{64f^3\cos^3\theta}$$

$$a_{12} = -\frac{\tan\theta}{8f^2} \; ; \quad a_{30} = -\frac{\sin\theta\cos\theta}{8f^2}$$

$$a_{40} = \frac{5\cos\theta\sin^2\theta}{64f^3} \; ; \quad a_{22} = \frac{3\sin^2\theta}{32\cos\theta f^3}$$

Plane

$R = \infty$; $\rho = \infty$; $a_{ij} \equiv 0$!

in terms of the other variables and the various a_{ij}. After making these expansions and substitutions one can express F as follows:

$$F = F_{000} + wF_{100} + \tfrac{1}{2} w^2F_{200} + \tfrac{1}{2} l^2F_{020} + \tfrac{1}{2} w^3F_{300} + \tfrac{1}{2} wl^2F_{120}$$

$$+ \tfrac{1}{8} w^4F_{400} + \tfrac{1}{4} w^2l^2F_{220} + \tfrac{1}{8} l^4F_{040}$$

$$+ lF_{011} + wlF_{111} + \tfrac{1}{2} w\, F_{102} + \tfrac{1}{4} w^2F_{202} + \tfrac{1}{2} w^2lF_{211} + ...$$

selecting the most important terms [4.3, 4.10] and using the notation of Noda et al [4.3].

Thus, for r, r' >> z, z'

$F_{000} = r + r'$

$F_{100} = Nk\lambda - (\sin\alpha + \sin\beta)$ grating equation

$F_{200} = (\cos^2\alpha/r) + (\cos^2\beta/r') - 2a_{20}(\cos\alpha + \cos\beta)$ Meridional focus

$F_{020} = (1/r) + (1/r') - 2a_{02}\,(\cos\alpha + \cos\beta)$ Sagittal focus

$F_{300} = [T(r,\alpha)/r]\,\sin\alpha + [(T(r',\beta)/r']\,\sin\beta - 2a_{30}(\cos\alpha + \cos\beta)$ Primary coma

$F_{120} = [S(r,\alpha)/r]\,\sin\alpha + [S(r',\beta)/r']\,\sin\beta - 2a_{12}(\cos\alpha + \cos\beta)$ Astigmatic coma

$$F_{400} = [4T(r,\alpha)/r^2]\,\sin^2\alpha - [T^2(r,\alpha)/r] + [4T(r',\beta)/r'^2]\,\sin^2\beta$$

$$- [T^2(r',\beta)/r'] - 8a_{30}\left[\frac{1}{r}\,(\sin\alpha\,\cos\alpha) + \frac{1}{r'}\,(\sin\beta\,\cos\beta)\right]$$

$$- 8a_{40}(\cos\alpha + \cos\beta) + 4a^2_{20}\left[\frac{1}{r} + \frac{1}{r'}\right]$$

$$F_{220} = [2S(r,\alpha)/r^2]\sin^2\alpha + [2S(r',\beta)/r'^2]\sin^2\beta$$

$$- [T(r,\alpha)S(r,\alpha)/r] - [T(r',\beta)S(r',\beta)/r']$$

$$+ 4a_{20}a_{02}(1/r + 1/r') - 4a_{22}(\cos\alpha + \cos\beta)$$

$$- 4a_{12}\left[\frac{1}{r}(\sin\alpha\cos\alpha) + \frac{1}{r'}(\sin\beta\cos\beta)\right]$$

$$F_{040} = 4a_{02}^2(1/r + 1/r') - 8a_{04}(\cos\alpha + \cos\beta) - [S^2(r,\alpha)/r] - [S^2(r',\beta)/r']$$

$$F_{011} = -\frac{z}{r} - \frac{z'}{r'}$$

$$F_{111} = -\frac{z}{r^2}\sin\alpha - \frac{z'}{r'^2}\sin\beta$$

$$F_{102} = \frac{z^2\sin\alpha}{r^2} + \frac{z'^2}{r'^2}\sin\beta$$

$$F_{202} = \left(\frac{z}{r}\right)^2\left[\frac{2\sin^2\alpha}{r} - T(r,\alpha)\right] + \left(\frac{z'}{r'}\right)^2\left[\frac{2\sin^2\beta}{r'} - T(r',\beta)\right]$$

$$F_{211} = \frac{z}{r^2}\left[T(r,\alpha) - \frac{2\sin^2\alpha}{r}\right] + \frac{z'}{r'^2}\left[T(r',\beta) - \frac{2\sin^2\beta}{r'}\right]$$

and $T(r,\alpha) = (\cos^2\alpha/r) - 2a_{20}\cos\alpha$

$S(r,\alpha) = (1/r) - 2a_{02}\cos\alpha$

and analogously for $T(r',\beta)$, $S(r',\beta)$.

The F_{ijk} terms which are not identified above contribute to coma, line shape, and line inclination.

It is useful to divide the light path function, F, into two parts

$$F^* = F_{000} + wF_{100}$$

and

$$F^{**} = \text{the rest!}$$

Application of Fermats' principle (eq. 2, 3) to F* yields the grating equation

$$Nk\lambda = \sin\alpha + \sin\beta.$$

Application of Fermats' principle to F** yields the expressions for the optical characteristics of the image at B for a given object at A and the surface P.

The main goal of this entire exercise is to determine the relationship between A, P and B on the one hand and the resolution, $\Delta\lambda$, that one can expect from a given system on the other. The dispersive contribution to resolution, $\Delta\lambda$, caused by aberrations stemming from F**, is derived as follows:

$$Nk\lambda = \sin\alpha + \sin\beta$$

$$\left(\frac{\partial\lambda}{\partial\beta}\right)_{\alpha = \text{const}} = \frac{1}{Nk}\cos\beta$$

$$\frac{dy'}{r'} = d\beta$$

$$d\lambda = \frac{1}{Nkr'}\cos\beta\, dy'$$

The deviation of the path function in the dispersive direction is

$$\frac{\partial F^{**}}{\partial w} = \delta(\cos \gamma_y) = d(\sin\beta) = \cos\beta \, d\,\beta = \frac{\cos\beta}{r'} \, dy'$$

and in the sagittal direction

$$\frac{\partial F^{**}}{\partial l} = \frac{1}{r'} \, dz'$$

where δ ($\cos \gamma_y$) is the change in the direction cosine from the Gaussian value (see Howells, 1980).

Then

$$\Delta\lambda = \frac{1}{Nk} \frac{\partial F^{**}}{\partial w}$$

and

$$\Delta\lambda = \frac{1}{Nk}\left[wF_{200}+\tfrac{3}{2}w^2F_{300}+\tfrac{1}{2}l^2F_{120}+\tfrac{1}{2}w^3F_{400}+\tfrac{1}{2}wl^2F_{220}+lF_{111}+\tfrac{1}{2}F_{102}+\tfrac{1}{2}wF_{202}+wlF_{211}\ldots\right]$$

We have thus arrived at the goal of this section and need now simply to insert the geometric parameters, a_{ij}, in the F_{ijk} relations above to obtain the expression for $\Delta\lambda$ (w, l, α, β, etc.) for a given surface.

4.3 The Toroidal/Spherical Grating Monochromator

For toroidal grating monochromators, and for the special case of spherical grating monochromators, where $\rho = R$, the relevant expressions for the terms in the optical path function are as follows:

$$F_{020} = \frac{1}{r} + \frac{1}{r'} - \frac{1}{\rho}(\cos\alpha + \cos\beta)$$

$$F_{200} = \left(\frac{\cos^2\alpha}{r} - \frac{\cos\alpha}{R}\right) + \left(\frac{\cos^2\beta}{r'} - \frac{\cos\beta}{R}\right)$$

$$F_{300} = \left(\frac{\cos^2\alpha}{r} - \frac{\cos\alpha}{R}\right)\sin\alpha + \left(\frac{\cos^2\beta}{r'} - \frac{\cos\beta}{R}\right)\sin\beta$$

$$F_{400} = \frac{4}{r^2}\left(\frac{\cos^2\alpha}{r} - \frac{\cos\alpha}{R}\right)\sin^2\alpha - \frac{1}{r}\left(\frac{\cos^2\alpha}{r} - \frac{\cos\alpha}{R}\right)^2$$

$$+ \frac{4}{r'^2}\left(\frac{\cos^2\beta}{r'} - \frac{\cos\beta}{R}\right)\sin^2\beta - \frac{1}{r'}\left(\frac{\cos^2\beta}{r'} - \frac{\cos\beta}{R}\right)^2$$

$$- \frac{1}{R^3}(\cos\alpha + \cos\beta) + \frac{1}{R^2}\left(\frac{1}{r} + \frac{1}{r'}\right)$$

$$F_{120} = \left(\frac{1}{r} - \frac{1}{\rho}\cos\alpha\right)\frac{\sin\alpha}{r} + \left(\frac{1}{r'} - \frac{1}{\rho}\cos\beta\right)\frac{\sin\beta}{r'}$$

$$F_{220} = \left(\frac{1}{r} - \frac{1}{\rho}\cos\alpha\right)\frac{2\sin^2\alpha}{r^2} + \left(\frac{1}{r'} - \frac{1}{\rho}\cos\beta\right)\frac{2\sin^2\beta}{r'^2}$$

$$- \frac{1}{r}\left(\frac{\cos^2\alpha}{r} - \frac{\cos\alpha}{R}\right)\left(\frac{1}{r} - \frac{\cos\alpha}{\rho}\right) - \frac{1}{r'}\left(\frac{\cos^2\beta}{r'} - \frac{\cos\beta}{R}\right)\left(\frac{1}{r'} - \frac{\cos\beta}{\rho}\right)$$

$$+ \frac{1}{\rho R}\left(\frac{1}{r} + \frac{1}{r'}\right) - \frac{1}{\rho R^2}(\cos\alpha + \cos\beta)$$

$$F_{040} = \frac{1}{\rho^2}\left(\frac{1}{r} + \frac{1}{r'}\right) - \frac{1}{\rho^3}(\cos\alpha + \cos\beta) - \frac{1}{r}\left(\frac{1}{r} - \frac{\cos\alpha}{\rho}\right)^2 - \frac{1}{r'}\left(\frac{1}{r'} - \frac{\cos\beta}{\rho}\right)^2$$

$$F_{202} = \left(\frac{z}{r}\right)^2\left[\frac{2\sin^2\alpha}{r} - \frac{\cos^2\alpha}{r} + \frac{\cos\alpha}{R}\right] + \left(\frac{z'}{r'}\right)^2\left[\frac{2\sin^2\beta}{r'} - \frac{\cos^2\beta}{r'} + \frac{\cos\beta}{R}\right]$$

$$F_{211} = \frac{z}{r^2}\left[\frac{\cos^2\alpha}{r} - \frac{\cos\alpha}{R} - \frac{2\sin^2\alpha}{r}\right] + \frac{z'}{r'^2}\left[\frac{\cos^2\beta}{r} - \frac{\cos\beta}{R} - \frac{2\sin^2\beta}{r}\right]$$

and F_{011}, F_{111} and F_{102} are as given above.

The two focussing terms F_{200}, F_{020}, arise from the fact that, for a single spherical optical element at other than normal incidence, two non-coincident focii are produced: one in the meridional plane and one in the sagittal.

Thus, for a vertically deflecting spherical mirror

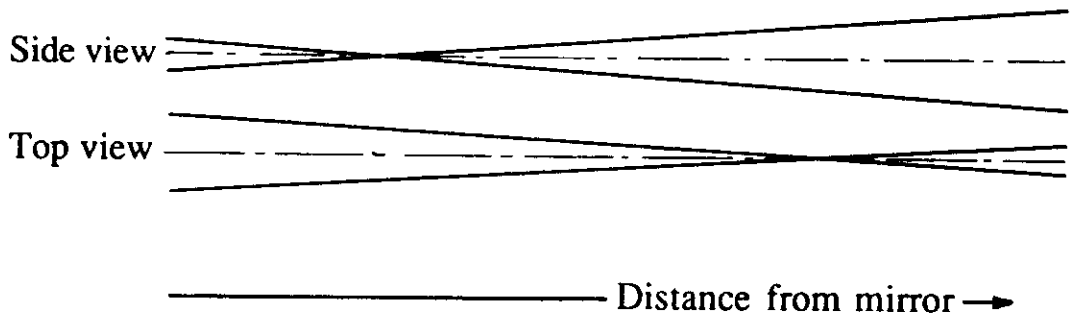

In a monochromator this is not necessarily a problem since only the focus in the dispersion plane affects the resolution. It can become a problem, however, if an absolute minimum of optical elements is required. This subject will be taken up again at a suitable point.

As shown in section 4.2, the resolution, $\Delta\lambda$, is related to the various terms by the following:

$$\Delta\lambda = \frac{1}{Nk}\left[wF_{200}+\frac{3}{2}w^2F_{300}+\frac{1}{2}l^2F_{120}+\frac{1}{2}w^3F_{400}+\frac{1}{2}wl^2F_{220}+lF_{111}+\frac{1}{2}F_{102}+\frac{1}{2}wF_{202}+wlF_{211}\ldots\right]$$

4.4 Some useful relationships

4.4.1 Magnification = M (λ)

The meridional magnification is defined by

$$M(\lambda) = \frac{s'}{s}$$

where s = entrance slit width i.e. in the dispersion direction
s' = exit slit width.

This is related to the optical parameters as follows:

$$\left(\frac{d\lambda}{d\alpha}\right)_\beta = \frac{\cos\alpha}{Nk}$$

$$\left(\frac{d\lambda}{\partial\beta}\right)_\alpha = \frac{\cos\beta}{Nk}$$

$$\Delta\alpha = \frac{s}{r}$$

$$\Delta\beta = \frac{s'}{r'}$$

$$\frac{\cos\alpha}{Nk}\Delta\alpha = \frac{\cos\beta}{Nk}\Delta\beta$$

$$\frac{s}{r}\cos\alpha = \frac{s'}{r'}\cos\beta$$

$$M(\lambda) = \frac{s'}{s} = \frac{r'}{r}\frac{\cos\alpha}{\cos\beta}$$

4.4.2 Slit limited resolution:

Entrance: $$\Delta\lambda_{ent} = \frac{1}{Nk}\frac{s}{r}\cos\alpha$$

Exit: $$\Delta\lambda_{exit} = \frac{1}{Nk}\frac{s'}{r'}\cos\beta$$

4.4.3 Contribution of rms tangent errors, σ_{TE}, to resolution:

$$(\theta = \frac{\alpha - \beta}{z})$$

$$\Delta\lambda_{Tan} = 2 \cdot \lambda \cdot \sigma_{TE} \cot \sin^{-1}\left(\frac{Nk\lambda}{2\cos\theta}\right)$$

or

$$\Delta\lambda_{Tan} = 2\frac{d}{m}\sigma_{TE}\cos\left(\frac{\Omega}{2}\right)$$

4.4.4 Diffraction limited resolution:

$$\Delta\lambda_0 = \frac{\lambda}{2kNw_o}$$

N = lines/mm
w_o = half illuminated width in dispersive direction
k = diffraction order

4.4.5 Horizon wavelength:

$$\lambda_H = \frac{2}{Nk}\cos^2\theta$$

4.4.6 Grating equation: $Nk\lambda = \sin\alpha + \sin\beta = 2\cos\theta\sin\phi$

where

$$\theta = \frac{\alpha - \beta}{2} \quad ; \quad \phi = \frac{\alpha + \beta}{2}$$

N.B. Note the sign convention for α and β! (see fig. 4.1)

4.4.7 The determination of the length of a grazing incidence mirror (grating):

r	= distance from the source to the mirror	p	= point of incidence of the central ray
$\pm m$	= ± divergence of the light beam	w_1	= nearer illuminated length of mirror
θ_g	= grazing angle of incidence of light on the mirror	w_2	= farther illuminated length of mirror
	$= \pi/2 - \theta$	N	= normal to the mirror

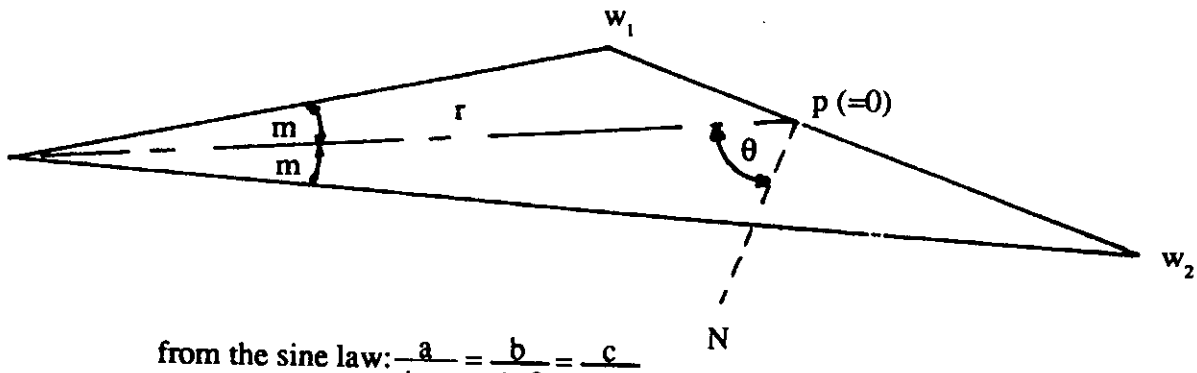

from the sine law: $\frac{a}{\sin\alpha} = \frac{b}{\sin\beta} = \frac{c}{\sin\gamma}$

$$w_1 = \frac{r \sin m}{\sin(\pi - \theta_g - m)} = \frac{r \sin m}{\sin(\theta_g + m)}$$

$$w_2 = \frac{r \sin m}{\sin(\theta_g - m)}$$

$$L = w_1 + w_2$$

For $\theta g >> m$

$$w_1 \approx w_2$$

$$\text{Length} \approx \frac{2 r \sin m}{\sin \theta_g}$$

Example:

r = 6500 mm; ± m = ± 2.5 mrad = ± 0.144°; θg = 2.5°
w_1 = 354.1 mm; w_2 = 397.4 mm
L = 751.5 mm
with the approximation one obtains

$$L \approx \frac{2 r \sin m}{\sin \theta g} = 749.0 \text{ mm}$$

4.4.8 Determination of a slit width or pinhole diameter

The width of a slit or the diameter of a pinhole may be determined by analysing the Fraunhofer diffraction pattern generated by the opening using coherent light (e.g. HeNe laser)

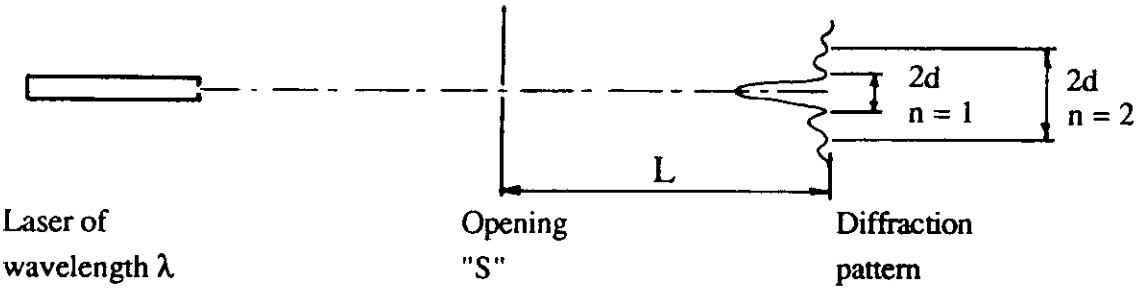

a) Slit (width much smaller than length)

$$\sin\left(\frac{d(n)}{L}\right) \approx \frac{d(n)}{L} = \frac{n\,\lambda}{S}$$

Note:

1. 2 d(n) represents the distance between intensity minima i.e. dark bands. These are more easily and accurately determined than the middle of the bright bands. "n" is the number of the dark band, i.e. first, second etc. from the central maximum.

2. The diffraction pattern is perpendicular to the slit length. It can be used to determine that the slit is horizontal to an accuracy of about 1° with the help of a plumb line.

b) Pinhole of diameter S

$$\sin\left(\frac{d(n)}{L}\right) \approx \frac{d(n)}{L} = \frac{X_n\,\lambda}{S}$$

where X_n corresponds to the zero value of the Bessel function, $J_1(X_n)$ divided by π. X_n = 1.220; 2.233; 3.238; 4.241; 5.243; 6.244; 7.245; 8.245; 9.246; 10.246 for the first ten dark rings.

The central bright spot is known as the Airy disk, encountered in the Rayleigh definition of resolution. The relative intensities of the bright bands are of the order of 1:0.05:0.02:0.01 for slits and 1:0.02:0.004:0.002 for pinholes.

4.4.9 The blaze angle of a diffraction grating

For a grating with a "saw tooth" groove profile, it is possible to choose the angle Ψ of the long side of the profile such that, for a particular wavelength, the diffraction direction coincides with the direction of specular reflection from the individual facets. This is shown in the figure below [3.1]. Note that N is the normal to the overall grating surface while N' is the normal to the individual facet.

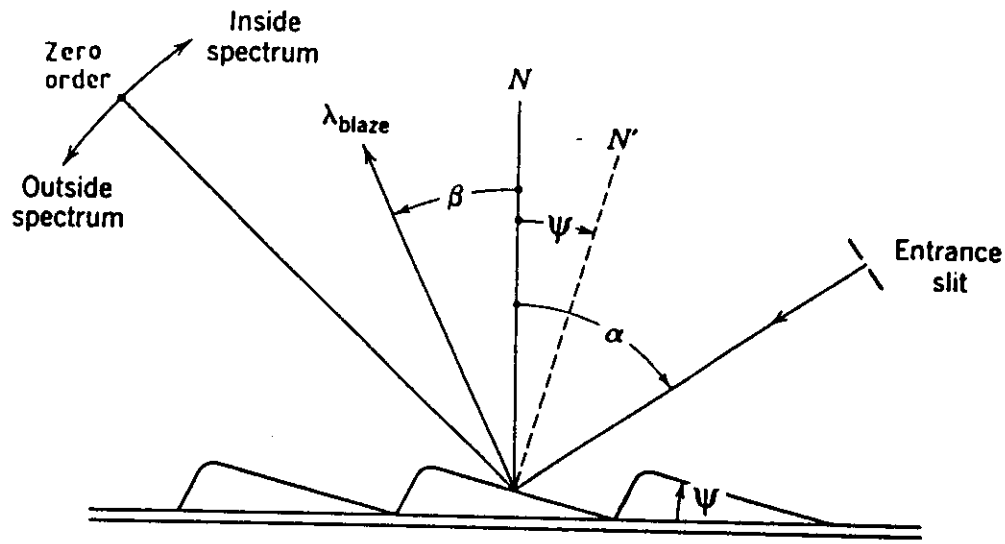

Evidently, the blaze condition is fulfilled

when $\alpha - \Psi = -\beta + \Psi$ (Note sign convention for β!)

Thus $\Psi = \frac{\alpha + \beta}{2}$.

Then, since $\lambda = \frac{2}{Nk}\cos\theta \sin\Psi$ (Eq. 4.4.6)

one finds

$$\lambda_{blaze} = \frac{2}{Nk}\cos(\alpha - \Psi)\sin\Psi$$

Ignoring other effects, a grating blazed for the wavelength λ_1 in first order (k = 1) is blazed for $\frac{\lambda_1}{2}$ in second order (k = 2) etc.

Comparison: RC-SGM with P-PGM

1. Goal: To define a high resolution monochromator for undulator radiation

2. Energy range: 90 - 800 eV

3. Boundary conditions: see extra sheet

4. Criteria: see table 4.0.1

5. Basic types of Monochromator:
   RC-SGM: Rowland circle spherical grating monochromator
   P-PGM: Petersen type (focussed at all λ's) plane grating monochromator

6. Comparisons made:
   a) Resolution for the same transmission
   b) Maximum resolution at the cost of transmission

Figure 4.5.1: **Optical Layout of a Focussing Spherical Grating Monochromator (F-SGM)**

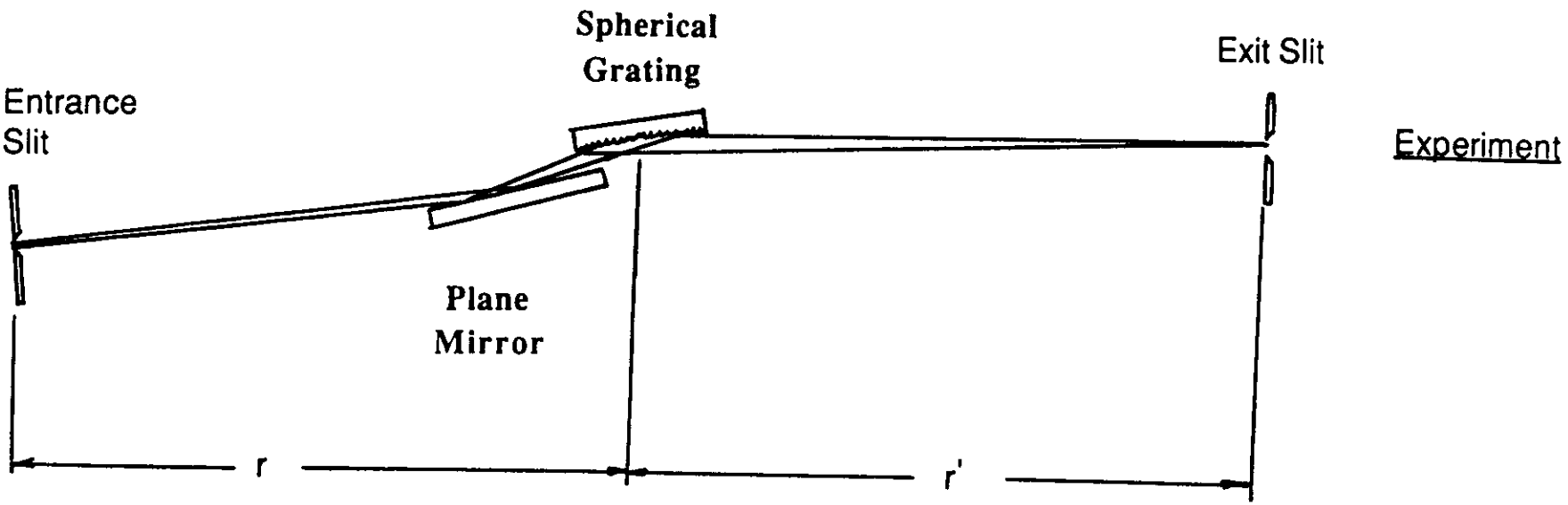

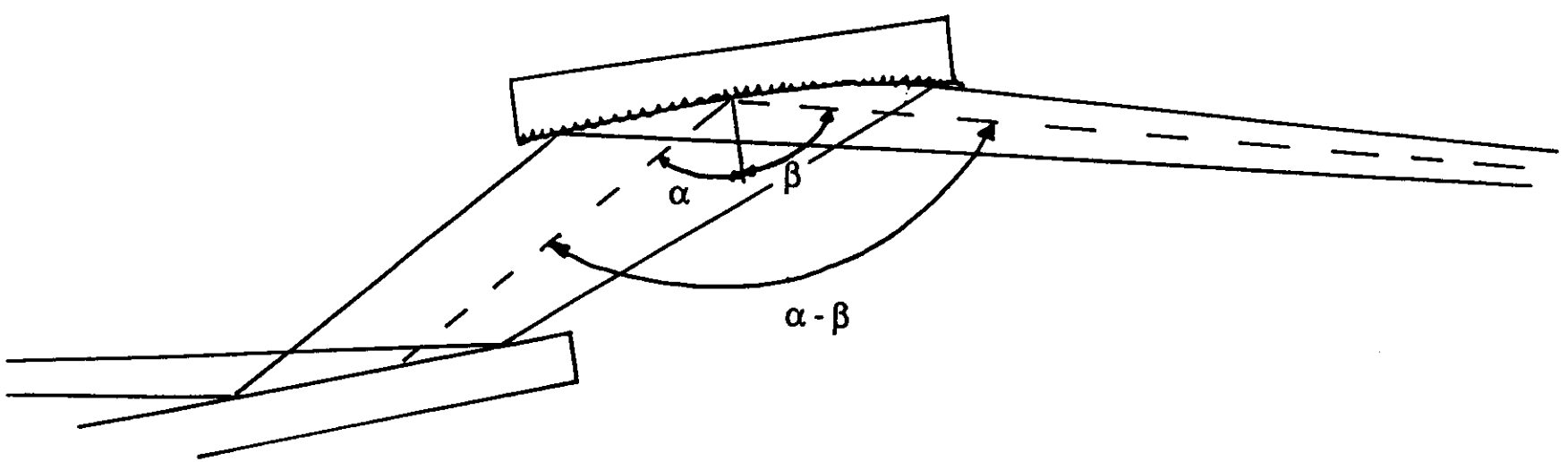

Figure 4.5.2: **Optical Layout of a Petersen Type Plane Grating Monochromator (P-PGM) [4.9]**

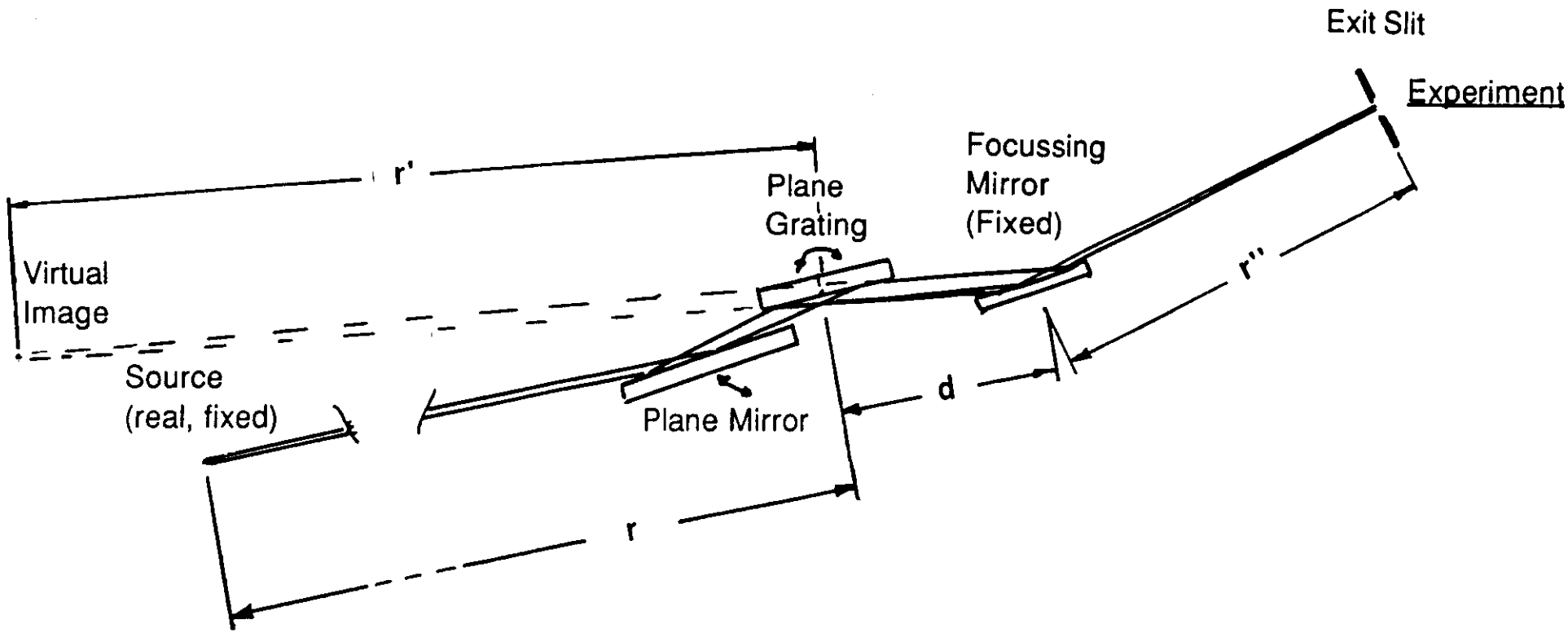

For Grating: $$-\frac{r'}{r} = \frac{\cos^2\beta}{\cos^2\alpha} = (2.25)^2 \quad \text{(Petersen)}$$

For Mirror: $$\left(\frac{1}{p} + \frac{1}{r''}\right)\frac{\cos\theta}{2} = \frac{1}{R} \qquad \text{where } p = r' + d$$

Magnification within a monochromator

i.e. optimal size of the exit slit for a given entrance slit or source size

1. Rowland Circle Monochromator

$$M = \frac{r' \cos \alpha}{r \cos \beta} \qquad \text{Eq. 4.4.1}$$

$r = R \cos \alpha$
$r' = R \cos \beta$ Rowland Conditions

$$\therefore\ M = \frac{R \cos \beta \cdot \cos \alpha}{R \cos \alpha \cdot \cos \beta} \equiv 1\ !$$

2. Petersen Type Plane Grating Monochromator

a) $\frac{r'}{r} = - \frac{\cos^2 \beta}{\cos^2 \alpha}$ F_{20} for Plane Grating

b) $M_{Grating} = M_G = \frac{r'}{r} \frac{\cos \alpha}{\cos \beta}$ Eq. 4.4.1

c) $M_{Mirror} = M_M = \frac{r''}{r'+d}$ see Fig. 4.5.2

d) $M = M_G \cdot M_M$

For constant focussing

$$\frac{r'}{r} = - \frac{\cos^2 \beta}{\cos^2 \alpha} = - c^2 \qquad \text{(Petersen [4.9], c = 2.25)}$$

then $$M = \frac{r' \cos \alpha}{r \cos \beta} \cdot \frac{r''}{r'+d} = \frac{r'}{rc} \cdot \frac{r''}{r'+d}$$

But $$r' = - r c^2$$

$$\therefore M = \frac{r''}{rc - d/c} \simeq \frac{r''}{rc}$$

5. Mirror Systems

It is the absorption coefficient of optical materials that makes the VUV and soft x-ray part of the spectrum so different from the visible: the high energy radiation (> 10 eV) interacts with essentially all materials with the result that nothing transmits and little reflects. Thus, there are no windows (for vacuum), no lenses, prisms, quarter wave plates, etc. and only poorly reflecting mirrors. Only at increasingly grazing angles is a reflected wave observed with increasing photon energy. In this section we encounter the relationships necessary to determine reflectivities, polarisation effects, etc. In addition, the focussing properties of some standard (and eminently useful!) geometries are provided. Finally, manufacturing errors and limits and their consequences are discussed.

5.1 Reflectivity and Polarisation

The relationship between the optical constants of a surface, the angle of incidence and the reflectivity is given by the generalized Fresnel equations for reflection [3.1, 5.5]:

$R_S = [(a-\cos\theta)^2 + b^2] / [(a+\cos\theta)^2 + b^2]$

= Reflectivity of the component whose E vector is perpendicular to the plane of incidence

$R_P = R_S [(a-\sin\theta\tan\theta)^2 + b^2] / [(a+\sin\theta\tan\theta)^2 + b^2]$

= Reflectivity of the component whose E vector is parallel to the plane of incidence

where

θ = Angle of incidence with respect to the surface normal

and

$$a^2 = \frac{1}{2}\{[(n^2-k^2-\sin^2\theta)^2 + 4n^2k^2]^{1/2} + (n^2-k^2-\sin^2\theta)\}$$

$$b^2 = \frac{1}{2}\{[(n^2-k^2-\sin^2\theta)^2 + 4n^2k^2]^{1/2} - (n^2-k^2-\sin^2\theta)\}$$

Hence, if one knows the optical constants of a material at some photon wavelength or energy, one can calculate the components of reflectivity at that energy.

i.e. $\tilde{n}(E) = n(E) + i\,k(E)$
where $\tilde{n}(E)$ is the complex index of refraction
$n(E)$ is the real part
and $k(E)$ is the imaginary part or extinction coefficient.

The optical constants for carbon, gold, platinum and nickel for energies between 100 - 1000 eV are shown in figure 5.1.2 [5.6].
Conversely, by measurements of the reflectivity and phase shift of s and p waves it is possible to determine the optical constants. Fortunately, for energies between ca. 30 eV and 10 keV, the optical constants for the elements can be calculated from the atomic scattering factors [5.4] Although the agreement between calculations and measurements is not always good [7.2, 7.3] (fig. 5.1.1) one can at least obtain a qualitative impression of the reflectivity from the calculations for elements for which measured data are lacking. The calculated reflectivities for many materials useful in the VUV and soft x-ray portion of the spectrum have been plotted in reference 7.4. Figure 5.1.3 illustrates the behavior to be found for carbon (C), gold (Au), platinum (Pt) and nickel (Ni) at angles of incidence of 80°, 82°, 84°, 86° and 88° for energies 100-1000 eV [5.6]. Note that at these energies and angles of incidence the Rs and Rp components are almost equal. At lower energies and steeper angles they differ dramatically (Fig. 5.1.4).

The degree of linear polarisation of radiation can be defined by

$$P = \frac{Is - Ip}{Is + Ip} .$$

where Is, Ip are the intensities of the s and p polarized radiation respectively. Radiation produced in a storage ring is almost 100% polarized: in the plane of the ring it is plane polarized with the E vector also in the plane of the ring. Above and below the plane of the ring it is elliptically polarised: that is both s and p waves are produced and exhibit a constant phase difference of 90°.

Figure 5.1.1: Comparison of Calculated and Measured Reflectivities

a) Carbon

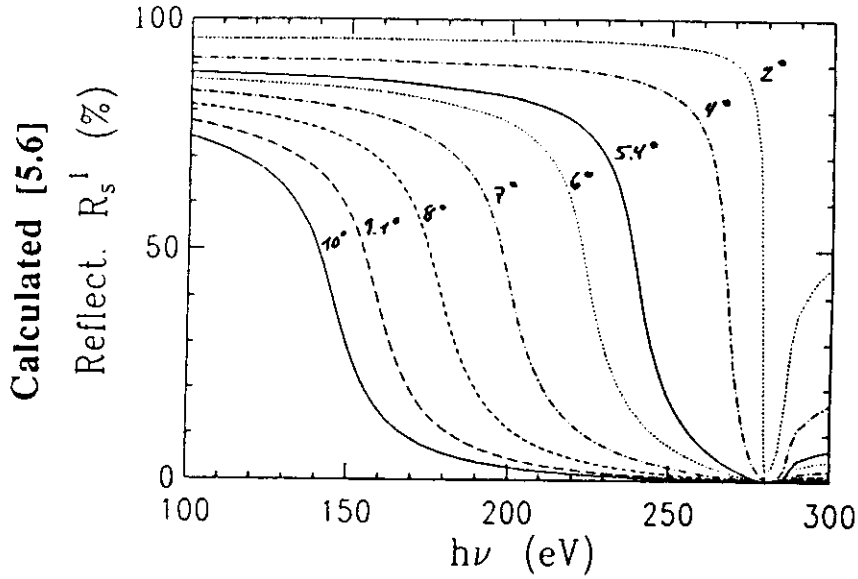

Carbon coating "Z"

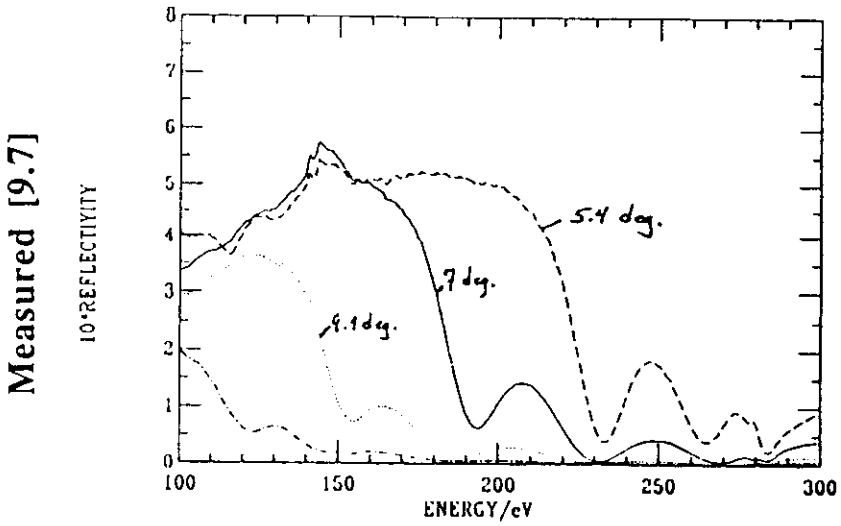

Carbon coating "T"

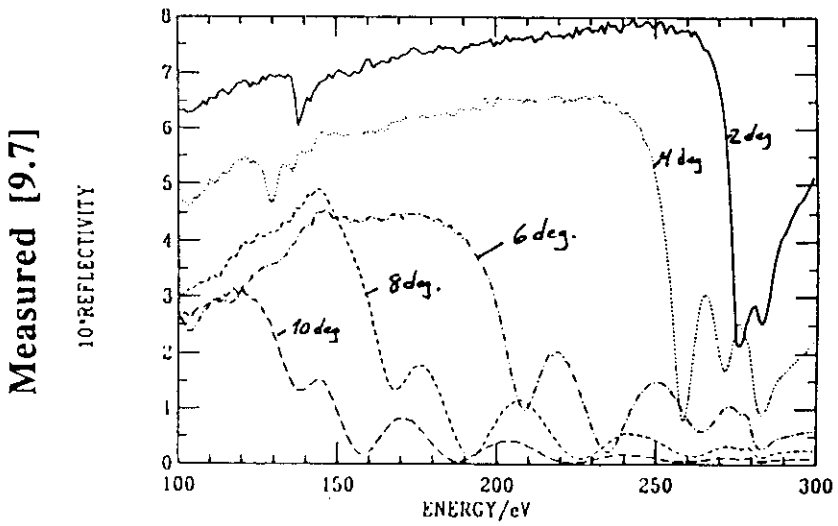

Grazing angles of incidence

Figure 5.1.1: **Comparison of Calculated and Measured Reflectivities**

b) Gold [5.6]

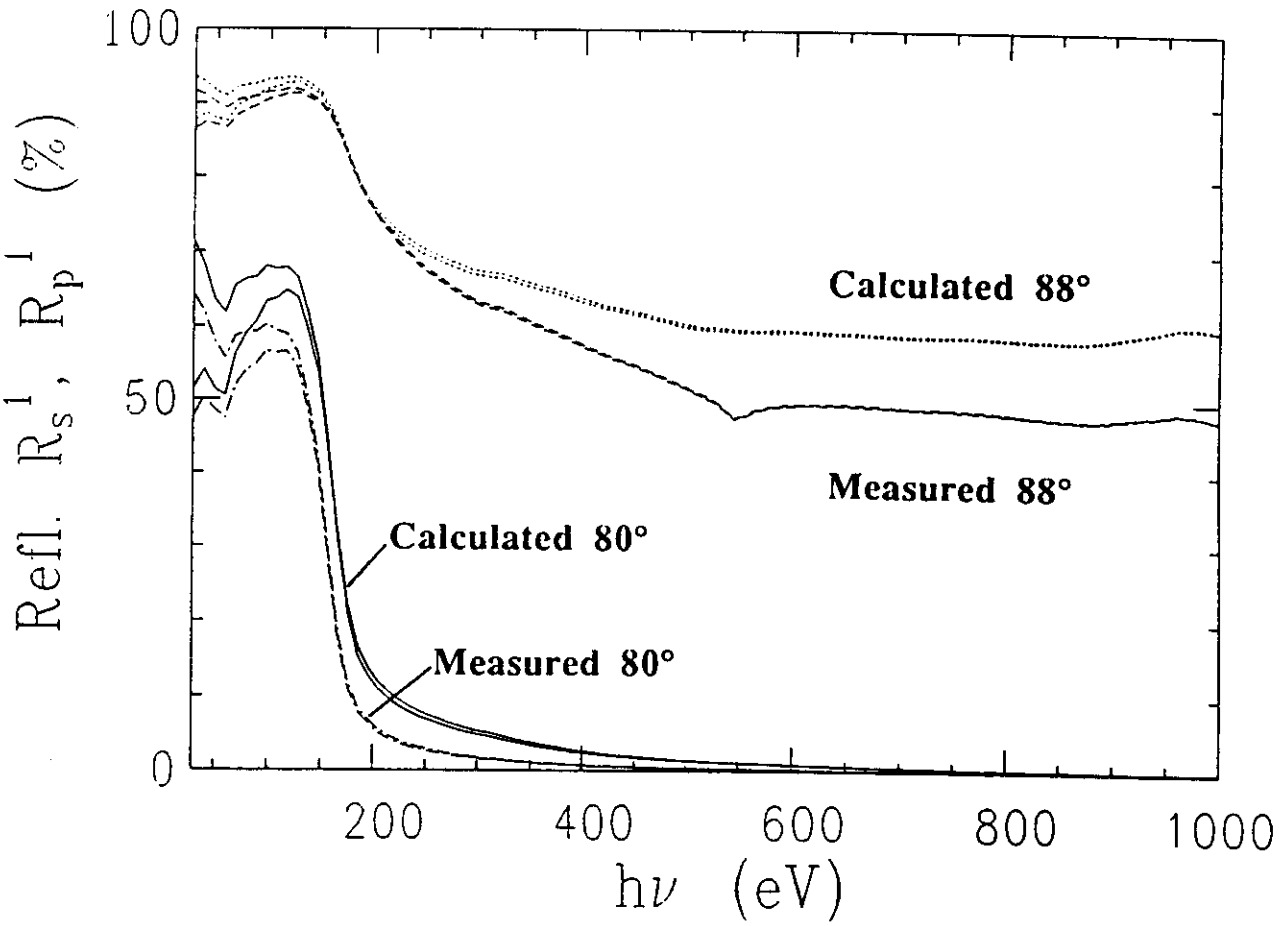

Figure 5.1.2: **The Optical Constants for C, Au, Pt, Ni [5.6]**

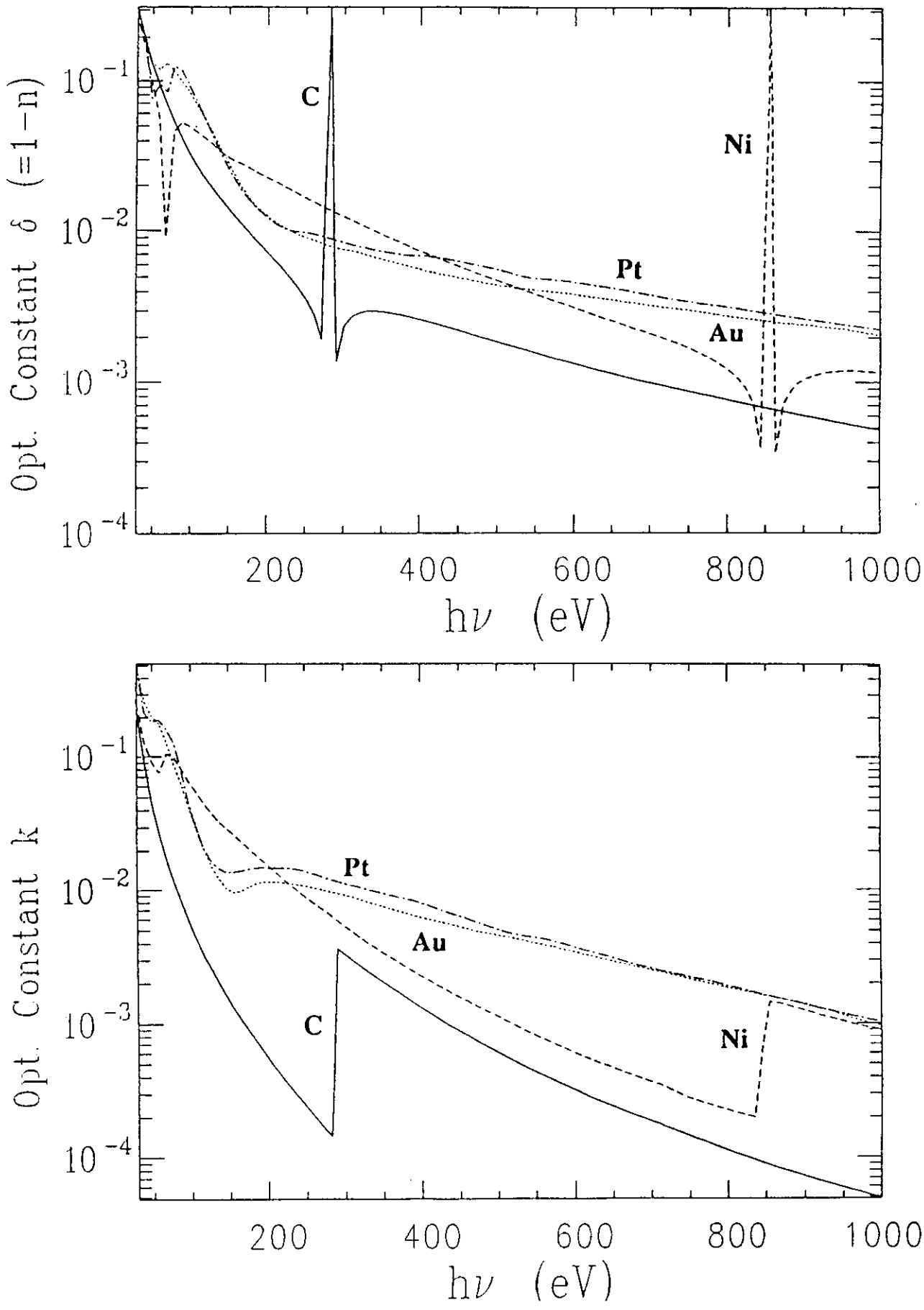

Figure 5.1.3: **Calculated Reflectivities of C, Au, Pt , Ni at Angles 80°, 82°, 84°, 86°, 88° [5.6]**

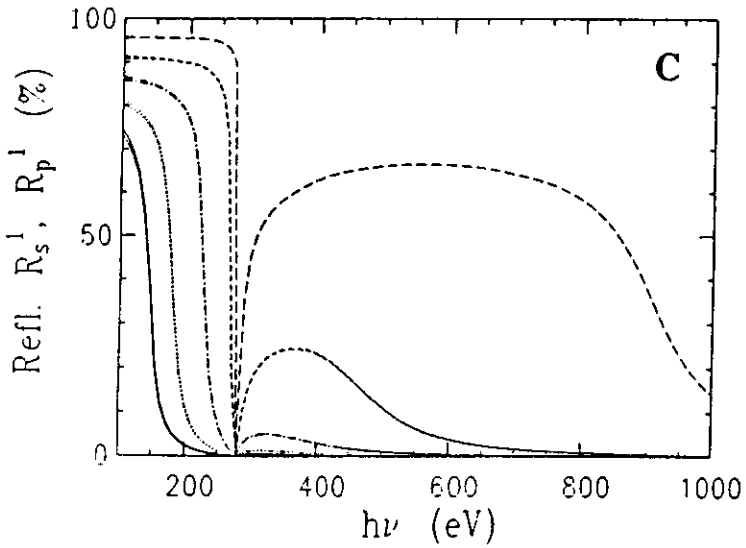

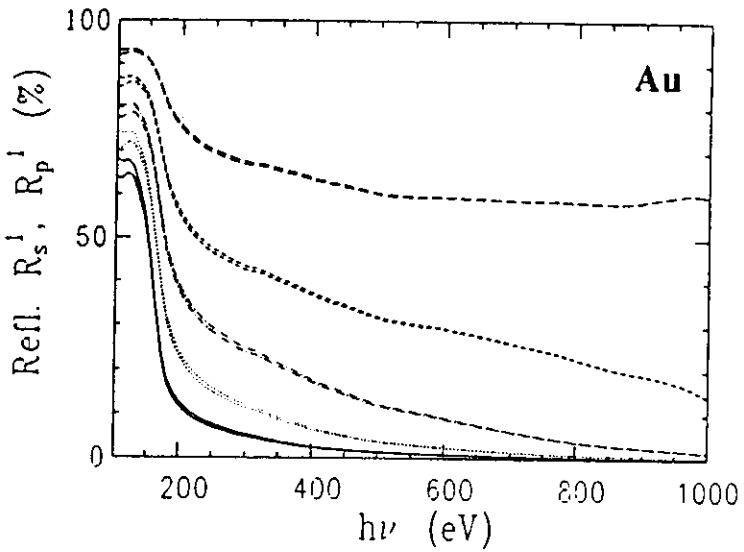

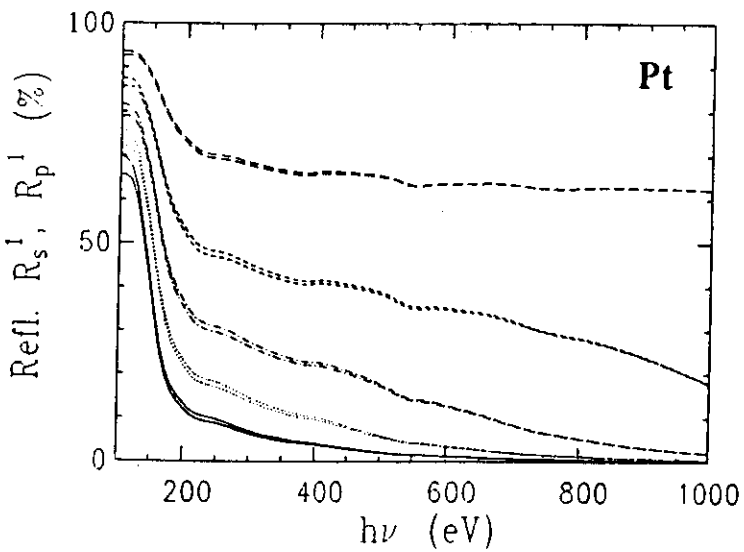

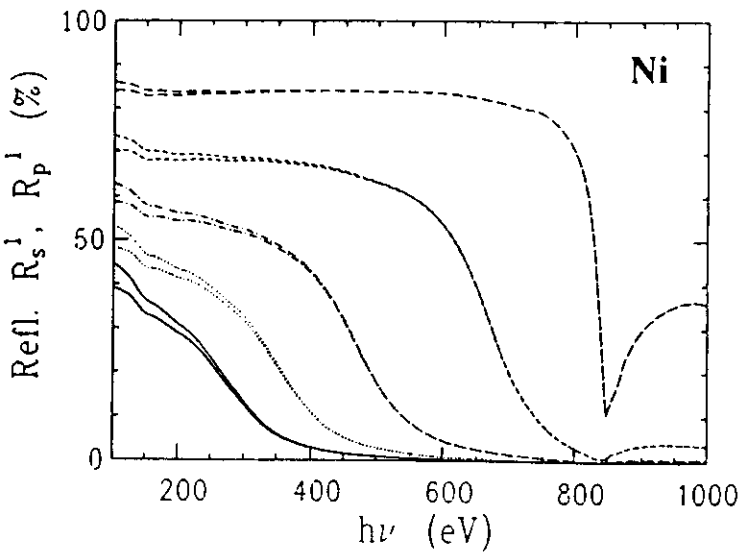

Figure 5.1.4: **Calculated Reflectivities of C, Au, Pt, Ni at Angles 50°, 60°, 70°, 80°, 88° [5.6]**

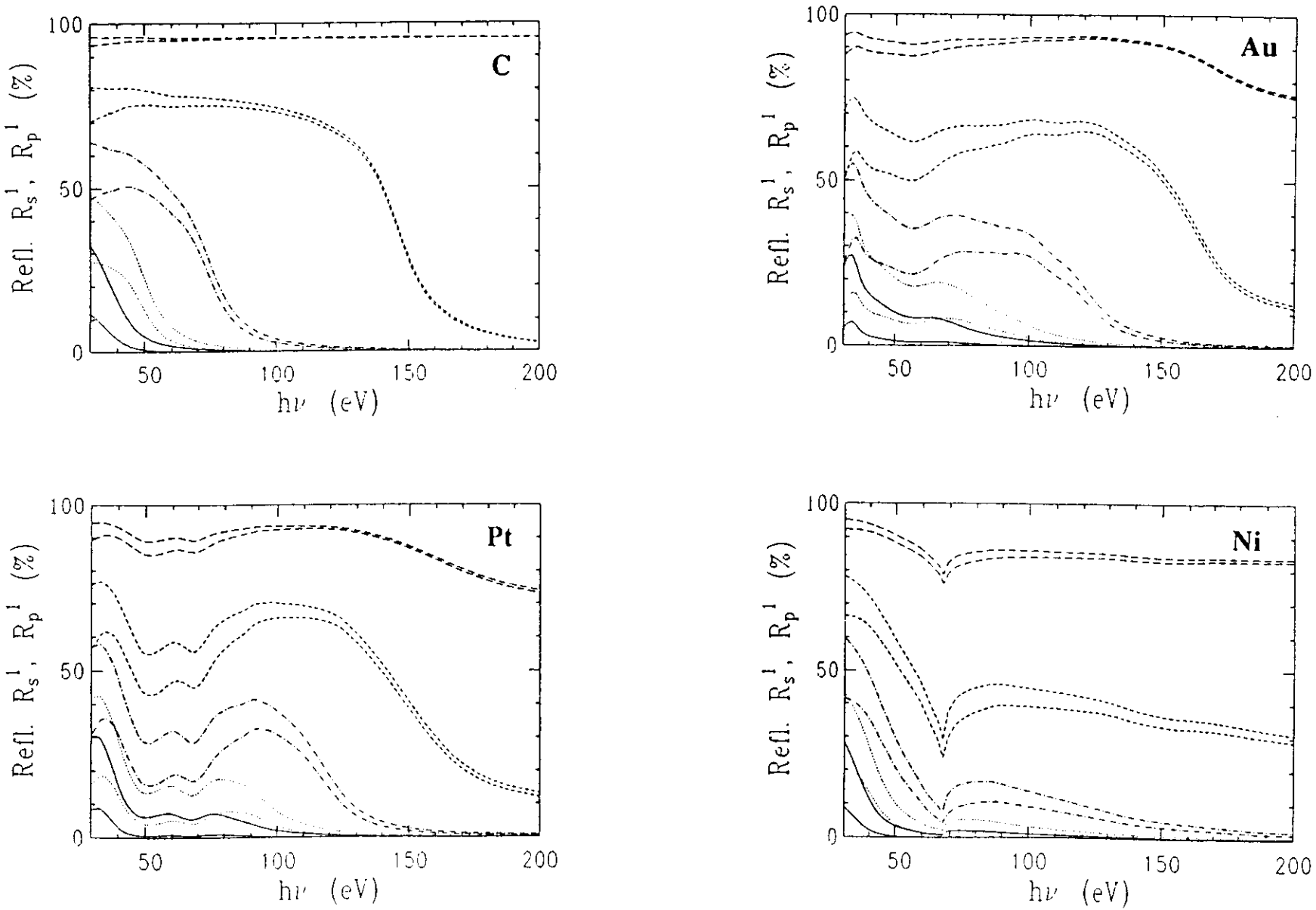

Figure 5.1.5: Elliptically Polarized Light: Various Cases [5.10]

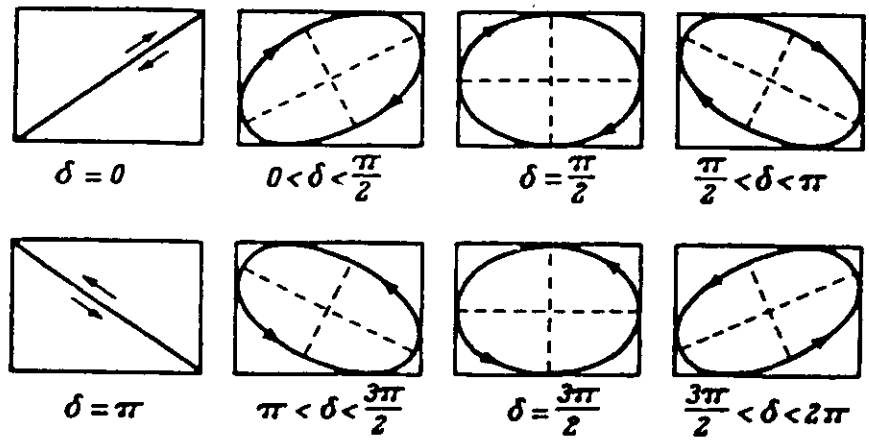

Table 5.1.1: Possible Observations with Polarized Light [5.19]

<table>
<tr><td colspan="3">A. No intensity variation with analyzer alone</td></tr>
<tr><td>I. If with λ/4 plate in front of analyzer</td><td colspan="2">II. If with λ/4 plate in front of analyzer one finds a maximum, then</td></tr>
<tr><td>1. One has no intensity variation,
one has
natural unpolarized light</td><td>2. If one position of analyzer gives zero intensity,
one has
circularly polarized light</td><td>3. If no position of analyzer gives zero intensity,
one has
mixture of circularly polarized light and unpolarized light</td></tr>
</table>

<table>
<tr><td colspan="4">B. Intensity variation with analyzer alone</td></tr>
<tr><td>I. If one position of analyzer gives</td><td colspan="3">II. If no position of analyzer gives zero intensity</td></tr>
<tr><td rowspan="2">1. Zero intensity,
one has
plane-polarized light</td><td colspan="3">2. Insert a λ/4 plate in front of analyzer with optic axis parallel to position of maximum intensity</td></tr>
<tr><td>a) If get zero intensity with analyzer,
one has
elliptically polarized light</td><td colspan="2">b) If get no zero intensity,</td></tr>
<tr><td></td><td>(1) But the same analyzer setting as before gives the maximum intensity,
one has
mixture of plane-polarized light and unpolarized light</td><td>(2) But some other analyzer setting than before gives a maximum intensity,
one has
mixture of elliptically polarized light and plane-polarized light</td></tr>
</table>

For equal amplitudes and a 90° or 270° phase difference one talks of circularly polarised light. Various cases are shown in figure 5.1.5 [5.10].

Upon reflection, the relative phase of the two components, δ, is altered by, Δ, as given by [3.1, 5.6]:

$$\tan\Delta = \frac{-2b\ \sin\theta\tan\theta}{a^2+b^2-\sin^2\theta\tan^2\theta} .$$

It is therefore easily checked mathematically if a given optical system will alter the polarisation characteristics of the incident radiation. Although the state of polarisation is defined by the amplitudes of the two linear components, a_1, a_2, and their relative phase, δ, it is convenient to use a different definition which corresponds more closely to the measured parameters, the Stokes parameters [5.17] first defined in 1852. For monochromatic radiation they are:

$S_o = a_1^2 + a_2^2 = I\ (0,0) + I\ (90,0)$ = total intensity
$S_1 = a_1^2 - a_2^2 = I\ (0,0) - I\ (90,0)$ = erect component
$S_2 = 2a_1a_2\ \cos\delta = I\ (45,0) - I\ (135,0)$ = skew component
$S_3 = 2a_1a_2\ \sin\delta = I\ (45,90) - I\ (135,90)$ = circular component

The intensities indicated $I\ (\Psi, \Delta)$ refer to the orientation of a polariser, Ψ, which produces a phase shift of Δ as analysed by a second polariser [5.6].

For monochromatic radiation which is 100% polarised, there is a further relationship between the Stokes parameters:

$$S_o^2 = S_1^2 + S_2^2 + S_3^2$$

If non-polarized light is present, as indicated by being unable to find a position of zero intensity with any orientation of a polariser with and without a quarter wave plate, the above equality is no longer valid i.e.

$$S_o^2 > S_1^2 + S_2^2 + S_3^2$$

In this case, one can define the degree of polarisation as follows

$$P = \frac{1}{S_o}(S_1^2 + S_2^2 + S_3^2)^{1/2}$$

The determination of the Stokes parameters in the VUV and soft x-ray region of the spectrum is made difficult by the lack of quarter wave plates in this region. Multiple reflectors provide the usual way around this problem, but the measurements and data evaluation are quite difficult. See for example reference 5.20 for details.

Finally, in order to give a better "feel" and understanding for this subject we refer to Table 5.1.1 which explains the observations one can make with a polariser and a quarter wave plate [5.19].

5.2 Focussing properties of single geometries

The equations relating object distance, r, image distance, r', and angle of incidence, θ, for a toroid (sphere), parabola/paraboloid and ellipse/ellipsoid are given below. For definitions see figure 5.2.1 [3.4, 5.7].

5.2.1 Toroid. For a sphere $\rho = R$.

Meridional focus $$\left(\frac{1}{r} + \frac{1}{r'}\right)\frac{\cos\theta}{2} = \frac{1}{R}$$

Sagittal focus $$\left(\frac{1}{r} + \frac{1}{r'}\right)\frac{1}{2\cos\theta} = \frac{1}{\rho}$$

For r = r' the image is identically free of coma.

5.2.2 Parabola $\Psi^2 = 4aX$

Paraboloid $\Psi^2 + Z^2 = 4aX$

where $a = f\cos^2\theta$

The location of the pole of the mirror, P, is given by

$$X_o = a\tan^2\theta$$
$$Y_o = 2a\tan\theta$$

5.2.3 Ellipse $$\frac{X^2}{a^2} + \frac{Y^2}{b^2} = 1$$

Ellipsoid $$\frac{X^2}{a^2} + \frac{Y^2}{b^2} + \frac{Z^2}{c^2} = 1$$

where $$a = \frac{r + r'}{2}$$

$$b = [a^2 (1-e^2)]^{1/2}$$

and the eccentricity, e, is given by

$$e = \frac{1}{2a} (r^2 + r'^2 - 2rr' \cos 2\theta)^{1/2}$$

The location of the pole of the mirror is given by

$$X_o = a\left(1 - \frac{Y_o^2}{b^2}\right)^{1/2}$$

$$Y_o = \frac{rr' \sin 2\theta}{2\ ae}$$

Figure 5.2.1 Three Geometries [3.4, 5.7]

Toroid

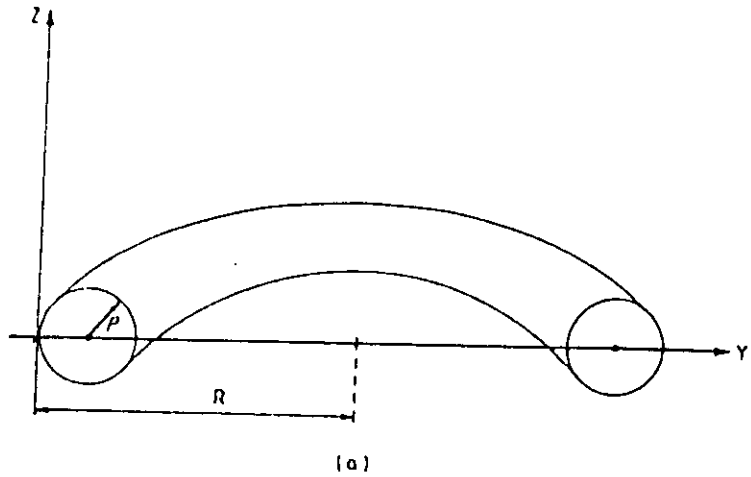

(a)

Parabola

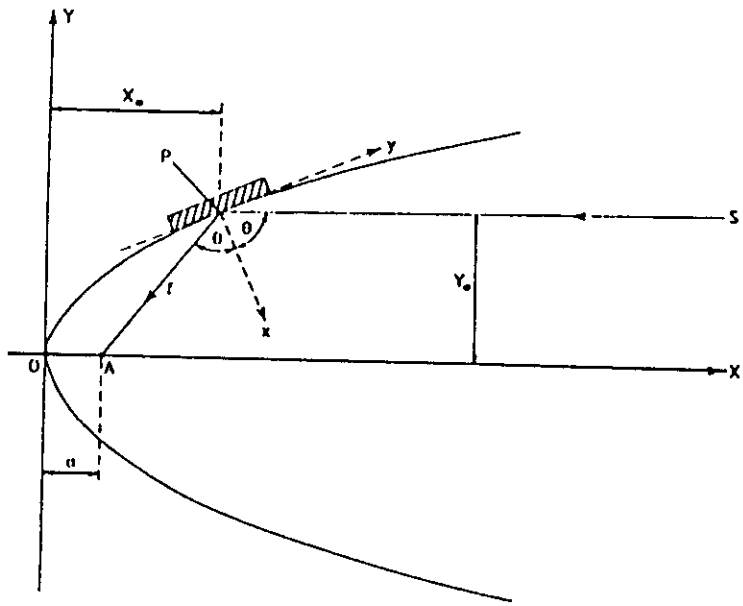

Ellipse

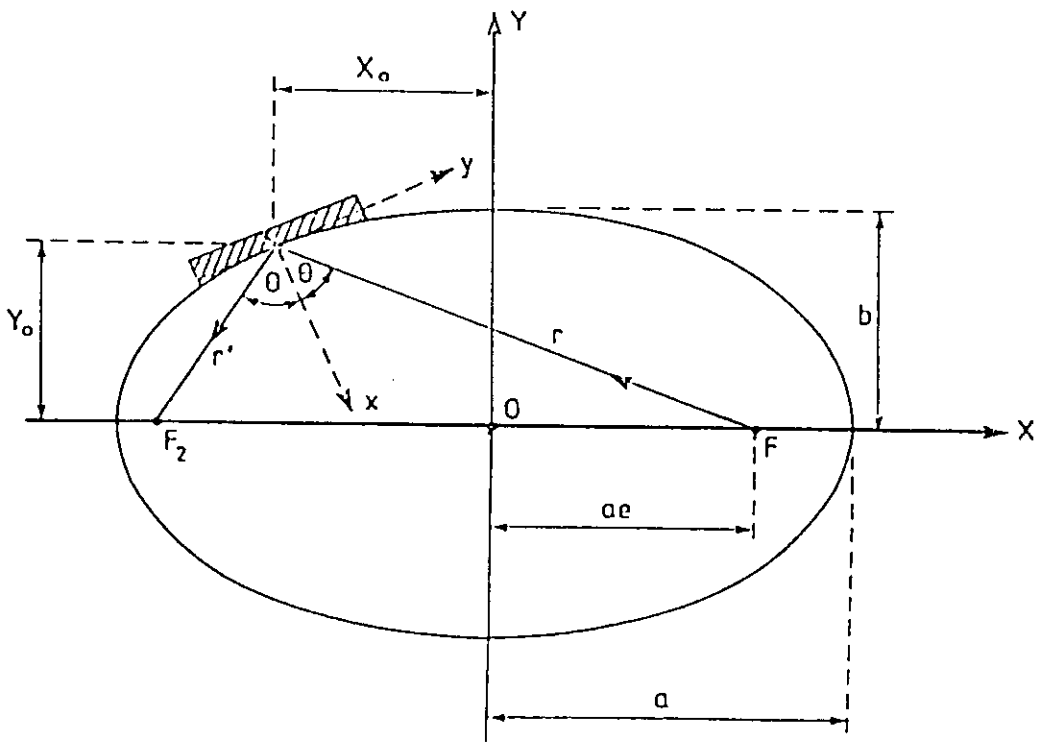

5.3 Two-Mirror Systems

Every optical system suffers from intrinsic optical aberrations which, in contrast to manufacturing limitations, can only be reduced by going to another system. A camera lens, for example, can be as simple as a pinhole, a triplett of lenses as in pocket cameras or a set of five or more individual lenses for more demanding uses. In this example, the main causes for the different systems are twofold: lens opening or f number and chromatic correction. The larger the transverse size of the lens, in comparison to the object or image distance, the more difficult the task of correcting for the intrinsic optical aberrations. Conversely, the smaller it is, the easier -- hence the pinhole lens!

In contrast to optical systems for visible light, we have seen that in the VUV and soft X-ray part of the spectrum no optical materials exist from which lenses can be made and only reflecting optics are available, and these with quite limited reflectivity (see sect. 5.1). Thus, the concept of "corrected" optical systems is of much more limited application than in the visible and, in general, instead of 3 - 7 optical elements for a "corrected" system only two elements are feasible. As will be seen in section 5.5 on figure errors, the accuracy with which a particular geometry can be manufactured is limited, plane and spherical surfaces being easier to produce to a high figure accuracy than parabolic, hyperbolic or ellipsoidal geometries. Unfortunately, the latter are generally required for "corrected" systems at short wavelengths. Finally, the ease and stability of the alignment of the elements of an optical system also depends upon their geometry, planes and spheres being the easiest having no plane of symmetry.

For the above reasons then, we will limit the discussion of two-mirror systems, designed to correct or to avoid particular optical aberrations, to the Kirkpatrick-Baez design [5.1]. Wolter, Schwarzschild and other systems, requiring the use of two aspheric mirrors will not be discussed here in monochromator design. It should be noted that their application in purely imaging systems for soft X-rays is quite widespread. Furthermore, we will assume that the monochromator has an entrance slit and that the two-mirror system is intended to focus the source on this entrance slit in the dispersion plane of the monochromator. The arguments for using an entrance slit can be

found in reference 4.20. Nevertheless, a two-mirror system is equally applicable to a monochromator with no entrance slit.

The Kirkpatrick-Baez arrangement [5.1] is shown in figure 5.3.1: two mirrors are employed to independently focus the object in the two orthogonal planes. Thus, it is possible to optimize geometry (intrinsic aberrations), figure accuracy and heat load aspects in the critical, resolution determining plane while solving or partially solving the "heat load" problem in the other plane. As will be seen in section 5.5 pp. 8 - 11, the influence of tangent errors of a mirror on the sagittal focussing characteristics of that mirror are reduced by the factor $\sin\theta_g$ where θ_g is the grazing angle of incidence on the mirror. For the application at hand θ_g is typically 2 - 3° and $\sin\theta_g$ is 0.035 - 0.052 or a factor of 29 or 19 respectively. That is, a mirror with a figure error of 1 arc sec will effectively have a figure error of $\frac{1}{29}$ or $\frac{1}{19}$ arc sec in the sagittal direction. The first mirror in a beamline, the one that receives the largest heat load, can be chosen to deflect and focus the source in the plane perpendicular to the resolution determining plane. Then, the geometrical errors of this mirror, caused by manufacturing deficiencies and by heat loading, are reduced by the factor $\sin\theta_g$ in that plane. The second mirror must intrinsically offer and, under illumination, should maintain an especially high geometric accuracy of its reflecting surface. Finally, and of great importance in the overall beamline design, the astigmatic errors of the rest of the beamline can be compensated for by the first mirror. In general, a small focus is desired at the experiment or on the exit slit of the monochromator. Thus, the first mirror can be designed to produce a focus in its plane at the rear of the beamline, if possible such that $r \approx r'$ which is free of coma in that plane. In addition, the light and heat density on the entrance slit of the monochromator are reduced, typically by a factor of 10 or so, thereby reducing the problem of deformation of the entrance slit by the heat load. Slit lengths of 10 - 30 mm do not produce new problems of consequence.

For the second mirror, one can choose between a cylindrical, a spherical or a plane elliptical mirror. The first two are essentially the same in their optical function: they produce a focus in their meridional plane according to equation 5.2.1. Sagittally, the cylinder produces no focus while the sphere focusses the source very weakly and negligibly in comparison to the other mirror in the

Figure 5.3.1: **The Kirkpatrick-Baez Optical System [5.1]**

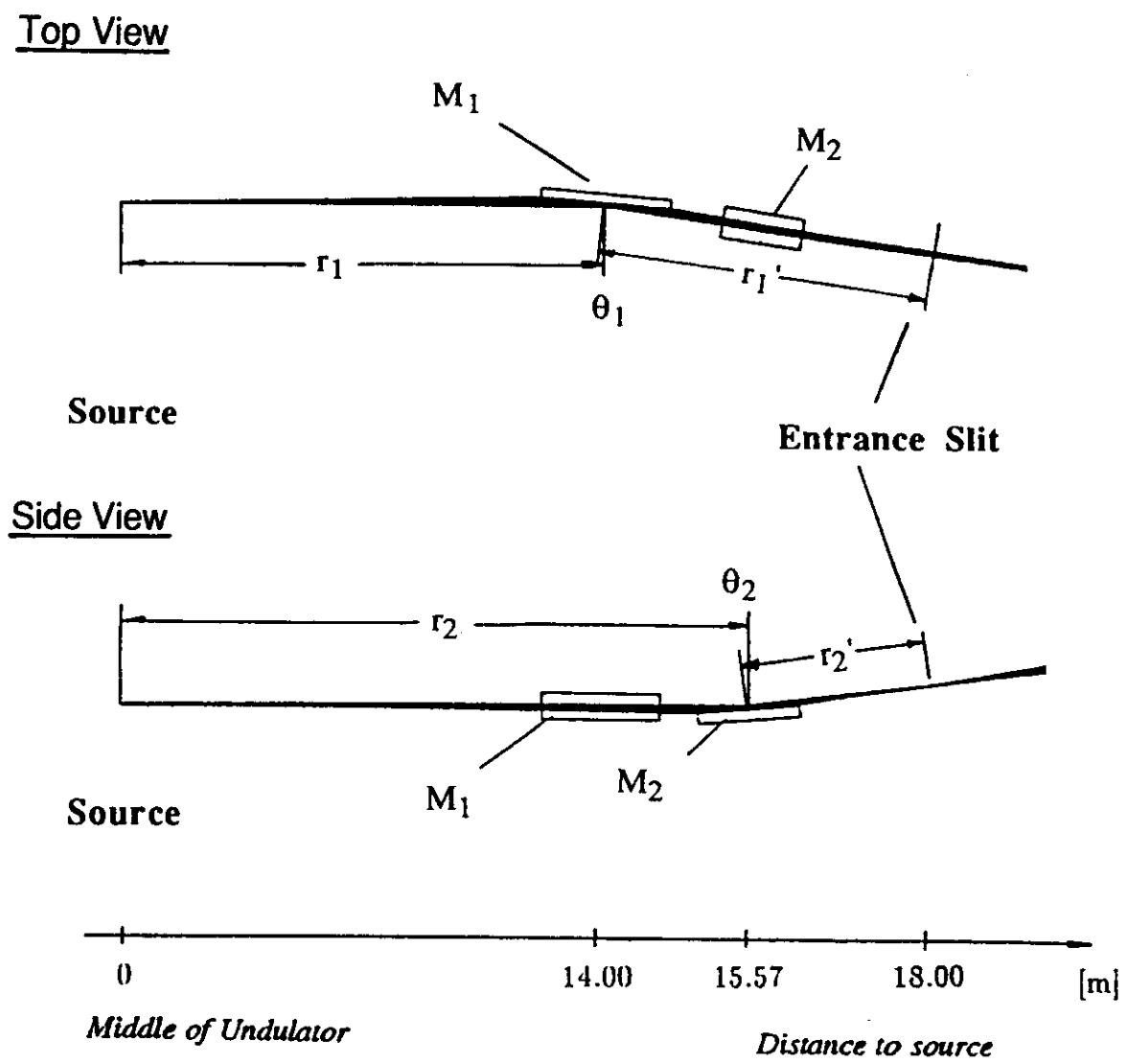

Figure 5.3.2: **The Namioka Conjugate Sphere System [5.3]**

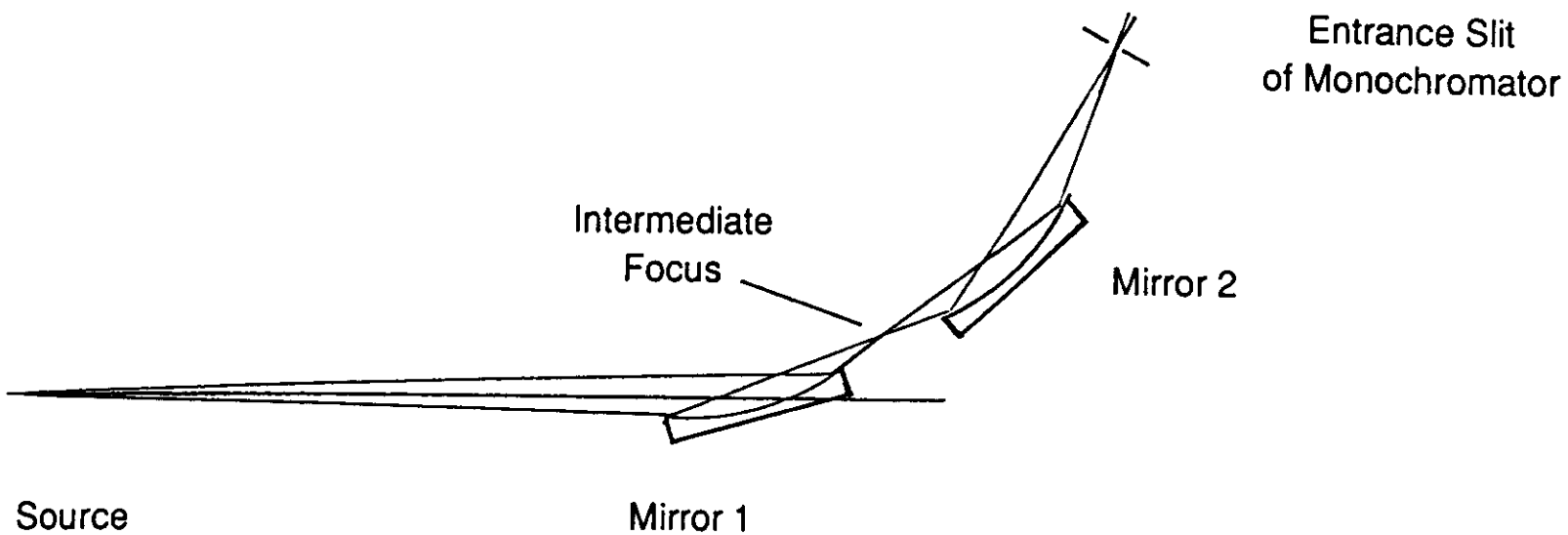

system. The advantages of the sphere over the cylinder are that it can be produced to a higher figure accuracy and that it has no symmetry plane, making alignment easier.

The plane elliptical geometry can be used for relatively large acceptance angles and produces an image free of coma and spherical aberrations. It is, however, more difficult (and expensive!) to produce, cannot be produced with as high a figure accuracy and has a very critical plane of symmetry.

A possible way around the first two criticisms of the plane elliptical geometry is presented by the Namioka conjugate sphere system in which coma and some spherical aberrations are identically eliminated [5.3]. Two spherical mirrors are employed such that an intermediary focus is produced by the first which is than refocussed by the second sphere, the aforementioned optical aberrations of the first image being cancelled by the action of the second sphere (Figure 5.3.2). Thus, the second mirror of the Kirkpatrick-Baez system is replaced by two tightly coupled spherical mirrors which produce a focus in their meridional plane.

The focussing equations for the Namioka system are:

$$\frac{1}{R_1} = \left(\frac{1}{r_1} + \frac{1}{r_1'}\right)\frac{\cos\theta_1}{2} \qquad \text{(eq. 5.2.1)}$$

and

$$M_1 = \frac{r_1'}{r_1} = \text{demagnification}$$

where R_1, r_1, r_1' and θ_1 are as usually defined and refer to the first mirror of the pair. Similarly, R_2, r_2, r_2', θ_2 and M_2 are defined for the second mirror.

The nominal demagnification of the Namioka system is given by

$$M = M_1 \cdot M_2.$$

Finally, the parameters of the second mirror are coupled to those of the first by the following relation:

$$r_2 = r_1' \frac{\tan\theta_1}{\tan\theta_2} \cdot \frac{(1-M_1^2)M_2^2}{(M_2^2-1)} \quad .$$

The focussing properties of the Namioka system are similar to those of a plane ellipse and are, for example, relatively independent of the acceptance of the system, in sharp contrast to a single sphere where coma dominates. An aperture can be located at the intermediate focus in order to mask out unwanted light. The disadvantages of this system are that two reflections are employed, that it has a plane of symmetry and that the relative position of the mirrors to each other is critical.

The optical characteristics of all three Kirkpatrick-Baez arrangements are quantitatively discussed with the help of ray tracings in the next section (section 5.4).

5.4 Extreme Demagnifications

In the quest for resolution, the size of the source of synchrotron radiation, the electron beam itself, has been significantly reduced in each new generation of storage rings. Along with the lateral dimensions, the divergence of the source has been reduced as well. That these two dimensions are coupled in the expression called emittance is an unavoidable fact (see chapter 2) and is an example of Liouville's theorem. The same holds true at the entrance slit of a monochromator: the emittance of the source cannot be reduced at the entrance slit, only the two quantities, lateral size and divergence, can be traded off against each other. Thus, in a beamline, the more the source size is reduced by an optical system, the larger the divergence of the light beam behind the slit. If no light is to be lost, the grating and mirrors in the monochromator must be made larger thereby increasing the problems of optical aberrations, figure errors and costs. This situation is shown in figure 1.1.1 of chapter 1. In addition to this, the ability of an optical system to reduce the size of the source decreases with increasing demagnifications. In order to illustrate this point, a ray-trace study has been made of three systems (Kirkpatrick-Baez) used to reduce the size of a realistic undulator source on a storage ring of the third generation. Only the dispersion plane is considered, the sagittal direction being irrelevant for the study. Although an extended source such as that in an undulator is more difficult to demagnify than a dipole source, the problematic is similar. The rest of this section is taken up with this study.

The source characteristics have been worked out for an undulator on a storage ring of the third generation and are given in table 2.5.5 of chapter 2. As shown there, the relevant parameters for ray trace studies are

σ_x	= 0.220 mm
σ_y	= 0.042 mm
z	= 4100 mm (not r.m.s.!)
σ'_{HSR}	= 0.080 - 0.160 mrad
σ'_{VSR}	= 0.055 - 0.110 mrad
r	= 17000 mm.

For the study two values of σ'_{VSR} have been used in order to test the systems for sensitivity to divergence: σ'_{VSR} = 0.040 and 0.080 mrad.

The idea is to determine the size of the entrance slit necessary to accept all of the SR from the source. Hence, the effective source size (95 % or 4 σ'_{VSR}) is 0.168 mm. An effective demagnification of 10 would mean that the entrance slit must be opened to 17 μm. If a slitwidth of 10 μm is necessary for the desired resolution, an effective demagnification of 17 is required. As shall be shown, the nominal demagnification, r/r', does not correspond well to the effective demagnification.

Shown in figure 5.4.1 are the point diagrams for a simple sphere with a nominal demagnification of 24. Immediately evident is a large coma tail resulting from the very asymmetric system ($\frac{r}{r'} = 24$). Equally evident is the fact that the extent of this tail is relatively independent of the figure error of the mirror, σ_{TE}. Since the coma aberration scales with the square of the illuminated length of the mirror, it should be significantly reduced if the acceptance, σ'_{VSR}, is reduced. This is shown in figure 5.4.1c. The effective demagnifications are found to be 168/37 = 4.5, 168/53 = 3.2 and 168/35 = 4.8 for the three cases respectively. A perfect sphere ($\sigma_{TF} = 0$) and an acceptance of 0.040 mrad yields an effective demagnification of 168/15 = 11! These results are summarized in figure 5.4.4a. The difference between the nominal demagnification and the effective demagnification is apparent. One should not forget that the divergence of the SR behind the slit has been increased, in this case by a factor of roughly 24! This too is easily shown with the help of raytraces. Thus, we conclude that a strong demagnification with a sphere is not only ineffective but impossible for the source under study!

The same approach was used for a plane elliptical mirror and the results shown in figure 5.4.2 and summarized in figure 5.4.4b. The line shape is much better than for a sphere because of the absence of coma but one must expect that the figure errors, σ_{TE}, are larger than for a sphere. Geometric errors resulting from a heat load would be the same in both cases making the effective figure error for the sphere more like that of the plane ellipse. Also seen in figure 5.4.4b is the insensitivity of the plane ellipse to acceptance, again resulting from the absence of coma. The best realistic effective demagnification is 168/29 = 5.8 for σ_{TE} = 1 sec. A perfect mirror would yield 168/12 = 14.

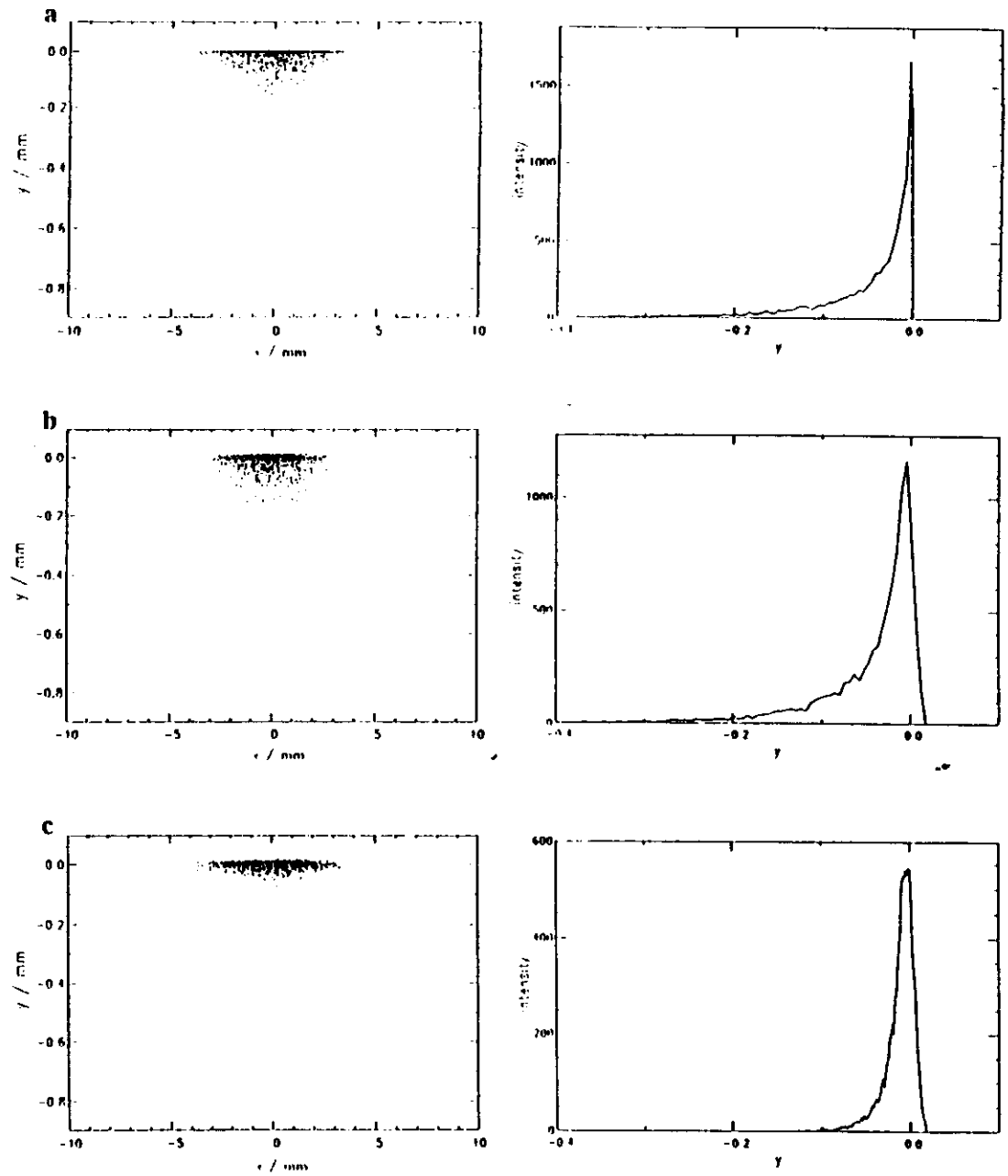

Figure 5.4.1: Focussing Characteristics of a Spherical Mirror

To the left the spot diagram. To the right the integrated vertical profile. Angle of incidence θ = 87.5°.

a) Demagnification = 24, σ_{TE} = 0, σ'_{VSR} = 80 μrad
b) Demagnification = 24, σ_{TE} = 1 sec, σ'_{VSR} = 80 μrad
c)) Demagnification = 24, σ_{TE} = 1 sec, σ'_{VSR} = 40 μrad

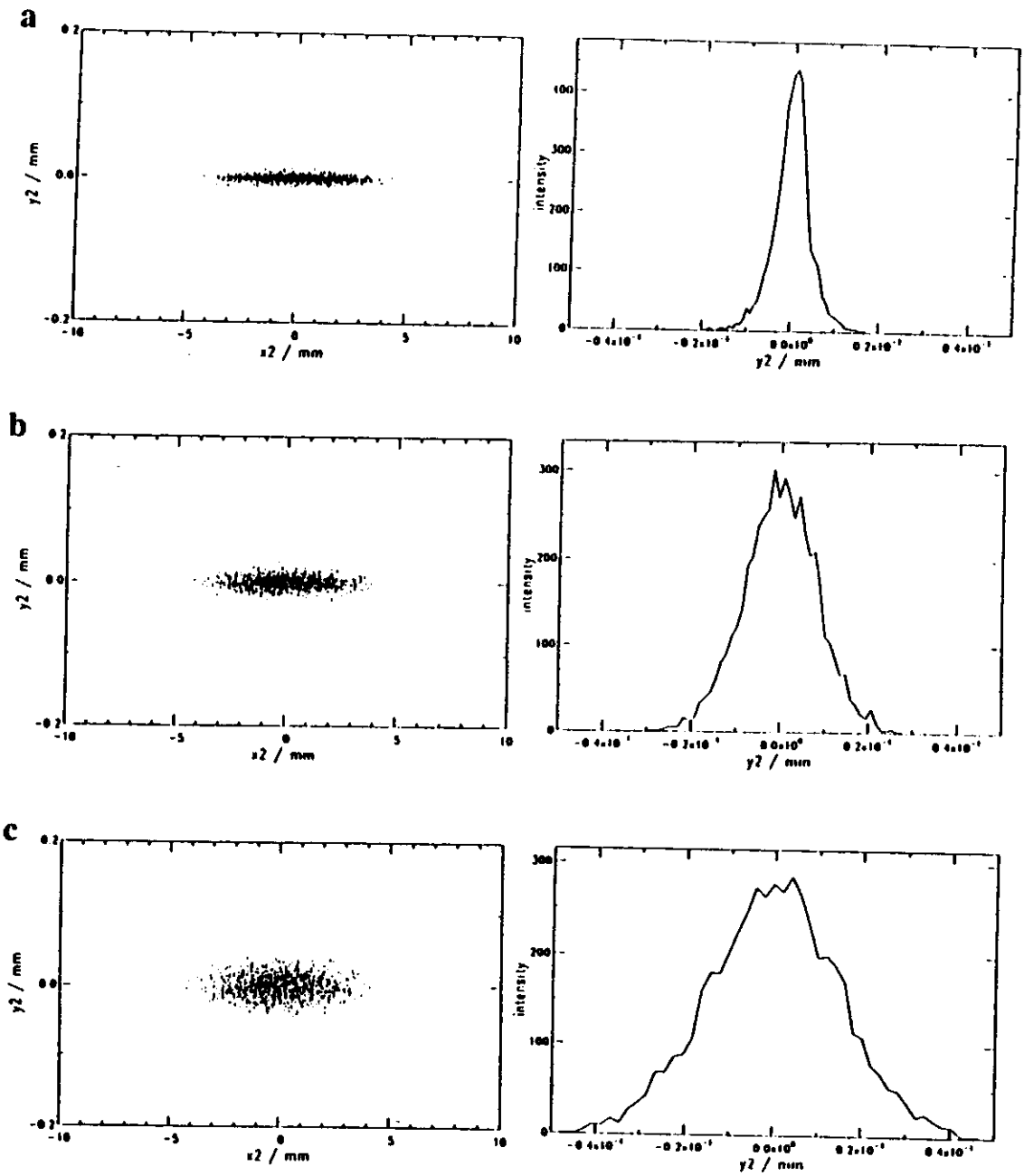

Figure 5.4.2: Focussing Characteristics of a Plane Elliptical Mirror

To the left the spot diagram. To the right the integrated vertical profile. Angle of incidence θ = 87.5°.

a) Demagnification = 24, σ_{TE} = 0, σ'_{VSR} = 80 μrad
b) Demagnification = 24, σ_{TE} = 1 sec, σ'_{VSR} = 80 μrad
c) Demagnification = 24, σ_{TE} = 2 sec, σ'_{VSR} = 80 μrad

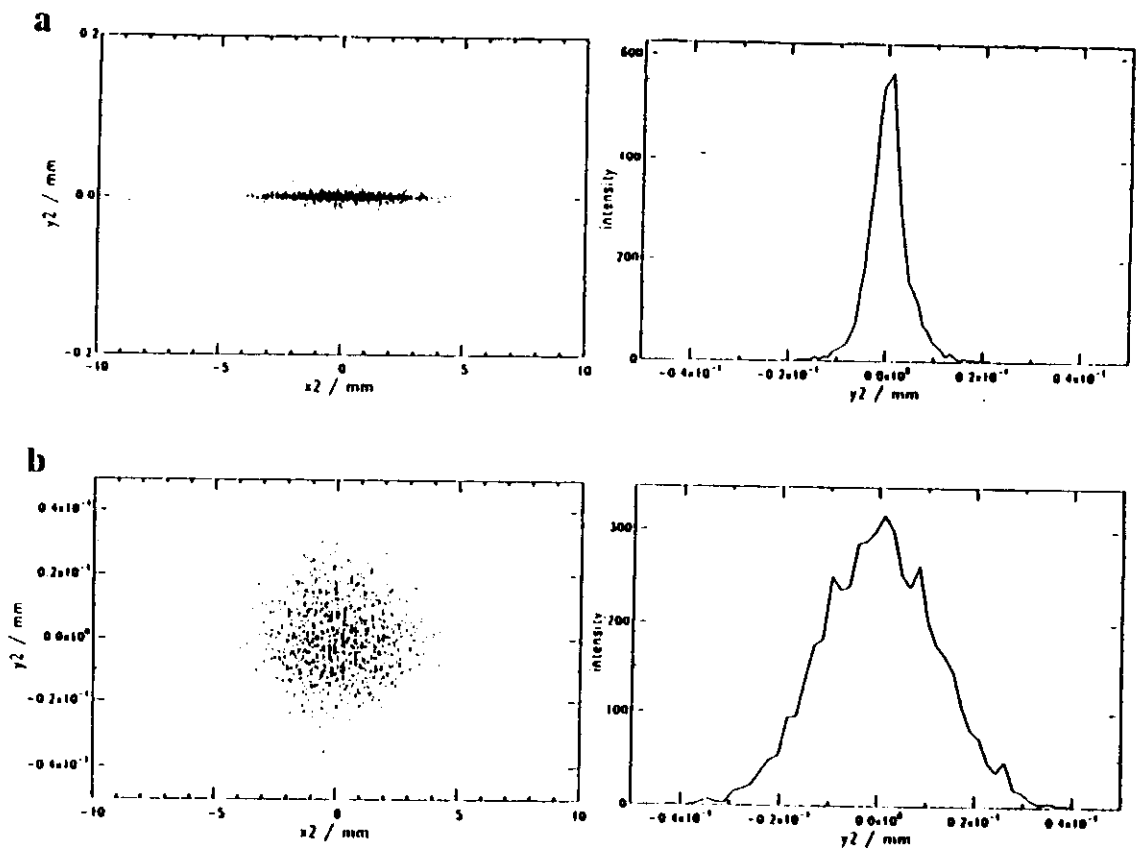

Figure 5.4.3: Focussing Characteristics of a Conjugate Sphere System

To the left the spot diagram. To the right the integrated vertical profile. Angle of incidence on each mirror θ = 88.0°.

a) Demagnification = 24, σ_{TE} = 0, σ'_{VSR} = 80 μrad

b) Demagnification = 24, σ_{TE} = 1 sec, σ'_{VSR} = 80 μrad

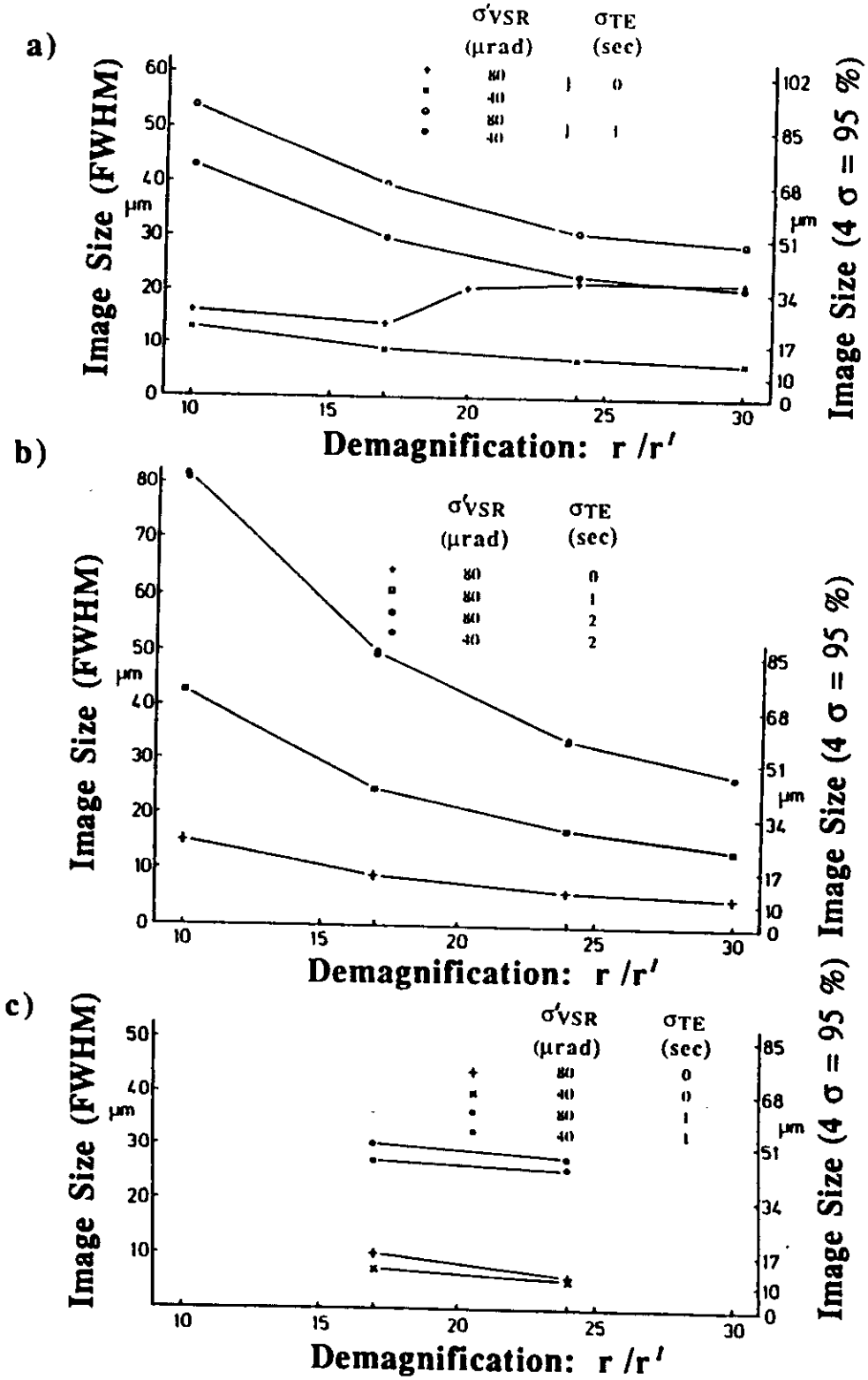

Figure 5.4.4: Demagnification of an Undulator Source on an Entrance Slit

Vertical image size as a function of demagnification for several tangent errors (σ_{TE}) and vertical acceptances (σ'_{VSR}). Source characteristics are given in table 2.4.4.
(a) Spherical mirror. (b) Plane elliptical mirror. (c) Conjugate sphere system.

The data for the conjugate spheres are shown in figures 5.4.3 and 5.4.4c. As seen in the former, the line shape is similar to that of the system with the plane elliptical mirror, the coma aberration of each sphere cancelling with that of the other. Only a weak dependence on acceptance is to be seen. The effective demagnifications are 168/48 = 3.5 (σ_{TE} = 1 sec) and 168/12 = 14 for perfect mirrors.

Making similar comparisons for a nominal demagnification of 10 yields the following results (with σ_{TE} = 1 sec and 0 sec respectively):

Spheres	168/89 = 1.9	effective demagnification
	168/28 = 6.0	effective demagnification
Plane ellipse	168/72 = 2.3	effective demagnification
	168/24 = 7.0	effective demagnification

In this case the resulting divergence is smaller and, in the case of the sphere, the line shape is much better.

In fact, it is to be recommended that a still smaller demagnification be employed in real systems. By choosing a demagnification of 5 - 8, one can easily show that a perfect sphere is almost as good as a perfect plane ellipse. Since the former can be manufactured with a better figure and at a lower cost than the latter and is more easily adjusted, there is little incentive to employ a plane ellipse for the premirror system to a monochromator. That the conjugate sphere system offers no advantage at such modest demagnifications should be evident from the foregoing.

5.5 Figure Errors

The equations given in other sections for describing mirror and grating geometries are for perfect surfaces. There we are confronted with optical aberrations stemming from the inability of particular geometries to produce a perfect image. In fact, however, it is not possible to obtain such surfaces from manufacturers and additional sources of optical aberrations must be considered. Thus, the designer of an optical system must evaluate the effect of deviations from a perfect geometry on the performance of the system. Such an evaluation is made difficult by the fact that often neither the manufacturer nor the user of the optical elements is in a position to determine the extent and nature of the imperfections - or only with great difficulty and incompletely. This is especially true in the vacuum ultraviolet and soft x-ray regions of the spectrum. The following points highlight the new situation:

a) The optical relations are different from those relevant to the visible region resulting from the necessity of employing grazing angles of incidence instead of (near) normal angles of incidence.

b) The most relevant optical tests can only be made with light of the wavelengths of interest. Thus, sources, vacuum systems and corresponding detectors are required. Most manufacturers and indeed users do not have such systems at their ready disposal.

c) With the coming of synchrotron radiation sources, the failings of the optical fabrication techniques have been brought to light (!). The requirements on mirrors and gratings for VUV and soft x-ray optics have forced manufacturers and users alike to develop measuring and test methods for optical components.

d) The availability of fast and inexpensive computers has made possible the development and widespread use of programs which geometrically trace the path of a ray of light through arbitrarily complicated optical systems. With such ray trace programs it is possible to deal with complex geometries of sources and optical elements and with optical errors associated with the latter (see e.g. references 1.2, 1.3).

Coming back to the question of errors in the geometry, it is necessary to distinguish between two types of errors:

1. Errors whose period (length) is comparable to the dimensions of the optical element and
2. Errors whose period is irregular and is much shorter than the dimensions of the optical element.

Errors of the first type must be considered in terms of the geometry of the optical element: a spherical mirror is specified as having a radius of curvature of, say, 100 m but in fact has somewhat different radii depending upon what portion of the mirror is measured. This is not a random error and, hence, cannot be treated as such. By masking out certain portions of the mirror it may be possible to achieve the performance of a nearly perfect mirror of R = 100 m.

Errors of the second type include such things as irregular machining marks on the one hand and residual roughness on the other. These two sorts of errors differ in their spatial frequency but can be displayed in a power spectrum of the surface (Fig. 5.5.1). If such data are available to the manufacturer, it may be possible to locate the source of a particular frequency in the manufacturing process and to reduce or eliminate it.

Errors of the first type are very common and cannot be treated in a statistical fashion. Each mirror or grating will have its own characteristics which cannot be extrapolated from general considerations. Its character may be discovered by examining its performance piecewise, by masking off the rest [5.7]. An example of such a case is shown in figure 5.5.2. In the 1980's highly precise measuring instruments were developed enabling one to ascertain this type of error [5.12, 5.13]. Unfortunately, such instruments are very expensive and only a few exist in the entire world at the present (1991). With the measurement data of such instruments the manufacturer can then rework the substrate thereby, iteratively, improving the basic geometry enormously. In practice, it is not uncommon for users to empirically find the best portion of a mirror or grating and to occlude the rest, when the additional performance is worth the cost in photon flux.

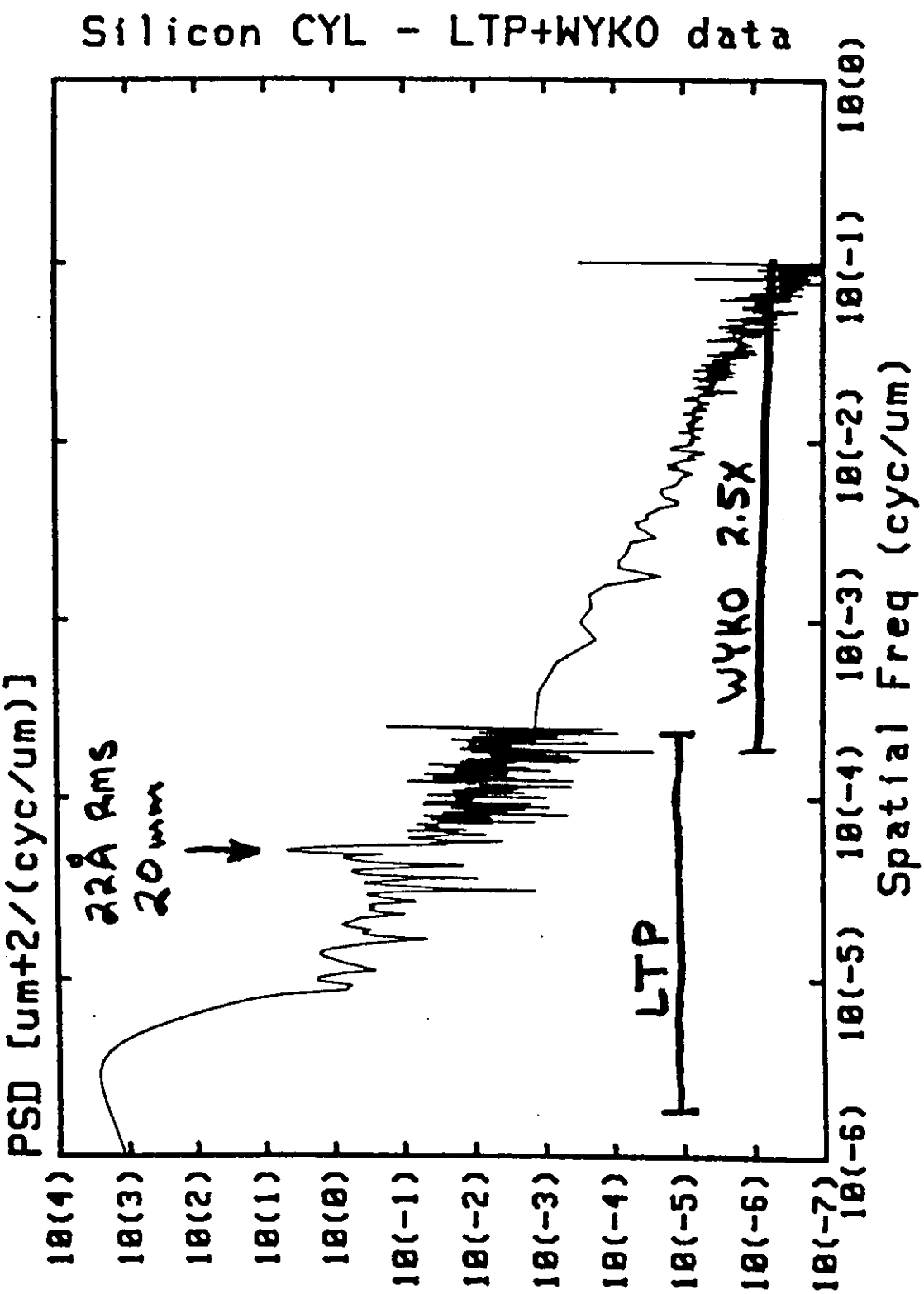

Figure 5.5.1: Power Spectrum of Surface Errors [5.11]

Figure 5.5.2: **Example of Figure Error of the First Type [5.12]**

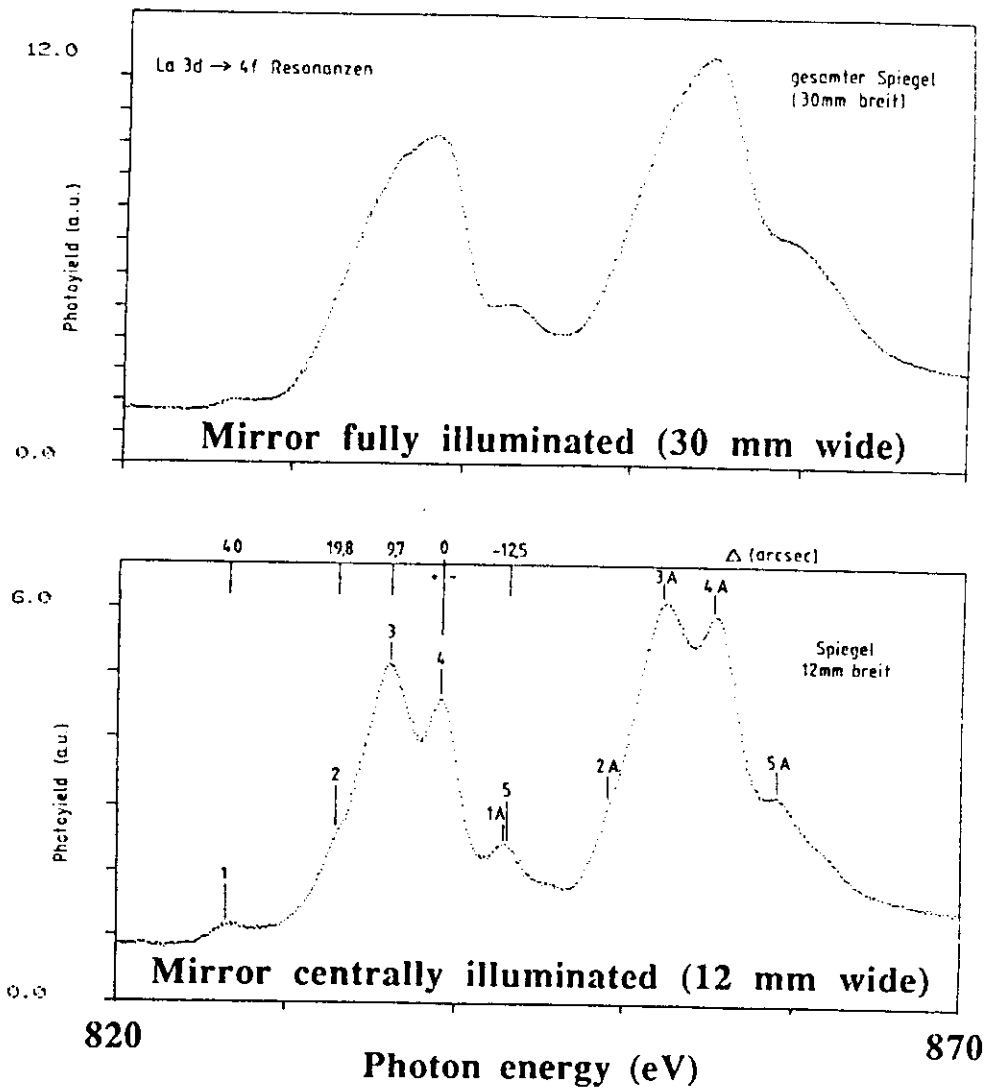

Photoyield spectrum of the La $3d_{3/2, 5/2} \rightarrow 4f$ resonances with a fully and a partially illuminated mirror. The well known spin-orbit pair is seen to appear five times. The corresponding (systematic) tangent error is indicated. The numbers correspond to the areas of the mirror given below.

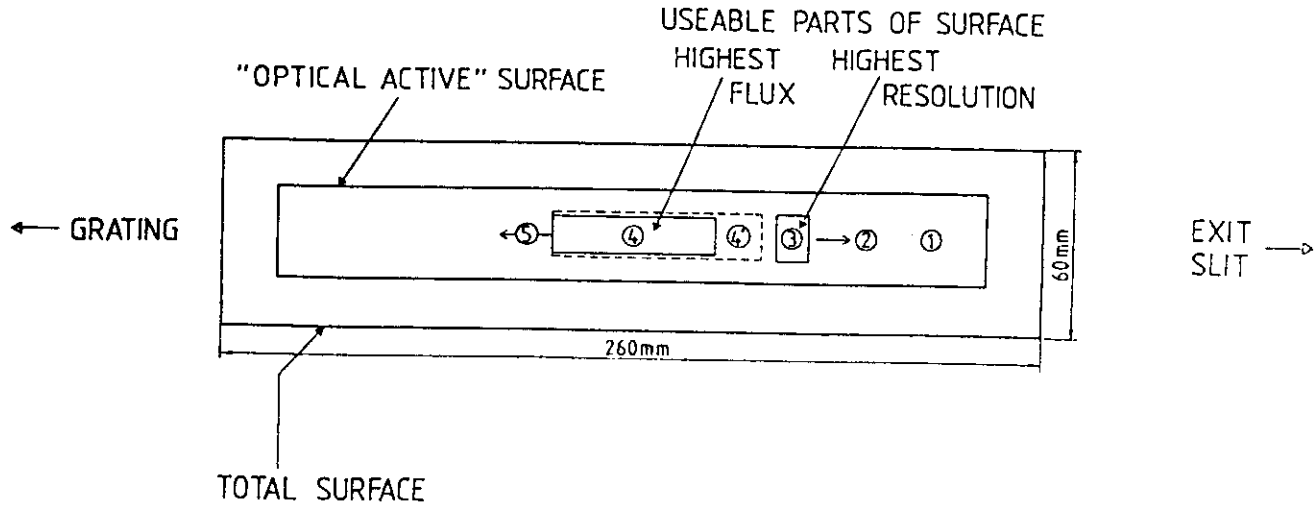

Errors of the second type are assumed, for simplicity, to obey a Gauß distribution and can, therefore, be dealt with mathematically in a straightforward fashion [5.9 - 5.11, 5.14 - 5.16]. At this point it is convenient to make a further subdivision of errors. Errors of the second type which contribute to the specular image we call, along with errors of the first type, figure or tangent errors. Thus we have systematic figure (tangent) errors (first type) and random figure (tangent) errors. Errors of the second type which do not contribute to the specular image but instead to scattered light we ascribe to surface roughness. Errors of this type will be discussed briefly in section 5.4.

Random figure errors are easily dealt with in ray-trace programs if their σ_{TE} or r.m.s. value of the random scatter of the tangents over the surface is known (see e.g. Ref. 1.3). Moreover, given σ_{TE}, one can readily estimate their effect on the image of a single optical element as shown below.

First, however, it should be pointed out that there is a significant difference in the effectiveness of meridional tangent errors, σ_{mer}, and sagittal tangent errors, σ_{sag}, in disturbing the image. This is easily explained:

NB: θ_g = grazing angle of incidence
Δ_s, Δ_{mer} is the full width half maximum value (FWHM)
i.e. 2.35 σ_s, σ_{mer} etc.

a) Meridional tangent error

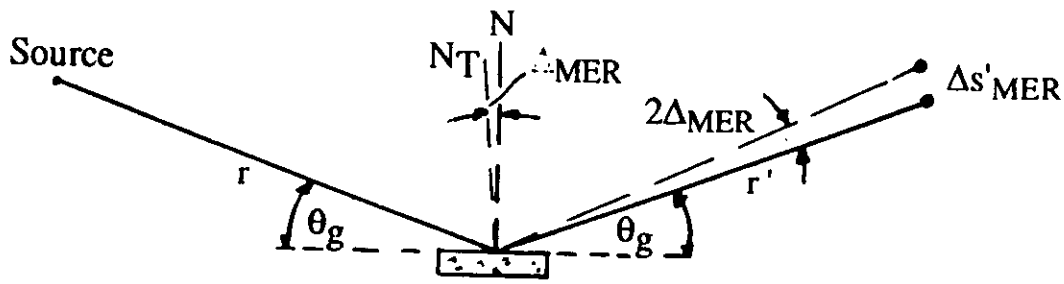

$$\Delta\, s'_{mer} = 2\, r'\, \Delta_{mer}$$

which is the same is if the source were at

$$\Delta\, s_{mer} = 2\, r\, \Delta_{mer}$$

b) Sagittal tangent error

$\Delta\, s'_{sag}$

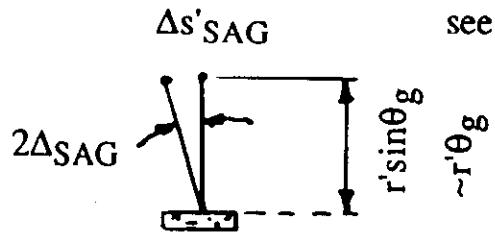

see picture above

end-on view

$$\Delta\, s'_{sag} = 2\, \Delta_{sag} \cdot r' \sin \theta_g$$

$$\approx 2\, \Delta_{sag} \cdot r' \theta_g$$

(good to < 0.5 % for $0 < \theta_g < 10°$)

c) The relative magnitudes of Δ_{mer} and Δ_{sag} which produce the same $\Delta s'$ is given by

$$\frac{\Delta s'_{mer}}{\Delta s'_{sag}} \equiv 1 \approx \frac{2r'\Delta_{mer}}{2r'\theta_g \Delta_{sag}}$$

$$\theta_g = \frac{\Delta_{mer}}{\Delta_{sag}}$$

$\theta_g = 5.73^\circ = 0.1$ rad
$\Delta_{sag} = 10\ \Delta_{mer}$

$\theta_g = 2^\circ = 3.5 \times 10^{-2}$ rad
$\Delta_{sag} = 29\ \Delta_{mer}$

Thus, for example, for a monochromator with a vertical dispersion plane mirrors which produce a horizontal deflection need not be as high quality as those producing a vertical deflection, or, it may be possible for a manufacturer to produce a more accurate finish in one direction than in the other: e.g. a mirror might be ground or cut in one direction rather in the other. In this case differing tangent errors will be produced and the mirror should be specified so as to yield a satisfactory tangent error in the dispersion plane.

Before we apply these equations, we'll examine the results of ray-trace calculations set up for the same purpose: to determine the effect of meridional and sagittal tangent errors on an image. Six trials are made, in which, for a symmetric optical system with an ellipsoidal focussing mirror and a point source, the image is generated with various values of tangent errors. The parameters and results are given in Table 5.5.1. The ray-trace diagrams are shown in Fig. 5.5.3. The image is also calculated for zero tangent error as reference (trial 1). Note that the effect of the errors is essentially orthogonal: meridional tangent errors have little effect on the sagittal halfwidth and vice-versa.

Figure 5.5.3: Effect of Tangent Errors on Line Width: Ray Trace Results

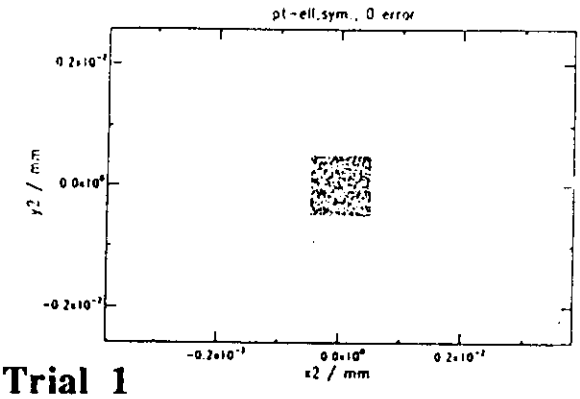

Trial 1

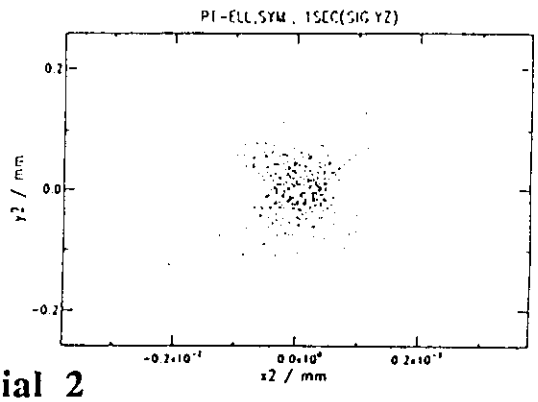

Trial 2

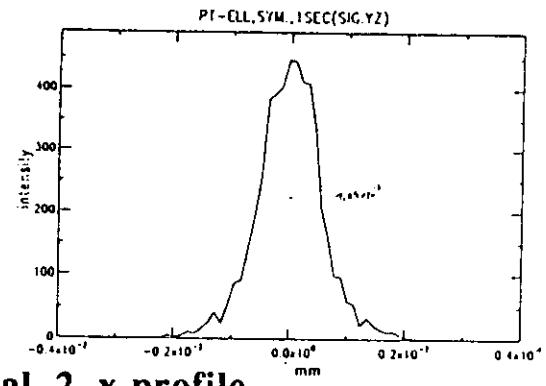

Trial 2 x-profile

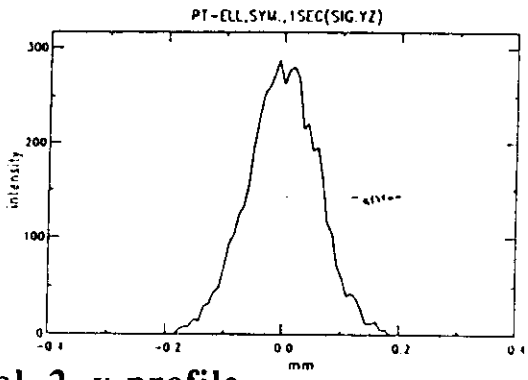

Trial 2 y-profile

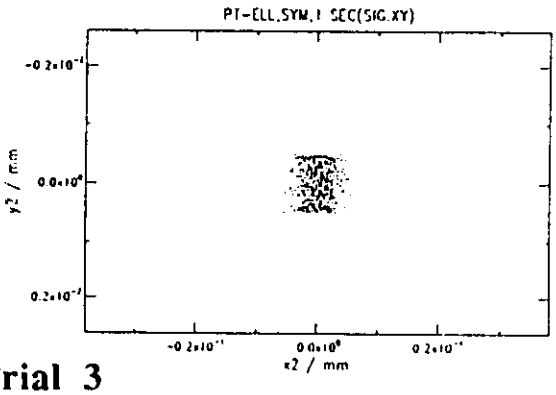

Trial 3

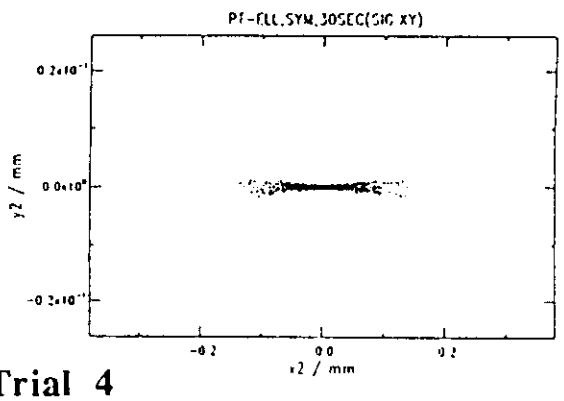

Trial 4

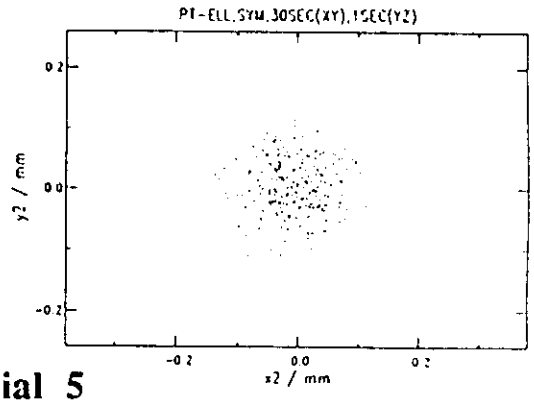

Trial 5

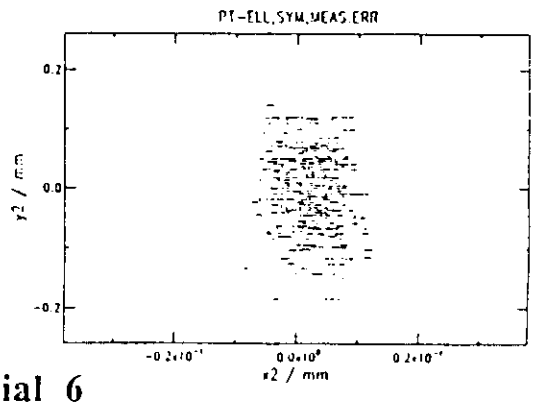

Trial 6

Table 5.5.1: Effect of Tangent Error on Line Width as Determined with Ray Traces

			Ray Traces*	
Trial	σ_{sag} (sec)	σ_{mer} (sec)	$FWHM_{sag}$ (mm)	$FWHM_{mer}$ (mm)
1	0	0	1.0×10^{-3}	1.0×10^{-3}
2	0	1	1.1×10^{-3}	0.134
3	1	0	4.9×10^{-3}	1.0×10^{-3}
4	30	0	0.14	1.1×10^{-3}
5	30	1	0.14	0.14
	measured tangent errors from a real mirror			
6	~ 2	~ 0.9	$8 - 11 \times 10^{-3}$	~ 0.11

* Ray-trace parameters

Source: $0.001\ mm^3$ x, y, z
1 mrad FWHM Divergence in the x and y planes
Isotropic distribution of source points and emission angles

Mirror: Ellipsoid
$r = r' = 6000$ mm
$\theta_g = 2° = 3.5 \times 10^{-2}$ rad $= \frac{1}{29}$ rad

Now we can take the formulas given above and calculate the image halfwidths resulting from the various tangent errors chosen.

2nd trial: $\Delta s'_{mer} = 2\, r' \Delta_{mer}$
$= 2 \cdot 6000 \cdot 1.14 \times 10^{-5}$ rad = <u>0.14 mm</u>

3rd trial: $\Delta s'_{sag} = 2\, r' \theta_g\, \Delta_{sag}$
$= 2 \cdot 6000 \cdot 3.5 \times 10^{-2}$ rad $\cdot$ 1.1×10^{-5} rad
$= 4.8 \times 10^{-3}$ mm

4th trial: $\Delta s'_{sag} = 2\, r' \theta_g\, \Delta_{sag}$
$= 2 \cdot 6000 \cdot 3.5 \times 10^{-2}$ rad $\cdot$ 3.4×10^{-4} rad
= <u>0.14 mm</u>

5th trial : $\sigma_{mer} = 1$ sec

$\theta g\, \sigma_{sag} = \frac{1}{29} \cdot 30 \simeq 1$ sec

The aberrations should be comparable (see trials 2 and 4 above).

6th trial: $\Delta s'_{mer} \approx 0.11 = 2 \cdot 6000\, \Delta_{mer}$
σ_{mer} = <u>0.81 sec</u>

$\Delta s'_{sag} \approx 9.5 \times 10^{-3} = 2 \cdot 6000 \cdot 3.5 \times 10^{-2}\, \Delta_{sag}$
σ_{sag} = <u>2.0 sec</u>

Similar trials were made for a 6:1 demagnifying system. The agreement between the σ's and the FWHM (ray trace) was as good as found above.

5.6 Surface Roughness

In contrast to the specular reflectance of a mirror at angles around $-\theta$, where θ is the angle of incidence, the intensity observed at other angles is not easily calculated. Such scattered reflectance results from the microroughness of the mirror surface (Figure 5.6.1 [5.11]). An useful relation for the reduction in reflectivity at a given wavelength and grazing angle of incidence is [5.18].

Figure 5.6.1: Surface Roughness [5.11]

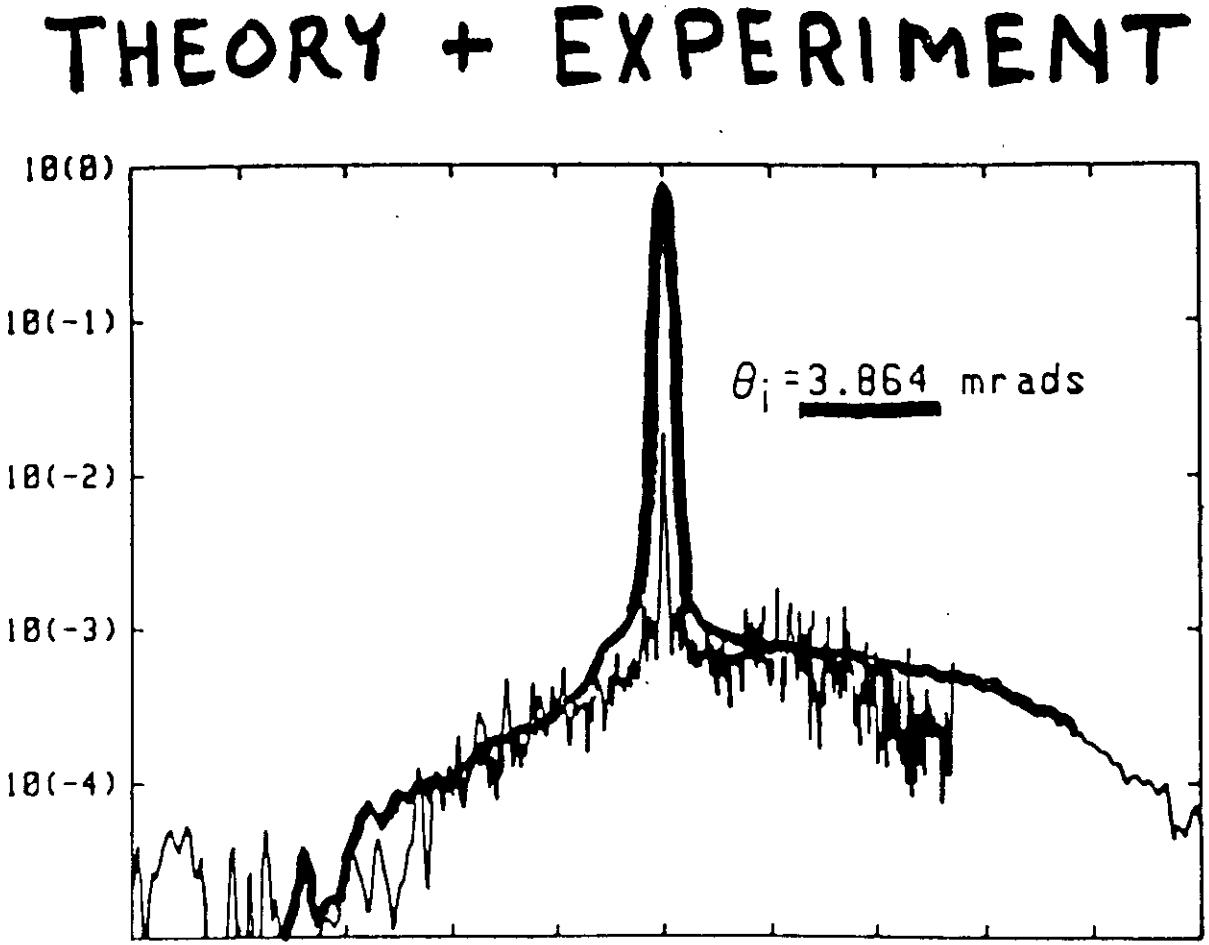

$$R = R_0 \exp - \left(\frac{4\pi \sigma \sin \theta_g}{\lambda}\right)^2$$

where R_0 = smooth surface reflectivity
R = attenuated reflectivity
θ_g = grazing angle of incidence
λ = Wavelength of incident light
σ = rms surface roughness

Attention is drawn to the references (5.8 - 5.11).

In general, surface roughness and figure error are coupled perversely: in the manufacturing process, the process that produces a better (smaller) rms micro-roughness simultaneously makes the figure worse. In recent years an rms microroughness of < 10Å is commonly available, with values down to 3 Å not uncommon.

Some Notes on the Design of Beamlines for Soft X-ray SR-Sources of the 3rd Generation

W.B. Peatman, BESSY, Berlin, FRG

10. References (given by section)

1. Introduction

1. For both general and specific treatments of the problems encountered here see the proceedings of the various national and international Synchrotron Instrumentation Meetings.
2. B. Lai, F. Cerrina, "Shadow: A Synchrotron Radiation Ray Tracing Program", Nucl. Instr. and Meth. A246, 337 (1986). For information contact Franco Cerrina, Center for X-Ray Lithography and Electrical and Computer Engineering Dept., University of Wisconsin, Madison, WI 53706, USA
3. Raytrace program RAY, J. Feldhaus, Fritz-Haber-Institute, MPG, Berlin; F. Schäfers, BESSY, Berlin. For information contact F. Schäfers, BESSY, Lentzeallee 100, D-1000 Berlin 33, Germany.
4. An example of a complete system, from multi-undulator to experiment.
   a) R.Z. Bachrach, R.D. Bringans, B.B. Pate, R.G. Carr, "The SSRL Insertion Device beam line 'WUNDER'", SPIE Proc. 582, 251-267 (1985)
   b) R.Z. Bachrach, R.D. Bringans, L.E. Swartz, I. Lindau, B.B. Pate, R.G. Carr, N. Nower, B. Youngman, H. Morales, P. Pianetta, "Multi-Undulator Beam Line V at SSRL: A Progress Report", Nucl. Instr. Meth. A266, 83 (1988)
5. a) G. Isoyama, S. Yamamoto, T. Shioya, H. Ohkuma, S. Sasaki, T. Mitsuhashi, T. Yamakawa, H. Kitamura, "Construction of a Multiundulator, Revolver No. 19, at the Photon Factory", Rev. Sci. Instrum. 60, 1863 (1989)
   b) A. Kakizaki, H. Ohkuma, T. Kinoshita, A. Harasawa, T. Ishii, "Simultaneous Scanning of Revolver Undulator and Monochromator at BL-19A of the Photon Factory", Rev. Sci. Instrum. in press (SRI-91)
6. "BESSY II, an Optimized Wiggler/Undulator Storage Ring Light Source for the VUV and XUV Spectral Regions" BESSY, Berlin (in German)
   (a) Part 1 1986 (b) Part 2 1989
7. U. Menthel, W.B. Peatman, F. Senf, "Conservation of Brightness in Undulator Beamlines", Rev. Sci. Instrum. in press (SRI-91)
8. G. Brown, K. Halbach, J. Harris, H. Winick, "Wiggler and Undulator Magnets - A Review", Nucl. Inst. Meth. 208, 65 (1983)
9. R.T. Avery, "Thermal Problems on High Flux Beam Lines", Nucl. Inst. Meth. 222, 146 (1984)

(W.B. Peatman, 10: References, con't)

2. SR-Source characteristics

1. S. Krinsky, M.L. Perlman, R.E. Watson, "Characteristics of Synchrotron Radiation and of its Sources" in "Handbook on Synchrotron Radiation", vol. 1, E.-E. Koch, Editor, North Holland, Amsterdam, 1983, chapter 2.
2. G. Brown, K. Halbach, J. Harris, H. Winick, "Wiggler and Undulator Magnets - A Review", Nucl. Instr. Meth. 208, 65-77 (1983)
3. C. Jacobsen, "SMUT" Undulator spectrum program with finite electron beam dimensions. Lawrence Berkeley Laboratory, Center for x-ray optics
4. C. Jacobsen, H. Rarback, "Predictions on the Performance of the Soft X-Ray Undulator", SPIE 582, 201-212 (1985)
5. H. Maezawa, Y. Suzuki, H. Kitamura, T. Sasaki, "Spectral Characterization of Undulator Radiation in the Soft X-Ray Region", Appl. Opt. 25, 3260-3268 (1987)
6. R.P. Walker, B. Diviacco "URGENT" Undulator spectrum program with finite electron beam dimensions. Sincrotrone Trieste, Italy
7. K. Molter, G. Ulm "Absolute Measurement of the Spectral and Angular Properties of Undulator Radiation with a Pinhole Transmission Grating Monochromator", Rev. Sci. Inst. in press (SRI-91)
8. J.M. Machado, P. Kuske "Horizontal Beam Profile at the BESSY Storage Ring" BESSY Technical Report TB 106/87 (1987) (in German)
9. F. Schäfers, W. Peatman, A. Eyers, Ch. Heckenkamp, G. Schönhense, U. Heinzmann "High-flux normal incidence monochromator for circularly polarized synchrotron radiation", Rev. Sci. Instrum. 57, 1032 (1986)
10. W. Peatman, J. Bahrdt "Undulator Radiation: Promises and Problems", Nucl. Instr. and Meth. A282, 448 (1989)
11. W. Peatman, C. Carbone, W. Gudat, W. Heinen, P. Kuske, J. Pflüger, F. Schäfers, T. Schroeter "The BESSY wiggler/undulator-TGM-5 beamline", Rev. Sci. Instrum. 60, 1445 (1989)
12. "An ALS Handbook" Lawrence Berkeley Laboratory Publication PUB-643 Rev. 2, April 1989
13. R.P. Walker "Multipole Wiggler Brilliance and Effective Source Size", Sincrotrone Trieste Technical Report ST/M-TN-89/24

(W.B. Peatman, 10: References, con't)

3. Requirements of the optical system:

Reviews of monochromators, mirrors, etc. for SR

1. J.A.R. Samson, "Techniques of Vacuum Ultraviolet Spectroscopy", Wiley, New York (1967), Chapters 2, 3
2. W. Gudat, C. Kunz, "Instrumentation for Spectroscopy and Other Applications" in "Topics in Current Physics", vol. 10, C. Kunz, Editor, Springer, Berlin, 1979, chapter 3
3. R.L. Johnson, "Grating Monochromator and Optics for the VUV and Soft X-Ray Region" in "Handbook on Synchrotron Radiation", Vol. 1, E.-E. Koch, Editor, North Holland, Amsterdam, 1983, chapter 3
4. J.B. West, H.A. Padmore, "Optical Engineering" in "Handbook on Synchrotron Radiation", Vol. 2, G.V. Marr, Editor, North Holland, Amsterdam, 1987
5. T. Namioka, K. Ito, "Modern Developments in VUV Spectroscopic Instrumentation", Phys. Scripta 37, 673-681 (1988)
6. D. Attwood, K. Halbach, K.-J. Kim "Tunable Coherent X-Rays", Science 228, 1265-1272 (1985)
7. M.R. Howells, M.A. Iarocci, J. Kirz "Experiments in X-Ray Holographic Microscopy Using Synchrotron Radiation", J. Opt. Soc. Am. A 3, 2171-2178 (1986)
8. E. Spiller "Soft X-Ray Optics and Microscopy" in "Handbook on Synchrotron Radiation", Vol. 1, E.E. Koch, Editor, North Holland, Amsterdam, 1983, Chapter 12

4. Gratings and monochromators

1. H.G. Beutler, "The Theory of the Concave Grating", J. Opt. Soc. Am. 35, 311-350 (1945)
2. H. Haber, "The Torus Grating", J. Opt. Soc. Am. 40, 153-165 (1950)
3. H. Noda, T. Namioka, M. Seya, "Geometric Theory of the Grating", J. Opt. Soc. Am. 64, 1031-1036 (1974)
4. T. Namioka, M. Seya, H. Noda, "Design and Performance of Holographic Concave Gratings", Jap. J. Appl. Phys. 15, 1181-1197 (1976)
5. M. Nevière, P. Vincent, D. Maystre, (Efficiency of Conical Diffraction), Appl. Opt. 17, 843-845 (1978)
6. W.R. McKinney, M.R. Howells, "Design Optimization of 'Straight Groove' Toroidal Grating Monochromators for Synchrotron Radiation", Nucl. Instr. Meth. 172, 149-156 (1980)
7. M.R. Howells, "Vacuum Ultra Violet Monochromators", Nucl. Instr. Meth. 172, 123-131 (1980)

(W.B. Peatman, 10: References, con't)

8. M.R. Howells, "Plane Grating Monochromators for Synchrotron Radiation", Nucl. Instr. Meth. 177, 127-139 (1980)
9. H. Petersen, "The Plane Grating and Elliptical Mirror: A New Optical Configuration for Monochromators", Opt. Commun. 40, 402-406 (1982)
10. H. Hogrefe, M.R. Howells, E. Hoyer, "Application of Spherical Gratings in Synchrotron Radiation Spectroscopy", SPIE Proc. 733, 274-285 (1986)
11. T. Harada, M. Itou, T. Kita, "A Grazing Incidence Monochromator with a Varied-Space Plane Grating for Synchrotron Radiation", SPIE Proc. 503, 114-118 (1984)
12. H. Petersen, "Plane Grating Monochromators: The Working Curve Concept as Implemented in the SX-700", SPIE Proc. 733, 262-264 (1986)
13. M. Pouey, "Dedicated Undulator Monochromators", Nucl. Instr. Meth. A 246, 256-259 (1986)
14. C.T. Chen, "Concept and Design Procedure for Cylindrical Element Monochromators for Synchrotron Radiation", Nucl. Instr. Meth. A 256, 595-604 (1987)
15. J.B. West, H.A. Padmore, "Optical Engineering" in "Handbook on Synchrotron Radiation", Vol. 2, G.V. Marr, Editor, North Holland, Amsterdam, 1987, Chapter 2
16. M.C. Hettrick, J.H. Underwood, P.J. Batson, M.J. Eckart, "Resolving Power of 35000 (5 mA) in the extreme Ultraviolet Employing a Grazing Incidence Spectrometer", Appl. Opt. 27, 200-201 (1988)
17. For several new monochromator designs see "Proceedings" of SRI-88 and SRI-91 in "Review of Scientific Instruments", 1989, 1992
18. REDUCE 3.3, A General Purpose Algebra System
    © A.C. Hearn (the RAND Corp.), 386 Based Computer Version, H. Melenk, W. Neun, Konrad Zuse Zentrum Berlin (1990)
19. E. Ishiguro, M. Suzui, J. Yamazaki, E. Nakamura, K. Sakai, O. Matsudo, N. Mizutani, F. Fukui, M. Watanabe "Constant Deviation Monochromator for the Range 100Å < λ < 1000Å" Rev. Sci. Inst. 60, 2105 (1989)
20. F. Senf, F. Eggenstein, W.B. Peatman "Simple, Constant Length Rowland Circle Monochromators for Undulator Radiation" Rev. Sci. Inst. ~~in press (SRI-91)~~ 63, 1326-1329 (1992)
21. W. Werner, H. Visser "X-Ray Monochromator Designs Based on Extreme Off-Plane Grating Mountings" Appl. Opt. 20, 487-492 (1981)

22. C. Buckley, H. Rarback, R. Alforque, D. Shu, H. Ade, S. Hellman, N. Iskander, J. Kirz, S. Lindaas, I.McNulty, M. Oversluizen, E. Tang, D. Attwood, R. DiGennaro, M. Howells, C. Jacobsen, Y. Vladimirsky, S. Rothman, D. Kern, D. Sayre "Soft-x-ray imaging with the 35 period undulator at the NSLS" Rev. Sci. Instrum. 60, 2444-2447 (1989)
23. F. Schäfers, W. Peatman, A. Eyers, Ch. Heckenkamp, G. Schönhense, U. Heinzmann "High-flux normal incidence monochromator for circularly polarized synchrotron radiation" Rev. Sci. Instrum. 57, 1032-1041 (1986)
24. Chien-Te Chen, F. Sette, N.V. Smith "Double-headed Dragon monochromator for soft x-ray circular dichroism studies" Appl. Optics 29, 4535-4536 (1990)
25. H. Petersen "Circularly Polarized Light in the 30-2000 eV Photon Energy Range at the SX700/3" Proceedings of the International Workshop High Performance Monochromators and Optics for Synchrotron Radiation in the Soft X-Ray Region held at BESSY GmbH, Berlin, Germany 26th - 28th March 1991

5. Mirror systems

1. P. Kirkpatrick, A.V. Baez, "Formation of Optical Images by X-Rays", J. Opt. Soc. Am. 38, 766-774 (1948)
2. W.A. Rense, T. Violett, "Method of Increasing the Speed of a Grazing-Incidence Spectrograph", J. Opt. Soc. Am. 49, 139-141 (1959)
3. T. Namioka, H. Noda, K. Goto, T. Katayama, "Design Studies of Mirror-Grating Systems for Use with an Electron Storage Ring Source at the Photon Factory", Nucl. Instr. Meth. 208, 215-222 (1983)
4. a) B.L. Henke, P. Lee, T.J. Tanaka, R.L. Shimabukuro, B.K. Fujikawa, "Low-Energy X-Ray Interaction Coefficients: Photoabsorption, Scattering and Reflection", Atomic Data Nucl. Data Tab. 27, 1 (1982)
   b) B.L. Henke, J.C. Davis, E.M. Gullikson, R.C.C. Perera, Lawrence Berkeley Laboratory, Berkeley, CA, LBL-26259 UC-411 (1988)
5. W.R. Hunter, "Measurement of Optical Constants in the Vacuum Ultraviolet Spectral Region" in "Handbook of Optical Constants of Solids", Ed. Palik, Academic, New York (1985) chapter 4
6. F. Schäfers "Description of the program REFLEC"
   BESSY Technical Report No. 157/1990 (in German)
7. M.R. Howells "Some Geometrical Considerations Concerning Grazing Incidence Reflectors", Brookhaven National Laboratory Report BNL-27416 (1980)
8. H. Petersen "Plane Grating Monochromators: Adjustment, Aspheric Mirror Analysis, Effects of Source Instabilities", BESSY Technical Report No. 118/1987 (in German)

9. E.L. Church, P. Takacs, "The Interpretation of Glancing Incidence Scattering Measurements", SPIE Proc. 640, 126-133 (1986)
10. P.Z. Takacs, E.L. Church, "Figure and Finish of Grazing Incidence Mirrors", Nucl. Instr. and Meth. A291, 253 (1990)
11. P.Z. Takacs, K. Furenlid, E.L. Church "Measurement of Surface Finish and Figure Accuracy" in Proceedings of the international workshop "High Performance Monochromators and Optics for Synchrotron Radiation in the Soft X-Ray Region" BESSY, Berlin 26th - 28th of March 1991
12. K. Becker, K. Beckstette "M 400 and P 400 - A Pair of Machines for Computer-Controlled Fine Correction of Optical Surfaces" in "Ultraprecision in Manufacturing Engineering", Springer, Berlin 1988
13. K. Beckstette, "Fabrication and Test of X-Ray Optics", SPIE 1140, 316 (1989)
14 H.E. Bennett, "Techniques for Evaluating the Surface Finish of X-Ray Optics", SPIE Proc. 184, 153-166 (1979)
15. K.H. Guenther, P.G. Wierer, J.M. Bennett, "Surface Roughness Measurements of Low-Scatter Mirrors and Roughness Standards", Appl. Opt. 23, 3820-3836 (1984)
16. H. Hogrefe, C. Kunz, "Soft X-Ray Scattering from Rough Surfaces: Experimental and Theoretical Analysis", Appl. Opt. 26, 2851-2859 (1987)
17. M. Born, E. Wolf "Principles of Optics", Pergamon Press Oxford, (1980)
18. E. Spiller "Soft X-Ray Optics and Microscopy" in "Handbook on Synchrotron Radiation", Vol. 1 E.-E. Koch, Editor, North Holland, Amsterdam, 1983 chapter 12
19. F.A. Jenkins, H.E. White "Fundamentals of Optics", 4th Edition, McGraw-Hill, New York, 1976
20. A. Gaupp, M. Mast "First Experimental Experience with a VUV Polarimeter at BESSY", Rev. Sci. Instrum. 60, 2213 (1989)
21. A.G. Michette "Optical Systems for Soft X-Rays" Plenum, New York 1986

6. Source stability

1. R.O. Hettel, "Beam Steering at the Stanford Synchrotron Radiation Laboratory", IEEE Trans. Nucl. Sci. NS-30, 2228 (1983)
2. L.H. Yu, J. Nawrocky, J. Galayda, "Studies of Positional Stability of the Electron Beam in the NSLS Storage Ring", IEEE Trans. Nucl. Sci. NS-32, 3394 (1985)
3. K. Huke, "Correlation Between the Movement of the Light Source Building and the Vibration of the Synchrotron Radiation Axis", Photon Factory Preprint KEK 86-48 (1986)

(W.B. Peatman, 10: References, con't)

4. M.A. Green, E.I. Majer, V.D. More, R.D. O'Connell, R.C. Shilling, "Ground Motion Measurements at the LBL Light Source Site, the Bevatron and at SLAC", Lawrence Berkeley Laboratory Report LBL-21519 (1986)
5. T. Katsura, Y. Kamiya, K. Haga, T. Mitsuhashi, "Beam Position Monitoring and Feedback Steering System at the Photon Factory", Part. Accl. Conf. 1987, IEEE Catalog No. 87CH2387-9, p. 538
6. W. Brefeld, "Beam Position Control System at DORIS II", Nucl. Instr. Meth. A 261, 22-26 (1987)
7. R.O. Hettel, "Beam Steering and Stabilizing Systems: Present Status and Considerations for the Future", Nucl. Instr. Meth. A 266, 155-163 (1988)
8. R.J. Nawrocky, J.W. Bittner, Li Ma, H.M. Rarback, D.P. Siddons, L.H. Yu, "Automatic Beam Steering in the NSLS Storage Rings Using Closed Orbit Feedback", Nucl. Instr. Meth. A 266, 164-171 (1988)
9. K.J. Kleman, "Beam Diagnostics and Control at ALADDIN", Nucl. Instr. Meth. A 266, 172-176 (1988)
10. E.D. Johnson, T. Oversluizen "Compact High Flux Photon Beam Position Monitor", Rev. Sci. Instrum. 60, 1947 (1989)
11. E.D. Johnson, T. Oversluizen "UHV Photoelectron X-Ray Beam Position Monitor", Nucl. Instr. Meth. A291, 427 (1990)
12. E.D. Johnson, P. Boccard, T. Oversluizen "Photoelectric Effect Photon Beam Position Monitors: Operation and Applications", Rev. Sci. Inst. in press (SRI-91)
13. F.-P. Wolf, W. Peatman "Synchrotron Radiation Diagnostics at BESSY", Nucl. Instr. Meth. A246, 408 (1986)
14. F.-P. Wolf, W. Peatman "Precise, Continuous Determination of Source Position and Emission Angle in Synchrotron Radiation Sources", Nucl. Instr. Meth. A278, 598 (1989)

7. Light of higher orders

1. E.S. Gluskin, E.M. Trachtenberg, A.S. Vinogradov, "A Simple System of the Short-Wave SR Prevention in the 30 Å to 180 Å Wavelength Range", Nucl. Instr. Meth. 152, 133-134 (1978)
2. R.J. Bartlett, D.R. Kania, R.H. Day, E. Källne, "Mirror Filter Systems for the Soft X-Ray Region", Nucl. Instr. Meth. 222, 95 - 98 (1984)
3. K. Ito, T. Namioka, Y. Morioka, T. Sasaki, H. Noda, K. Goto, T. Katayama, M. Koike, "High-Resolution VUV Spectroscopic Facility at the Photon Factory", Appl. Opt. 25, 837-847 (1986)
4. W. Peatman, "High-Order-Light Suppressor for Monochromators", BESSY Technical Report TB 160/90, 1990

(W.B. Peatman, 10: References, con't)

5. M. Krumrey, E. Tegeler, "Self-Calibration of Semiconductor Photodiodes in the Soft X-Ray Region", Rev. Sci. Inst. in press (SRI-91)

8. Heat loading and radiation damage

1. T. Ohta, T. Fujikawa, "Computer Simulation of the Heating Effect on Mirrors by Synchrotron Radiation", KEK Technical Report (Japan, in english) KEK 81-10 (1981)
2. V. Rehn, "Optics for Insertion-Device Beam Lines", SPIE Proc. 582, 238-250 (1985)
3. R. Di Gennaro, W.R. Edwards, E. Hoyer, "Predicting Thermal Distortion of Synchrotron Radiation Mirrors with Finite Element Analysis", SPIE Proc. 582, 273-280 (1985)
4. R.T. Avery, "Thermal Problems on High Flux Beamlines", Nucl. Instr. Meth. 222, 146-158 (1984)
5. P.Z. Takacs, T.L. Hursman, J.T. Williams, "Application of Silicon Carbide to Synchrotron Radiation Mirrors", Nucl. Instr. Meth. 222, 133-145 (1984)
6. J.B. Kortright, P. Plag, R.C.C. Perera, P.L. Cowan, D.W. Lindle, B. Karlin, "Multilayer Coated Mirrors as Power Filters in Synchrotron Radiation Beamlines", Nucl. Instr. Meth. A 266, 452-456 (1988)
7. W. Peatman, J. Bahrdt, "Undulator Radiation: Promises and Problems", Nucl. Instr. Meth. A 282, 448 (1989)

9. Contamination of optical components

1. K. Boller, R.-P. Haelbick, H. Hogrefe, W. Jark, C. Kunz, "Investigation of Carbon Contamination of Mirror Surfaces Exposed to Synchrotron Radiation", Nucl. Instr. Meth. 208, 273-279 (1983)
2. W.R. McKinney, P.Z. Takacs, "Plasma Discharge Cleaning of Replica Gratings Contaminated by Synchrotron Radiation", Nucl. Instr. Meth. 195, 371-374 (1982)
3. T. Koide, S. Sato, T. Shidara, M. Niwano, M. Yanagihara, A. Yamada, A. Fujimori, A. Mikuni, H. Kato, T. Miyahara, "Investigation of Carbon Contamination of Synchrotron Radiation Mirrors", Nucl. Instr. Meth. A 246, 215-218 (1986)
4. T. Koide, T. Shidara, M. Yanagihara, S. Sato, "Resuscitation of Carbon-Contaminated Mirrors and Gratings by Oxygen Discharge Cleaning. 2: Efficiency Recovery in the 100 - 1000 eV Range", Appl. Opt. 27, 4305-4313 (1988)
5. E.D. Johnson, R.E. Garrett, "In Situ Reactive Cleaning of X-Ray Optics by Glow Discharge", Nucl. Instr. Meth. A 266, 381-385 (1988)

(W.B. Peatman, 10: References, con't)

6. R.A. Rosenberg, D.B. Crossley, "Oxygen RF-Discharge Cleaning: Plasma Characterization and Implementation on a Grasshopper Beam Line", Nucl. Instr. Meth. A 266, 386-391 (1988)

7. B.R. Müller, F. Schäfers, F. Eggenstein, J. Feldhaus "Cleaning of Carbon Contaminated VUV-Optics: Influence on Surface Roughness and Reflectivity" Rev. Sci. Inst. in press (SRI-91)

Some Notes on the Design of Beamlines for Soft X-ray SR-Sources of the 3rd Generation

W.B. Peatman
Berliner Elektronenspeicherring-Gesellschaft
für Synchrotronstrahlung mbH (BESSY)
Lentzeallee 100, D-1000 Berlin 33, FRG

List of Tables

Some Notes on the Design of Beamlines for Soft X-ray SR Sources of the 3rd Generation

W.B. Peatman
Berliner Elektronenspeicherring-Gesellschaft
für Synchrotronstrahlung mbH (BESSY)
Lentzeallee 100, D-1000 Berlin 33, FRG

List of Figures